Fakultät TUM School of Life Sciences

Technische Universität München

Rescuing motor behavior in a Parkinson´s disease model by aCRISPR mediated reprogramming of striatal astrocytes into induced neurons

Jessica Giehrl-Schwab

Vollständiger Abdruck der von der Fakultät TUM School of Life Sciences der Technischen Universität München zur Erlangung des akademischen Grades eines

Doktors der Naturwissenschaften

genehmigten Dissertation.

Vorsitzender:

Prof. Dr. Erwin Grill

Prüfende der Dissertation:

1. Prof. Dr. Wolfgang Wurst
2. Prof. Angelika Schnieke, Ph.D.
3. Prof. Dr. Magdalena Götz

Die Dissertation wurde am 20.05.2020 bei der Technischen Universität München eingereicht und durch die Fakultät TUM School of Life Sciences am 14.10.2020 angenommen.

omnes viae neuronum ducunt

Contents

1 Abstract

Parkinson´s disease is a neurodegenerative disorder, mainly characterized by the specific degeneration of nigrostriatal dopaminergic neurons in the substantia nigra *pars compacta* (SN*pc*). This cell population is particularly important for the control of voluntary movement, wherefore its deficiency concludes in motor behavior deficits like tremor, bradykinesia and rigidity. So far no causal treatment option exists and therapy is primarily symptomatic. However, several attempts are realized utilizing cell replacement therapy of dopaminergic neurons as curative option. To circumvent *ex vivo* cell source and the associated GMP requirements, *in situ* direct cellular reprogramming appears as valuable alternative strategy. Several *in vitro* and *in vivo* studies exist, indicating that by the overexpression of specific transcription factors, somatic cells, like fibroblasts or astrocytes, can be converted into induced dopaminergic neurons. As so far efficiencies of generating functional dopaminergic neurons were not satisfying and most *in vitro* results were not transferable *in vivo*, this work focused on the development of a new tool for facile, multiplexed *in vivo* activation of transcription factors to reprogram astrocytes into dopaminergic neurons.

For this purpose, a new knock-in mouse line was generated, harboring the CRISPR activation system (aCRISPR), the so-called dCas9-Activator Mouse (*dCAM*). In a toxin-induced Parkinson´s disease model the two transcription factor combination *Ascl1*, *Lmx1a*, *Nr4a2* (*ALN*) and *Ascl1*, *Lmx1a*, *NeuroD1,* miRNA218 (*ALNe-218*), known to produce dopaminergic neurons *in vitro* and the latest even *in vivo*, were endogenously activated in astrocytes, by the AAV-based delivery of sgRNAs. Results demonstrate that the implemented aCRISPR system is able to activate the endogenous genes and efficiently reprogram astrocytes into functional induced neurons *in vivo*. To extent the applicability of the system to a broader scientific field, an aCRISPR system, solely based on viral delivery, independent of transgenic recipients was generated, called dCas9-Activator System (*AAV-dCAS*), making it versatile and applicable across species barriers, for example in different model organisms, including potential use for gene therapeutic approaches, by minimal modifications. With this approach the results obtained with the transgenic model could be reproduced, confirming the efficient production of induced neurons.

Only the neurons reprogrammed with the factor combination *ALN* exhibited a mature firing pattern and were integrated in striatal circuits. Immunohistochemistry and scRNA-seq analysis revealed their GABAergic identity. By using this transcription factor combination measurable improvement in voluntary movement could be detected in the toxin-induced Parkinson´s disease mouse model, with ameliorated disease symptoms.

In summary, with the aCRISPR approach it was possible to reprogram astrocytes into functional, mature GABAergic neurons integrated into striatal circuits. Interestingly, these

induced GABAergic neurons were capable of improving voluntary motor behavior. These results suggest a novel intervention strategy for Parkinson´s disease relevant aspects, beyond the restoration of dopamine levels. Thus, the transgenic-independent *AAV-dCAS* approach may enable clinical therapies for Parkinson´s disease by reprogramming striatal astrocytes.
The aCRISPR system is able to specifically manipulate target loci and reliably activate endogenous genes. Due to the facile multiplexing, extension of target genes is easily feasible, whereby it can potentially be used to treat a wide range of human diseases.

2 Zusammenfassung

Morbus Parkinson ist eine neurodegenerative Erkrankung, hauptsächlich gekennzeichnet durch die spezifische Degeneration der nigrostriatalen dopaminergen Nervenzellen in der Substantia nigra *pars compacta* (SN*pc*). Diese Zellpopulation ist speziell bei der Durchführung spontaner Bewegungsabläufe wichtig, weshalb ihre Abwesenheit unter anderem zu Bewegungsstörungen, wie Tremor, Bradykinesie und Steifheit führt. Bisher existieren keine kausalen Therapieansätze und die Behandlung erfolgt symptomatisch. Jedoch wurden einige Versuche unternommen Behandlungen mittels Zellersatztherapie der dopaminergen Nervenzellen durchzuführen. Um jedoch den *ex vivo* Zellursprung und die damit verbundenen GMP Anforderungen zu vermeiden, erscheint die *in situ* direkte Zellreprogrammierung als eine geeignete Alternative. In verschiedenen *in vitro* und *in vivo* Studien wurde gezeigt, dass durch gezielte Überexpression von Transkriptionsfaktoren somatische Zellen, wie Fibroblasten oder Astrozyten, in induzierte dopaminerge Nervenzellen umgewandelt werden können. Da die bisherigen Ansätze jedoch nur zu unzureichendem Erfolg geführt haben und die meisten *in vitro* Resultate nicht direkt *in vivo* übertragbar sind, wurde in dieser Arbeit versucht ein neues Hilfsmittel zu generieren, mit welchem unmittelbar mehrere Gene endogen angeschaltet werden können, um Astrozyten in dopaminerge Nervenzellen umzuprogrammieren.

Zu diesem Zweck wurde eine neue knock-in Mauslinie generiert, welche das CRISPR Aktivierungssystem (aCRISPR) beinhaltet, die sogenannte dCas9-Activator Mouse (*dCAM*). In einem Toxin-induzierten Parkinsonmausmodel wurden zwei verschiedene Transkriptionsfaktorenkombinationen endogen durch die Bereitstellung von sgRNAs mittels AAVs aktiviert. *Ascl1*, *Lmx1a*, *Nr4a2* (*ALN*) und *Ascl1*, *Lmx1a*, *NeuroD1,* miRNA218 (*ALNe-218*), wobei von beiden bekannt ist, dass sie dopaminerge Nervenzellen *in vitro*, die letztere Kombination sogar *in vivo*, produzieren können. Mittels beider Kombinationen konnten effizient Astrozyten in induzierte Nervenzellen umgewandelt werden. Um dieses System nun auch in einem umfangreicheren Maß zum Einsatz zu bringen, wurde ebenfalls ein aCRISPR System entwickelt, welches nur aus viral-basierter Verabreichung der Komponenten besteht, unabhängig von der transgenen Mauslinie, das dCas9-Activator System (*AAV-dCAS*). Dieses System kann nun auch in anderen Spezies, z.B. anderen Tiermodellen oder letztendlich auch als gentherapeutischer Ansatz im Menschen, mittels minimaler Modifikationen angewandt werden. Mit diesem Ansatz konnten alle Ergebnisse aus dem transgenen Modell reproduziert werden, wodurch die Effizienz dieses Systems nochmal validiert werden konnte.

Nur die Nervenzellen, welche mittels der Faktorenkombination *ALN* reprogrammiert wurden, wiesen elektrophysiologische Charakteristika von vollentwickelten Nervenzellen auf und waren in die neuronalen Schaltungen integriert. Immunohistochemie, sowie scRNA Sequenzieranalysen offenbarten die GABAerge Identität der neu generierten Nervenzellen.

Durch die Verwendung dieser Transkriptionsfaktorenkombination konnte in dem Toxin-induzierten Parkinsonmausmodel nachweislich eine Verbesserung der Bewegungsabläufe, d.h. verbesserte Krankheitssymptome, erzielt werden.
Zusammenfassend konnte mit dem aCRISPR Ansatz eine Reprogrammierung von Astrozyten in funktionale, vollentwickelte GABAerge Nervenzellen erreicht werden, welche in striatale neuronale Schaltkreise integriert sind. Interessanterweise sind diese neugenerierten GABAergen Nervenzellen in der Lage eine Verbesserung der Bewegungsabläufe zu erwirken. Diese Resultate legen eine neue alternative Behandlungsstrategie von Morbus Parkinson nahe, unabhängig von der Wiederherstellung des dopaminergen Systems. Der transgen-unabhängige Ansatz könnte eine klinische Anwendung des Zellreprogrammierungsansatzes zur Behandlung von Morbus Parkinson ermöglichen.
Mit diesem System können spezifisch endogene Loci manipuliert und verlässlich mehrere endogene Gene aktiviert werden. Durch die einfache Durchführbarkeit der mehrfachen Genaktivierung, hat dieses System das Potential, gentherapeutisch für die Behandlung eines breiten Spektrums an Krankheiten eingesetzt werden zu können.

3 Introduction

One of the main focuses of scientific research is to identify mechanisms how to prolong lifespan and to increase quality of life. Nowadays, better medical care and higher life standards in developed countries have raised health and life expectancy from around 70 years in the 1970s to around 80 years nowadays, whereas the trend goes even upwards [1, 2]. This development leads to a shift of the prevalent occurring maladies from more infectious diseases like tuberculosis or gastrointestinal disease, to more age-related ones such as cancer, cardiovascular disease or degenerative diseases [3].

By definition degenerative diseases are diseases, which negatively affect the function and structure of a tissue or an organ over time [4]. Nowadays, people receive more health checks and generally become diagnosed earlier, however depending on which organ or tissue is affected, more or less efficient medication exists. Considering for example the pancreas, people suffering from type II diabetes, which often arises with age, have good chances for high quality of life and less disease symptoms, as insulin treatment is very effective and noninvasive. Yet people contracted with a neurodegenerative disease, like Parkinson´s disease, have less good prospects, as the brain is a very complex and hard to target organ. For Parkinson´s disease, state-of-the-art-research led to several treatments that attenuate the symptoms and increase quality of life. But as so far, no curative therapy exists and there are still many obstacles to overcome. With this work it is tried to add some more insights into the basic understanding of this multifactorial disease.

“Parkinson's is my toughest fight. No, it doesn't hurt. It's hard to explain. I'm being tested to see if I'll keep praying, to see if I'll keep my faith. All great people are tested by God. “

[Muhammed Ali, 2012]

3.1 Parkinson´s disease

The shaking palsy was originally described in 1817 by the British surgeon James Parkinson in his work *´An Essay on the Shaking Palsy´*. Nowadays, it is generally known as Parkinson´s disease (PD), a designation which was introduced in 1865 by William Rutherford Sanders [5]. After Alzheimer´s disease it is the second most common neurodegenerative disorder. The main neuropathological characteristics are a specific degeneration of the dopaminergic neurons in the substantia nigra *pars compacta* (SN*pc*) and the formation of intracellular protein aggregates, so called Lewy bodies, which mainly consist of α-synuclein. However, also other neuronal subtypes are effected including norepinephrinergic, GABAergic, glutamatergic, cholinergic, and serotonergic neurons [6]. The cardinal signs of the disease are the well-known motor symptoms (rigidity, bradykinesia, tremor, and postural instability), that occur once 60-70% of the dopaminergic neurons are degraded [7]. In addition, the neuropathological alterations outside the SN*pc* could be correlated to non-motor PD symptoms that appear in the prodromal phase, like olfactory dysfunction, autonomic dysfunction, psychiatric symptoms and sleeping disorder [8]. Therapies for PD are at present symptomatic, as so far, no curative treatment exists. Much effort is put into neurorestorative research, as in most cases the disease is diagnosed when motor symptoms enchase and most dopaminergic neurons are already degraded. In addition, diagnostic procedures begin to change, to facilitate the cognition of the disease in the prodromal phase and to be able to intervene in a neuroprotective fashion before degradation occurs [9].

3.1.1 Epidemiology and etiology

Being the second most common neurodegenerative disorder, Parkinson´s disease has a global prevalence of approximately 0.3% [10]. Disease occurrence is rare before the age of 50, but rises strongly with increasing age, whereas prevalence raises up to 4% in people over the age of 80 [11]. Improved health care and better understanding of disease mechanisms led to revised disease management and prolonged survival of patients, which is associated with increased prevalence of PD over time, with an expected doubling of patient counts from 2005 to 2030 [12, 13].

Several studies indicate that prevalence and incidence of PD are approximately two times higher in men than in women. Age of onset, severity and type of symptoms differ significantly between sexes, whereas in women onset seems to be postponed and motor symptoms milder [14]. This protective effect might be explained due to hormonal, environmental or genetic differences. Estrogens have been shown to have a neuroprotective effect in animal models [15, 16]. However, clinical trials using estrogen replacement therapy in post-menopausal PD patients did not indicate a clear beneficial effect, remaining the understanding of the influence

of estrogens on PD inconclusive [17]. Despite the sex-specific hormone differences, also different lifestyles between men and women could have tremendous effects. It was shown that lifestyle and exposure to environmental factors have a big impact on the occurrence of the disease. Physical activity and consumption of caffeine or nicotine lead to a significant lower incidence of PD, whereas pesticides and diseases like traumatic brain injury or melanoma are associated with elevated disease appearance [18]. The influence of race and ethnicity on the appearance of the disease could not be defined properly, as data is sparse and inconsistent. Also no representative multiracial cohort exists to investigate these factors without the influence of geographical and environmental cues [10]. However, some populations exhibit a specific high disease prevalence, like the Ashkenazj Jews in Israel, but this increased occurrence is rather associated with shared genetic factors, in this case with a higher mutation rate in the PD associated genes *LRRK2* and *GBA,* than with the ethical or racial background [19]. Most PD cases are of sporadic, idiopathic nature, less than 5% are related to specific monogenic mutations. With large scale GWAS studies over 40 loci could be associated with an increased disease risk [20].

3.1.2 Neuropathophysiology

The two main pathological characteristics of PD are the specific degradation of the dopaminergic neurons in the SN*pc* and the occurrence of α-synuclein enriched neuronal protein inclusions, so-called Lewy bodies [21]. These two features independently also occur in other neurodegenerative diseases, however in combination they emerge specifically in PD.

Reduced dopamine levels in the basal ganglia are mainly responsible for the occurring motor dysfunctions. The nigrostriatal system, which is decisively involved in movement control, persists of the dopaminergic neurons in the SN*pc* that project to the dorsal striatum and liberate dopamine [22]. In PD selectively this midbrain population is degraded prominently. Literature suggests several major factors for their high vulnerability:

1. High oxidative stress due to pacemaker activity and dopamine as neurotransmitter
2. Highly branched and long axonal arbor, which is accompanied with high trafficking expenses
3. Impaired mitochondrial dynamics and function in disease state [23, 24].

However, PD is a multifactorial disease, and specifically the non-motor symptoms are provoked due to changes in other neurotransmitter systems like the cholinergic, serotonergic, glutamateric, noradrenergic or GABAergic system [25]. The disrupted biochemical interplay between the neuronal circuits accounts for the wide variety of disease symptoms.

3.1.3 Basal ganglia and neuronal circuits

In PD a progressive cellular degeneration in many brain regions occurs, however the most obviously affected cells are the dopaminergic neurons of the substantia nigra *pars compacta*, these in turn make up only one part of the cortico-basal ganglia-thalamocortical loop, which becomes disturbed due to their degeneration. In the next paragraph this complex signaling network will be elucidated in a simplified manner. Figure 1 depicts the basic model of the basal ganglia (BG) which are the interconnected subcortical nuclei [26].

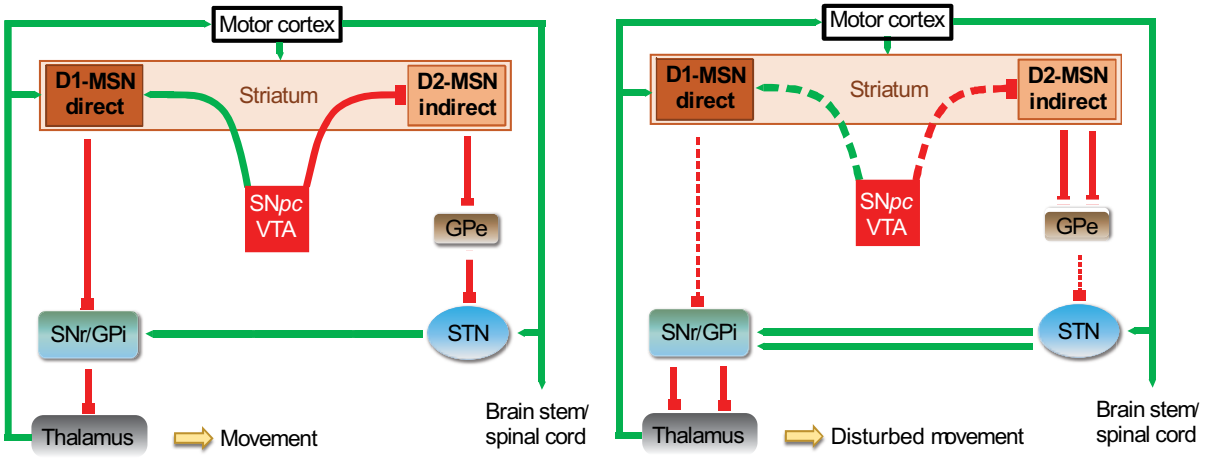

Figure 1: Schematic illustration of the basal ganglia circuity in normal and Parkinson´s disease state.

The striatum is the main input structure of the basal ganglia, receiving glutamatergic input from the cortex and the thalamus and dopaminergic input from the substantia nigra *pars compacta* and the ventral tegmental area. In Parkinson ´s disease state the dopaminergic input is disturbed, leading to an imbalance in the activity of the D1-, respectively D2-receptor positive medium spiny neurons. This imbalance between the striatonigral and striatopallidal pathway concludes in disturbed motor behavior. Abbreviation: D1 – dopamine D1 receptor; D2 – dopamine D2 receptor; MSN – medium spiny neuron; STN – subthalamic nucleus; SNr – substantia nigra reticulata; GPi – globus pallidus internus; GPe – globus pallidus externus; SN*pc* – substantia nigra *pars compacta*; VTA – ventral tegmental area.

A central input nucleus of the BG is the striatum, it receives massive excitatory glutamatergic input from the cortex and is densely innervated by dopaminergic projections. The main cell type (approximately 95%) represent GABAergic medium spiny neurons (MSN) which, based on dopamine receptor expression (D1 or D2), facilitate or suppress motor behavior by sending inhibitory projections to surrounding nuclei [27]. D1-MSNs (striatonigral) send projections directly to the globus pallidus internus (GPi) and the substantia nigra reticulata (SNr), the main output nucleus of the BG, and therefore it is called the direct pathway. The inhibition of the SNr/GPi disinhibits the thalamocortical projections, leading to the promotion of motor behavior. D2-MSNs act on the opposing, the indirect pathway, which ultimately leads to suppression of

motor behavior. D2-MSNs (striatopallidal) send their inhibitory projections to the globus pallidus externus (GPe), which leads to a disinhibition of the subthalamic nucleus (STN), and ultimately to an activation of the basal ganglia´s output nuclei and thus an inhibition of the thalamocortical circuitry. A central regulatory role within these network plays the SN*pc*, which activates, respectively inhibits, the D1- and D2-MSNs via their striatal dopaminergic projections [28]. However, this is a very simplified explanation of the complex BG networks, as also feedback loops, collateral branching and additional projections from other nuclei to the striatum exist and influence the BG output [27].

Additionally, other neurons reside in the striatum influencing its output signals, like cholinergic and GABAergic interneurons [26, 28]. Approximately 1% of striatal neurons are tonically active cholinergic interneurons (TAN), the residual 4% consist of GABAergic interneurons. This class of neurons is composed of mainly three specific subgroups, the fast-spiking parvalbumin-expressing interneurons (FSI), the low threshold spiking somatostatin/NPY-expressing interneurons (LTS), and the low threshold spiking calretinin-expressing interneurons (CRI) [29]. Despites the small amount of striatal interneurons, they exert the major cortico-basal ganglia information processing. Their function is controlled by excitatory cortical input, as well as cholinergic input from CHAT-expressing interneurons. In addition to the dopaminergic neurons, they are the main regulators of the GABAergic striatal output neurons (MSNs). Seemingly, due to the greater responsiveness of the interneuron to the cortical input, they are able to balance the asymmetric innervation onto MSNs from cortex and interneurons (10.000 cortical synapses vs. 4-27 FSI synapses onto MSNs), concluding in their major basal ganglia control function [30].

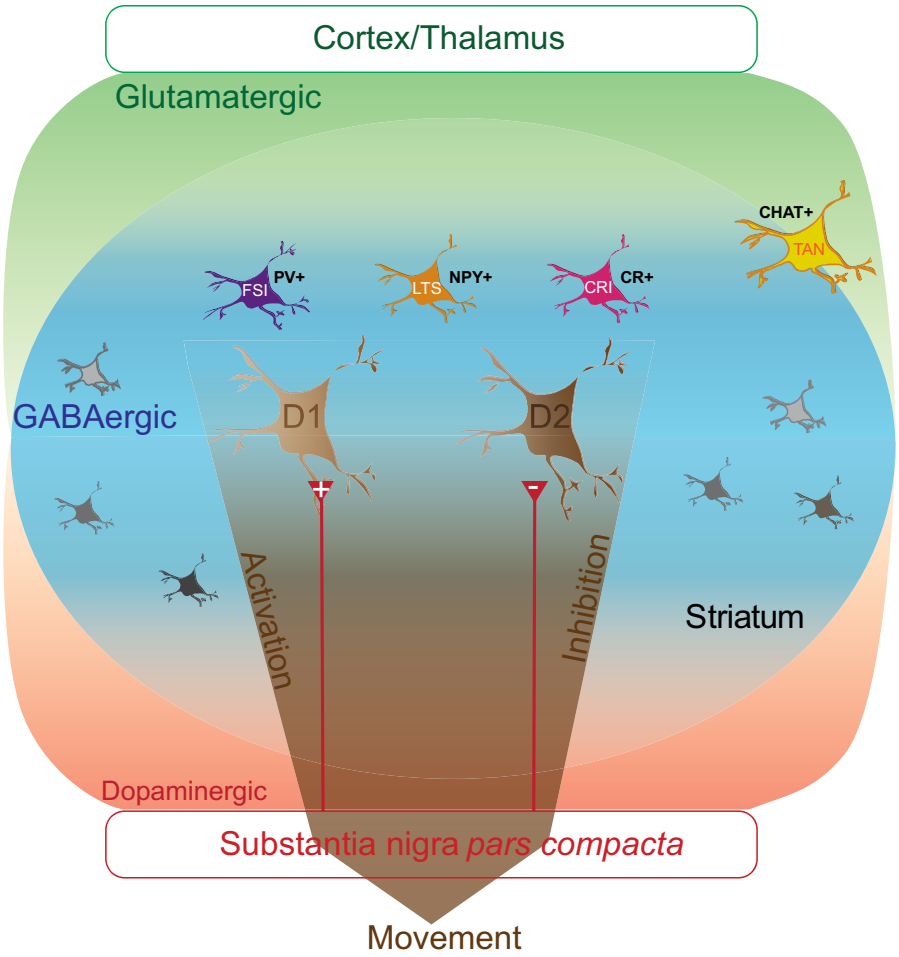

Figure 2: Heterogeneity and complexity of striatal neurons and neurotransmitter influence on basal ganglia function.

The striatum consists to 95% of GABAergic medium spiny neurons, either expressing D1 or D2 dopamine receptor, these cells send projections to basal ganglia output nuclei to control motor behavior. The residual neurons are mainly GABAergic interneurons, whereas three main subclasses exist: Fast spiking interneurons, low threshold interneurons and calretinin-positive interneurons, other marginally characterized subtypes shown in grey. The main neurotransmitter influences are the dopaminergic from the substantia nigra *pars compacta*, the glutamatergic from the cortex as well as thalamus and the internal, striatal GABAergic signaling. However, also cholinergic influence is described resulting from the approximately 1% of striatal tonically active cholinergic interneurons.
Abbreviation: D1 – dopamine D1 receptor; D2 – dopamine D2 receptor; MSN – medium spiny neuron; FSI – fast spiking interneurons; LTS – low threshold interneurons; CRI – calretinin-positive interneurons; TAN – tonically active interneurons.

It is widely accepted that in PD the main motor behavior phenotype results from the disbalance between the direct and indirect pathway [31]. In the disease pattern, it occurs that the indirect pathway is overrepresented, while the direct pathway is underrepresented, leading to a disrupted movement pattern with dyskinesia, freezing and bradykinesia.

3.1.4 Treatment options

For PD so far, no causal treatment option exists, however several approaches subsist to alleviate specifically the motor symptoms of the disease. The main therapeutic approach is disease intervention using drugs, like dopamine agonists, COMT inhibitors, MAO-B inhibitors or anticholinergic drugs, however the most prominent medication is the pharmacological dopamine replacement treatment with the dopamine precursor L-DOPA, which is able to cross the blood-brain-barrier, to compensate the depressed dopamine levels within the brain [32, 33]. Though often accompanied with this treatment are several serious side effects, like dyskinesia or movement freezing, which might occur due to the pulsatile dopamine stimulation of the hypersensitive, denervated striatum, leading to supersensitivity [33, 34]. Furthermore, there is a high inter-individual variability, with some patient even exhibiting drug resistance.

Other studies are performed to increase dopamine levels in the diseased striatum by the gene therapeutic delivery of enzymes necessary for dopamine production (aromatic amino acid decarboxylase, tyrosine hydroxylase and guanosine triphosphate cyclohydrolase) into non-degrading medium spiny neurons [34, 35]. Despite promising results, the high overexpression of these genes in the different neuronal context, might also lead to harmful side effect and further follow-up studies need to be performed.

Another strategy is the surgical intervention, whereas several possibilities exist. One approach is the inhibition of basal ganglia output nuclei due to the introduction of a lesion, often targeted is the GPi or the STN, or their decorrelation from the BG network using deep brain stimulation [28, 36, 37]. A second approach is cell transplantation therapy of fetal mesenchymal tissue or the injection of embryonic stem cell (ES) - or induced pluripotent stem cell (iPS) - derived dopaminergic neurons and neuronal precursors into the denervated striatum to increase the dopamine level in a more environmental controlled fashion, circumventing side effects induced by L-DOPA. However, not only the embryonic origin holds its ethical problematic, the ES and iPS cells also still harbor some totipotency, possibly leading to tumor formation [38, 39]. To circumvent this problematic, as well as difficulties meeting GMP requirements and logistical issues associated with extrinsic cell source, nowadays research focuses more and more in the direction of direct cellular reprogramming, whereas cells already residing within the brain are targeted and processed in a way they dedifferentiate and develop into a wanted cell type, for example in PD into dopaminergic neurons [40].

This PhD thesis focuses on the reprogramming of striatal astrocytes into dopaminergic neurons to ameliorate PD symptoms in a toxin-induced murine neurodegeneration model.

3.2 Direct cellular reprogramming

During development, uncommitted stem cells acquire specific transcriptional profiles and epigenetic landscapes. Traditionally this concept of early lineage commitment has been considered unidirectional and irreversible and was firstly described by C.H. Waddington in 1957 [41, 42]. However, since then a lot of discoveries have been made, unmasking this model as to simplified, at the latest since the discovery of induced pluripotent stem cells it is clear, that cells are much more plastic than expected [43].

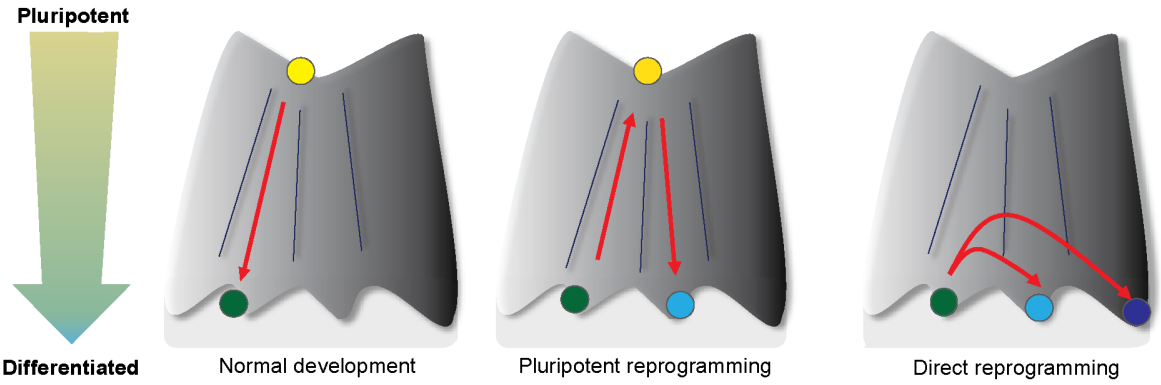

Figure 3: Waddington´s epigenetic landscape model.

During normal development an uncommitted cell achieves a specific transcriptional profile and epigenetic landscape, ultimately acquiring a terminated fate. During pluripotent reprogramming the program of the terminally differentiated cell is completely wiped out, reaching again a pluripotent state from which the cell can be programmed into another fate. In direct reprogramming the differentiated cell is forced to change their fate without reaching another level of pluripotency.

For the reprogramming of one cell type into another, specific cellular pathways and gene expression profiles of the target cell need to be activated. This can either be done by the treatment with small molecules and/or the enhanced expression of key transcription factors [44, 45].

The first direct transdifferentiation within one germlayer was shown in 1987, whereat fibroblasts were reprogrammed into myoblasts by the overexpression of *MyoD1*. However, it took until 2010 to show that reprogramming between different germ layers is also possible, by the overexpression of the three factors *Ascl1*, *Brn2* and *Myt1l* fibroblasts were reprogrammed into functional glutamatergic neurons [46]. The possibility to make new functional cells is of high interest in terms of degenerative diseases, specifically neurodegenerative diseases.

3.2.1 Direct neuronal reprogramming

Applying the knowledge of direct reprogramming onto the field of neurogenesis holds great promise, as replacing lost neurons in the brain, due to brain injury or neurodegenerative diseases, is still a big hurdle. One of the key publications showing that reprogramming of non-neuronal cells into neuronal cells within one germlayer is possible, was published in 2002 and showed that astrocytes can be reprogrammed into neurons by the overexpression of the neurogenic transcription factor (TF) *Pax6* [47]. Since then, many improvements on reprogramming efficiencies have been made by the expression of TFs, miRNAs or the treatment with small molecules that influence the developmental pathways of the cell, pushing it into a neurogenic fate. It became clear that several incidents have huge influence on the success of the reprogramming efficiency, like the cellular environment, the starter cell identity and the deployed transcription factors [48]. Still the molecular mechanisms underlying direct reprogramming are poorly understood. Nowadays an increasing amount of publications deal with metabolic changes occurring during the cellular switch, as cell death is a major issue during this process [49]. However, the major goal in terms of neuronal reprogramming is still finding the correct gene combination that needs to be activated to get a specific neuronal subtype. As cellular environment plays a main role in cell specification, studies done *in vitro* cannot directly be transferred *in vivo*, making the investigation laborious and difficult [45]. In this PhD thesis it is tried to solve this problem by the introduction of a new knock-in mouse model, which facilitates *in vivo* screening of gene combinations. By the knock-in of the aCRISPR system into a safe harbor locus, a facile activation of multiple endogenous genes is possible only by the introduction of short RNA sequences, so-called sgRNAs, a detailed description of the system will be elucidated in the following.

As this work focuses on Parkinson´s disease, in which specifically the meso-diencephalic dopaminergic neurons are degraded, it is tried to directly reprogram astrocytes into functional dopaminergic neurons *in situ* [50]. For this purpose specific transcription factor combinations were chosen to reprogram astrocytes into dopaminergic neurons, the individual transcription factors will be elucidated hereinafter.

- The Achaete-Scute Family bHLH Transcription Factor 1 (*Ascl1*) is known as pioneer transcription factor, able to bind to closed chromatin and actively open it up without the need of other factors [51]. Additionally, it is a well-studied proneuronal factor sufficient to solely reprogram murine fibroblasts into induced neurons [52, 53].
- The Neurogenic Differentiation 1 factor (*NeuroD1*) is a proneuronal bHLH transcription factor, which is primarily expressed in late nervous system development and important for terminal differentiation, maturation and survival [54]. It was shown to enable astrocyte to neuron conversion *in vivo* [55, 56].

- The Nuclear Receptor Related 1 (*Nr4a2*, also known as *Nurr1*) is a proneuronal transcription factor, specifically important for the differentiation, maturation and maintenance of midbrain dopaminergic neurons [57, 58]. Furthermore, it was associated with the inhibition of inflammatory signals and upregulation of survival genes, which might be pivotal during the reprogramming process, in which metabolic changes occur, accompanied with increased amounts of reactive oxygen species [49, 59].
- The LIM Homeobox Transcription Factor 1 Alpha (*Lmx1a*) is a homeodomain transcription factor necessary for the formation of the midbrain floor plate during embryogenesis and important for the specification of midbrain dopaminergic neurons [58, 60].

In one approach the transcription factor combination *Ascl1*, *Lmx1a* and *Nr4a2* was endogenously activated, as the forced expression of this lineage-specific factor combination was previously reported to reprogram fibroblasts into dopaminergic neurons *in vitro* and showed evidence to reprogram $NG2^+$ oligodendrocyte precursors into induced neurons *in vivo*, when overexpressed in the striatum of intact brains [61, 62]. In a second approach the transcription factor combination *Ascl1*, *Lmx1a* and *NeuroD1* was endogenously activated, together with the overexpression of the miRNA218. In the study from Rivetti di Val Cervo *et al.* this combination of lineage-defining factors was reported to directly reprogram astrocytes into functional dopaminergic neurons *in vitro,* as well as *in vivo* in the striata of lesioned brains [63]. In this work a detailed *in vivo* analysis was performed for both factor combinations, elucidating their reprogramming efficiencies when using the aCRISPR tool.

3.3 The CRISPR/Cas9 system and its applicability in genome engineering

3.3.1 Natural occuring – adaptive immune system of bacteria and archaea

The term CRISPR, standing for clustered regularly interspaced short palindromic repeats, was first introduced almost 20 years ago, in 2002 by Jansen *et. al* [64]. At this time CRISPR and its CRISPR associated genes (Cas) have been identified as repetitive structures, occurring in archaea and bacteria, but not in eukaryotes or viruses. However, it was not until 2005 that researchers elucidated the role of these sequences in the organism´s immune system. At the same time three groups claimed that CRISPR plays a role in the adaptive immune system of bacteria [65-67]. They found that the conserved palindromic CRISPR arrays were discontinued by variable sequences that show sequence homologies to viruses [68]. Upon base pairing of these variable sequences with viral DNA the Cas endonucleases are able to cleave the foreign DNA and protect the organisms from another infection. Nowadays several different types of the CRISPR system are known, which differ based on their Cas proteins [69]. The Cas enzymes are able to bind foreign DNA due to the homologous sequences, however another requirement has to be met, namely the protospacer adjacent motif (PAM). This short motif is

juxtaposed to the complementary region in the target DNA and differs between the different Cas enzymes [70]. One of the most studied system is the *Streptococcus pyogenes* Cas9 (SpCas9) associated type II system, which requires the relative simple PAM sequence 5´-NGG, facilitating a wide-area of binding sites within the genome, its mechanism is depicted in Figure 4. In the following, the mechanism of immunization and immunity shall be outlined shortly.

Immunization:

1. First infection of virus, invasion of viral DNA
2. The Cas proteins cleave the foreign DNA into spacers
3. Spacers are inserted into the CRISPR array

Immunity:

1. Second infection with virus, invasion of viral DNA
2. CRISPR array is transcribed, tracrRNA is complementary to repetitive sequences and hybridizes with CRISPR RNA transcript
3. Endogenous RNase III processes pre-crRNA strand into single tracrRNA – crRNA hybrids
4. The endonuclease SpCas9 forms a complex with the tracrRNA – crRNA hybrid
5. RNA guided SpCas9 nuclease recognizes foreign DNA due to complementarity to the crRNA sequence
6. Foreign DNA can be cleaved [71].

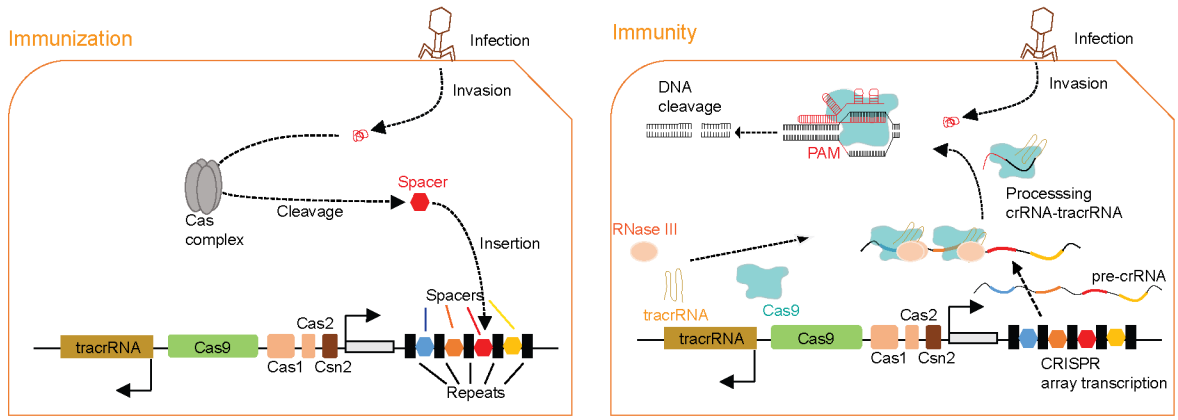

Figure 4: Type II CRISPR/Cas9 immune system.

Depicted on the left is the immunization process due to viral infection. Outlined on the right is the reaction occurring due to adapted immunity.

Abbreviation: CRISPR – Clustered regularly interspaced short palindromic repeats; Cas – CRISPR associated genes; tracr-RNA – trans-activating crRNA.

Having a system that is able to bind to double stranded DNA and introduce targeted double strand breaks opens a wide variety of possibilities in terms of genome engineering. This aspect shall be discussed in the following chapter.

3.3.2 Repurposing of the technology for genome engineering

Since whole genome sequencing became an affordable tool for scientists the prospects for personalized medicine increased drastically. Nowadays the genetic basis for many diseases is known and researchers are able to model these alterations via knock-in, knock-out or mutagenesis of genes *in vitro* and *in vivo* [72].

Besides CRISPR/Cas9 also other genome engineering technologies exist, like the zinc-finger nuclease (ZFN) and the transcription activator-like nuclease (TALEN). But although the CRISPR/Cas9 system is the most recently discovered one, it is the widely used one. Its discovery made genome engineering disposable for all research laboratories, as it is easy to handle and not cost intense. Another advantage over the other two approaches is the possibility to target multiple loci at once [73].

CRISPR/Cas9 consists of two components the SpCas9 endonuclease and the single-guide RNA (sgRNA, chimeric hydrid of tracrRNA – crRNA), which targets the nuclease to any locus in the genome with correct sequence homology and an adjacent PAM motif [74]. Today, more and more subtypes of CRISPR/Cas systems are discovered, having different endonucleases, PAM sequences and even different targets (RNA instead of DNA) [75, 76]. However, SpCas9 is still the gold standard, several modified versions exist making it a versatile tool. For example the nuclease-deficient Cas9 (dCas9) version can be targeted to genomic loci without introducing double strand breaks. By coupling it to specific effector proteins is can be applied for genetic labelling, to introduce epigenetic modifications or for transcriptional activation/repression of endogenous genes [77, 78].

In this work the CRISPR/dCas9 system is used for transcriptional activation.

3.3.3 Gene activation using CRISPR activation (aCRISPR)

In 2013 it was first shown that in mammalian cells endogenous genes can be activated by targeting the nuclease-deficient dCas9 coupled to activator domains to their promoter regions [79]. Since then many improvements have been made to increase the activation capacity. Here two activation systems shall be highlighted that will be applied in this study. The dCas9-VP64-p65-Rta (VPR) system, in which four times the activator domain of the *Herpes simplex virus* protein vmw65 (VP64), the transactivator domain of the p65 NF-κB subunit (p65) and the activator domain of the Regulator of transcription of the *Human herpesvirus 8* (Rta) are coupled to the C-terminal part of dCas9 (Figure 5 a) [80]. And the synergistic activator mediator (SAM) system, that is composed of specific sgRNAs, with loops extended by RNA aptamers to enable

binding by the MS2 bacteriophage coat protein. The MS2 is coupled to the activator domains of p65 and the transactivator domain of the human heat shock factor 1 (HSF1). Additionally, VP64 is fused to the C-terminus of the dCas9 (Figure 5 b) [81].

Both systems have been shown to lead to efficient endogenous activation in various species [82]. In this study both systems are used independently and in combination, as depicted in Figure 5 c.

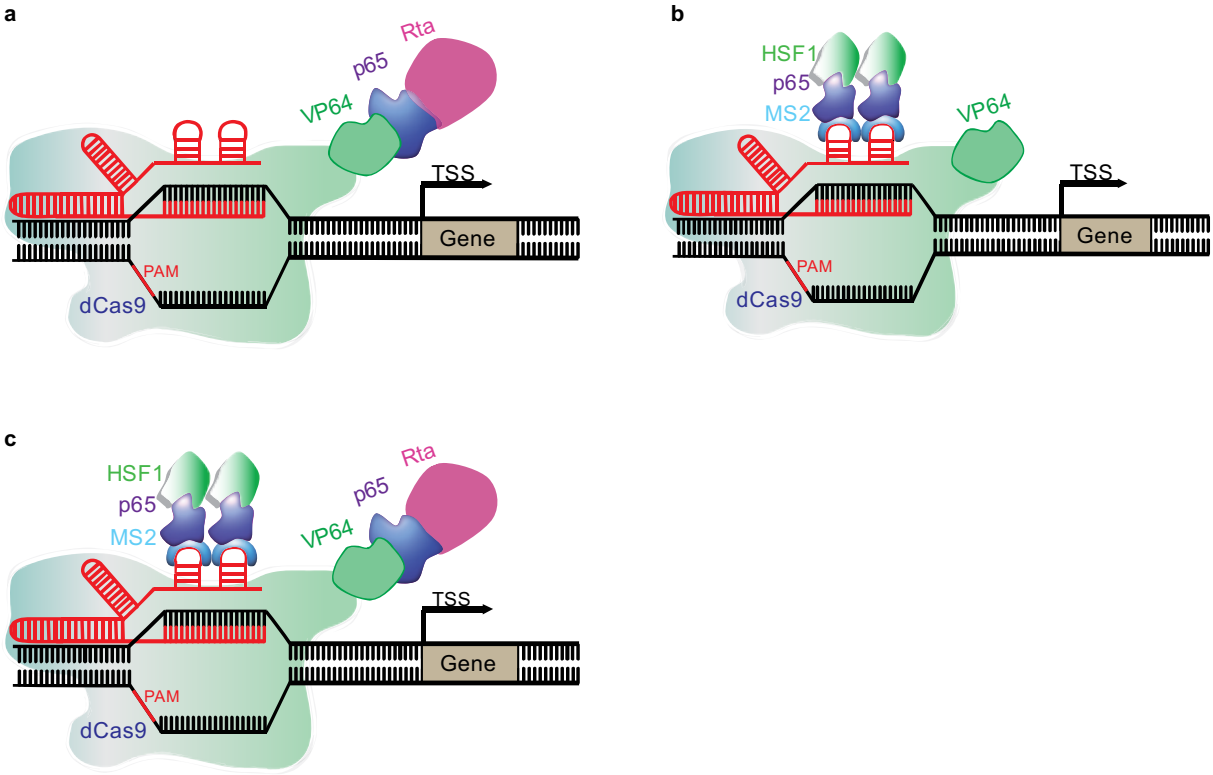

Figure 5: dCas9 transcriptional activator systems.

a, dCas9-VPR system, the activator domains of VP64 (4x VP16), p65 and Rta are C-terimally coupled to the dCas9. **b,** The synergistic activator mediator (SAM) system. sgRNA loops are extended by RNA aptamers to enable binding by the MS2 bacteriophage coat protein coupled to the activator domains of p65 and the heat-shock factor 1 (HSF1), the VP64 activator domain is C-terminally coupled to the dCas9. **c,** Combination of the VPR and the SAM system.

Abbreviations: dCas9 – dead (nuclease-deficient) Cas9; VP64 - 4x VP16 herpes simplex virus protein vmw65; p65 - p65 subunit of human NF-κB; Rta - Regulator of transcriptional activation; HSF1 – heat shock factor 1; MS2 - MS2 bacteriophage coat protein; PAM – protospacer adjacent motif; TSS – transcriptional start site.

4 Aim of the Thesis

Direct cellular reprogramming and cell replacement therapies are of specific interest for neurodegenerative diseases like Parkinson´s disease. So far no curative treatments exist, the replacement of lost neurons and the accompanied restoration of the neuronal circuits may be possible with this approach. As in PD specifically the dopaminergic neurons of the SN*pc* are degraded, the aim of the thesis was to develop a new strategy to improve the reprogramming of astrocytes into dopaminergic neurons *in vivo*, to restore neuronal circuits. Several studies are published using the overexpression of specific transcription factor combinations to directly reprogram cells into dopaminergic neurons, however so far none of them showed satisfying efficiencies. Furthermore, most of the studies were done *in vitro*, but as the microenvironment plays an important role for the reprogramming efficiency these results are hardly comparable to *in vivo* studies.

In this thesis an aCRISPR based system, enabling multiplexed activation of endogenous genes *in vivo* was established. A knock-in mouse line, as well as an AAV-based split-dCas9 activator system was generated. Both systems were used to address the reprogramming potential of different transcription factor combinations *in vivo*, in terms of induced neuron number, functionality and phenotypical output. With this animal study, it is intended to gain more insights into the complex genetic interplays that are necessary for efficient, cell-type specific reprogramming. Additionally, it is tried to elucidate the effects of reprogrammed neurons onto neuronal circuits in parkinsonian state.

5 Results

5.1 Rosa26 knock-in dCas9 Activator Mouse (*dCAM*)

5.1.1 Generation of the conditional Rosa26 dCas9-Activator Mouse (*dCAM*) and the *in vitro* validation

To facilitate the comprehensive and efficient application of CRISPR/Cas9 activation (aCRISPR) *in vivo*, a dCas9-activator knock-in mouse line in the safe harbor locus *Gt(ROSA)26Sor* was generated, combining the two previously described activation systems dCas9-VPR and SAM (synergistic activation mediator). Conditionally controlled by a *LoxP*-puro-stop-*LoxP* cassette, the ubiquitous CAG promoter is driving the expression of the *FRT*-flanked SAM components (aptamere-fused activator domains of p65 and HSF1) separated via a P2A element from dCas9, which is C-terminally coupled to the transcriptional activator domains VP64, p65 and Rta (VPR). Flanking the SAM activator with *FRT* sides enables the removal of this part of the double activator system, thus generating a simple dCas9-VPR knock-in line [80, 81]. To revise appropriate expression of the inducible system and to verify the correct cleavage of the P2A sequence between the dCas9-VPR and the SAM activator, a western blot analysis was performed on protein lysates from Neuro2A cells (Figure 6 a, b). The *Rosa26* homology arms are extending 1 kb upstream and 4 kb downstream from the integration site within the first intron [83]. The integration was confirmed via southern blot, the F1 generation showed normal Mendelian heritance (Figure 6 c, d). To ensure functionality *in vivo* the Rosa26-dCas9-activator mouse *(dCAM)* was crossed with the *Gfap-Cre* (*B6.Cg-Tg(Gfap-Cre)77.6Mvs/2J*) line, resulting in astrocyte-specific cassette expression. Western blot analysis from primary astrocyte lysates of these animals confirmed Cre-dependent astrocytic dCas9 expression (Figure 6 e). For further characterization, Christoph Breunig tested primary fibroblasts of the *dCAM* line, using a GFP reporter system. *GFP* under a minimal CMV promoter, together with a sgRNA targeting the promoter were transfected. Due to dCas9-activator binding, *GFP* expression was facilitated, which could be confirmed in a FACS analysis (Figure 6 f). No *GFP* expression could be recognized as long as the puro-stop cassette was introduced, confirming tight control of cassette expression.

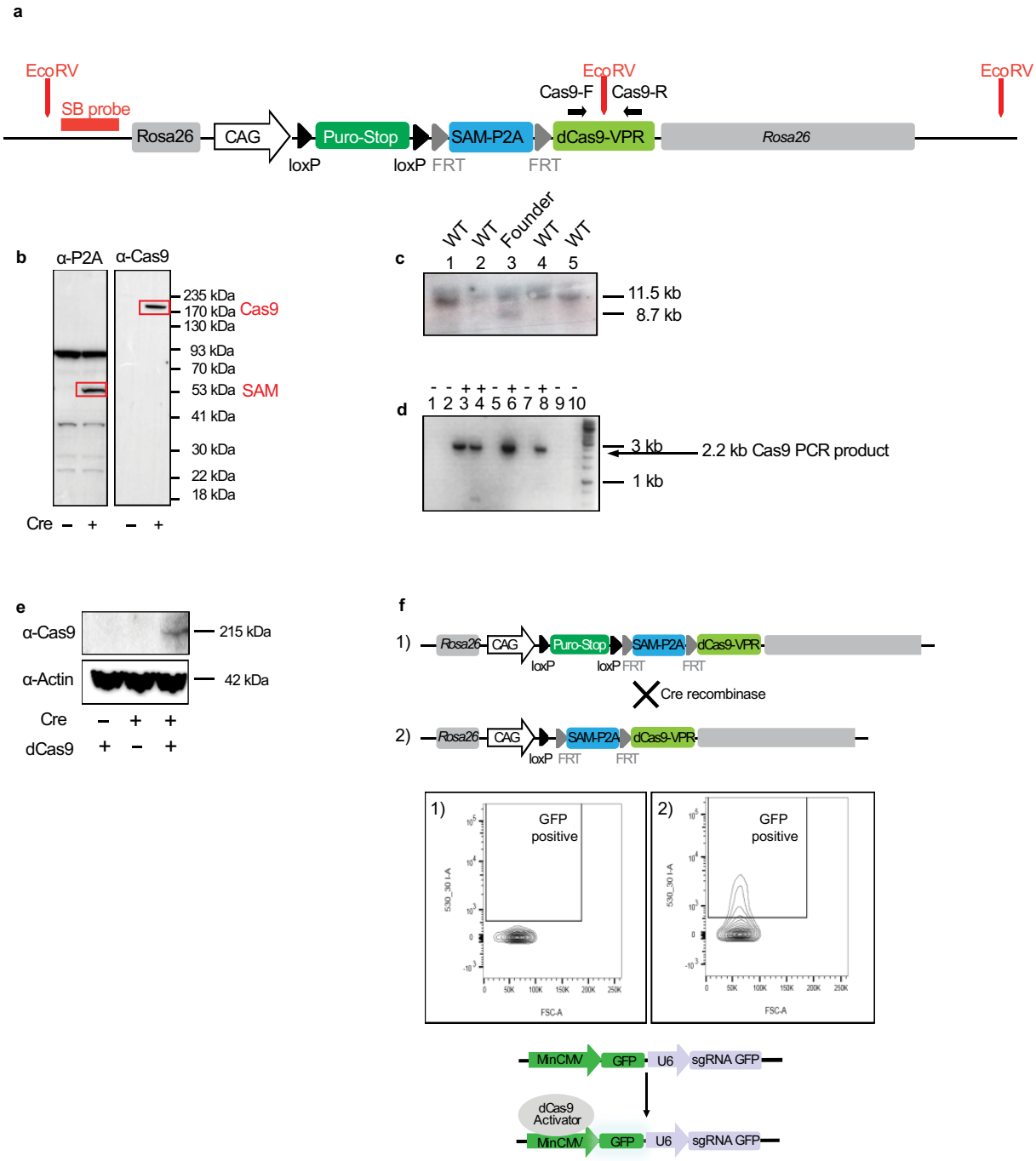

Figure 6: Design and evaluation of the *dCAM* mouse line.

a, Rosa26 knock-in design, long homology arms are used 5´arm 1 kb and 3´arm 4 kb long. **b,** Western blot. Left blot –Test of the P2A sequence for appropriate cleavage. Antibody binds 5´part of the P2A, SAM-5´-P2A runs at 55 kDa. No fusion products were observable. Right blot – Test of the puro-stop-cassette. Without Cre no Cas9 protein visible. **c,** Southern blot analysis of the founder animals. EcoRV was used for gDNA digest, as seen in **a**, with knock-in two bands occur at 11.5 kb – wild type band and at 8.7 kb – knock-in band. Mouse number 3 showed double band and was used for further breeding. **d,** Genotyping PCR of F1 generation using Cas9 F and Cas9 R primers, 4 out of 10 animals showed knock-in. **e,** Western blot from primary astrocytes of the *dCAM x Gfap-Cre* line. Cas9 was only detected when

Cre was expressed. **f,** Test of primary fibroblasts of the *dCAM* line using a minimal-CMV-GFP reporter. GFP can only be expressed when dCas9-activators binds to the minimal CMV promoter to enhance the transcription. 1) Fibroblasts containing the puro-stop-cassette were transfected with the reporter, in the FACS almost no GFP^+ cells could be counted. 2) Fibroblasts were transduced with a lenti-Cre virus to remove the puro-stop-cassette and transfected with the reporter, in the FACS a rise in GFP^+ cells could be recognized.
Abbreviations: Puro – puromycin resistance; SAM - synergistic activation mediator, MS2 - MS2 bacteriophage coat protein, p65 - p65 subunit of human NF-κB, HSF1 - Heat shock factor 1; P2A – 2A self-cleaving peptide; dCas9 - deadCas9 (nuclease-deficient); VPR: VP64 - 4x VP16 herpes simplex virus protein vmw65, p65, Rta - Regulator of transcriptional activation; CAG - CMV early enhancer/chicken β actin promoter.

For *in vivo* gene activation, the delivery of target-specific sgRNAs, including stem loops for SAM-aptamere binding, is required. Gold standard for the delivery are adeno-associated viruses (AAVs), as they exhibit low immunogenicity and ensure high and sustained expression [84, 85]. Their regular packaging limit of about 4.7 kb is sufficient to deliver up to six sgRNAs together with individual Pol III promoters and a FLExed-*GFP* marker gene by one AAV [86]. If more sgRNAs shall be delivered, two AAVs can be used together with a split-FLExed-*GFP* (Figure 7) [87].

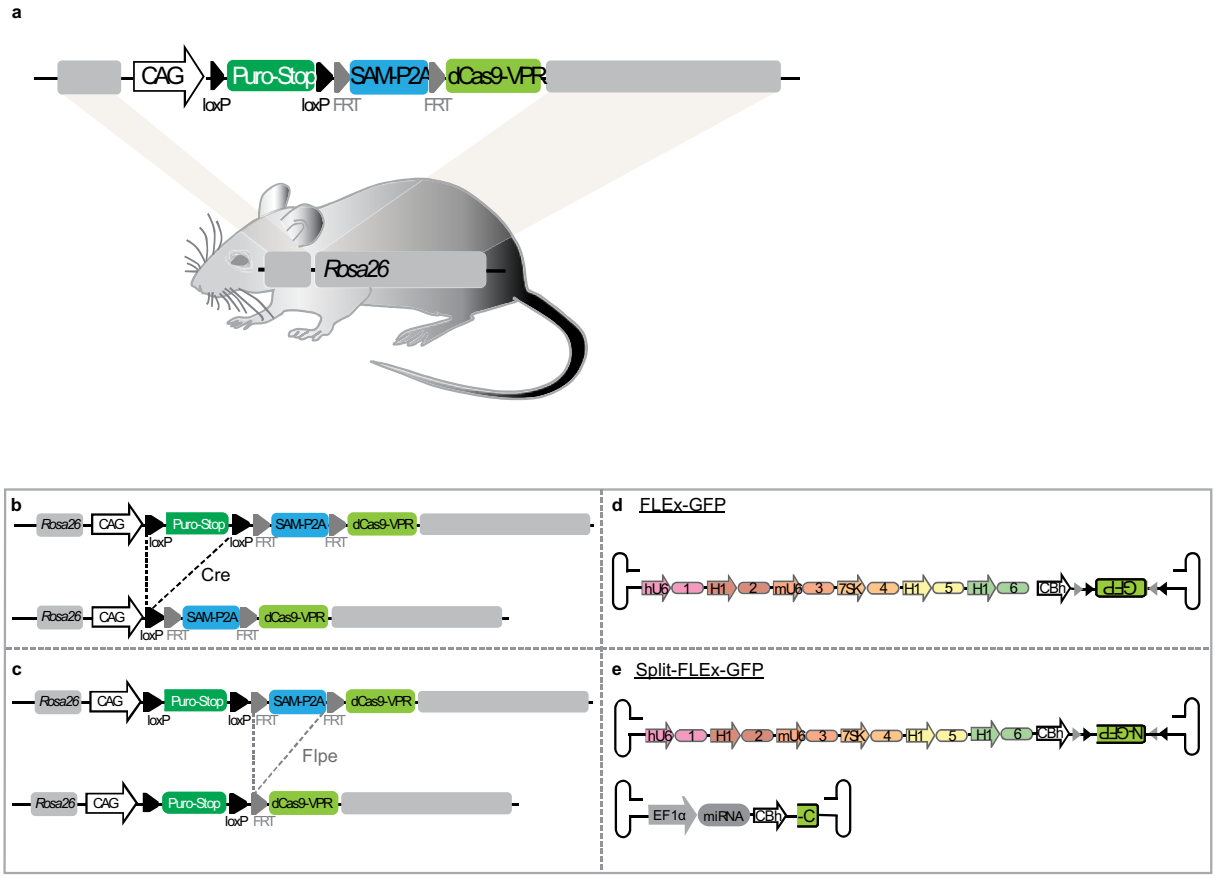

Figure 7: Rosa26 knock-in dCas9 Activator Mouse (*dCAM)*

a, Knock-in of a conditional dCas9-VPR-P2A-SAM expression cassette into the *Gt(ROSA)26Sor* locus enables flexible multiplexed endogenous gene activation *in vitro* and *in vivo.* Expression cassette is composed of *LoxP*-puro-stop-*LoxP* followed by the SAM activator (flanked by *FRT* sites), a P2A sequence and the dCas9-VPR. Expression is driven by the strong, ubiquitous CAG promoter. **b,** The *LoxP*-flanked puro-stop cassette ensures highly specific knock-in expression. **c,** Variable activation levels can be achieved, as the SAM activator is flanked by *FRT* sites and can be removed. **d,** For *in vivo* activation an AAV containing 6 sgRNAs and a reporter gene can be applied. **e,** If more than 6 sgRNAs shall be used for *in vivo* activation two AAVs containing 12 sgRNAs or 6 sgRNAs and a miRNA expression cassette can be applied with a split-reporter gene. AAVs contain sgRNAs, expression is driven by the different Pol III promoters (H1, hU6, mU6 and 7SK), and the marker gene FLEx-*GFP*, respectively split-FLEx-*GFP*, is expressed by the CBh promoter and also delivered by AAVs.
Abbreviations: Puro – puromycin resistance; SAM - synergistic activation mediator: MS2 - MS2 bacteriophage coat protein, p65 - p65 subunit of human NF-κB, HSF1 - Heat shock factor 1; P2A – 2A self-cleaving peptide; dCas9- deadCas9 (nuclease-deficient), VPR: VP64 - 4x VP16 herpes simplex virus protein vmw65, p65, Rta - Regulator of transcriptional activation; CAG - CMV early enhancer/chicken β actin promoter; CBh - chicken ß–actin hybrid promoter.

For endogenous gene activation, different conditions, including various distances to the transcriptional start side and using multiple sgRNAs were tested and best gene induction was

obtained using two sgRNAs, targeting sequences 200 bp prior to the transcriptional start site, as described by Konermann *et al.* (Figure 8) [81].

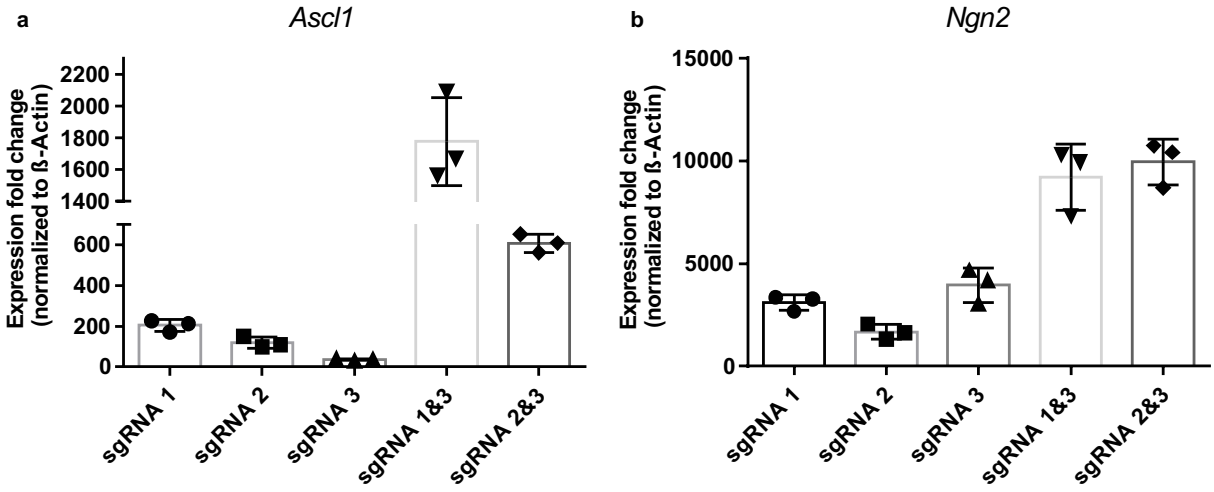

Figure 8: Comparison single and multiple sgRNAs at different genomic loci (within the region -200 bp to TSS) for their endogenous gene activation potential.

a, Endogenous activation of *Ascl1* (sgRNA1 203 ± 29, sgRNA2 119 ± 28, sgRNA3 35 ± 5, sgRNA1&3 1777 ± 280, sgRNA2&3 607 ± 45). **b,** Endogenous activation of *Ngn2* (sgRNA1 3108 ± 376, sgRNA2 1671 ± 366, sgRNA3 3952 ± 835, sgRNA1&3 9206 ± 1630, sgRNA2&3 9944 ± 1097). Experiments were performed in Neuro2A cells. Activation levels are depicted as fold change between cells transfected with and without sgRNAs. All levels were normalized to β-Actin.
Error bars represent mean ± SD.

Due to the viral delivery of the sgRNAs the activation of the endogenous genes can be timed exactly. Having three levels to control gene activation, namely activation level, cell-type specificity and time, makes this transgenic model a valuable, universal tool to induce expression of multiple endogenous genes to study complex processes like cellular reprogramming *in vivo*.

5.1.2 Multiplexed gene activation in primary astrocyte cultures

One of the main advantages of the *dCAM* system over the traditional transgene overexpression approach is the ease of multiplexed activation of endogenous genes by small sgRNAs. This study focused on the usage of the system to reprogram striatal astrocytes into induced neurons. As proof-of-principle, Benedict Rauser, a former PhD student of our laboratory, reprogrammed astrocytes into induced neurons, using the aCRISPR (activation-CRISPR/Cas9 – dCas9 coupled to activators) system. He lentivirally transduced primary astrocytes with the system components and sgRNAs to active endogenous *Ascl1,* a bHLH transcription factor known to reprogram fibroblasts into neurons [46]. As depicted in Figure 9,

he was able to reprogram astrocytes into MAP2$^+$ neurons (dsRed 1.6 ± 0.8% vs. aCRISPR/Cas9 15.0 ± 2.0%).

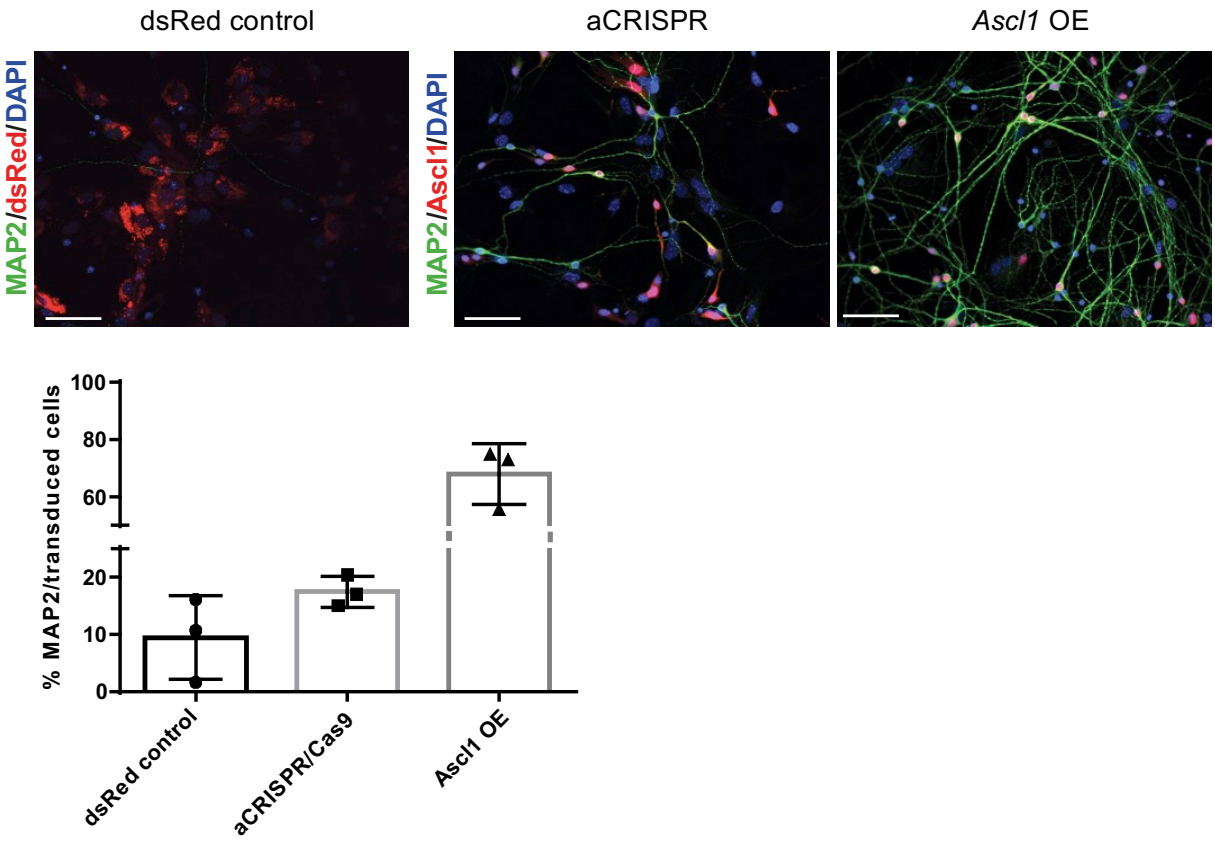

Figure 9: Successful conversion of astrocytes into induced neurons utilizing the aCRISPR/Cas9 system delivered by lentiviral transduction.

Immunocytochemistry analysis of reprogrammed cells 16 days after transduction with aCRISPR components revealed successful reprogramming of astrocytes into neurons. Quantification of MAP2$^+$ neurons per transduced cells. dsRed control showed 1.6 ± 0.8% MAP2$^+$/transduced cells indicating the basal fraction of neurons transduced by viruses. The aCRISPR showed an increase in MAP2$^+$/transduced cells to 15.0 ± 2.0% indicating successful conversion of astrocytes into neurons. The overexpression condition of *Ascl1* exhibited 75.0 ± 1.4% MAP2$^+$/transduced cells. Three independent experiments were performed. Data from representative experiment is shown. Error bars represent mean ± SD. Scale bars indicate 50 µm.
Abbreviations: aCRISPR – CRISPR activation system; OE – overexpression.

To test for multiplexed gene activation two transcription factor combinations were activated, known to convert non-neuronal cells into induced neurons *in vitro* and *in vivo*. The first combination *Ascl1*, *Lmx1a* and *Nr4a2* (*ALN*) was shown to reprogram mouse and human fibroblast into induced dopaminergic neurons *in vitro*, and could be confirmed to reprogram NG2$^+$ oligodendrocyte precursors into induced neurons *in vivo* [61, 62]. The second

combination *Ascl1*, *Lmx1a*, *NeuroD1* and miRNA218 *(ALNe-218)* showed *in vitro* and *in vivo* potential to reprogram mouse and human astrocytes into induced dopaminergic neurons [63]. As proof-of-principle of the transgenic system a multiplexed gene activation of these combinations was attempted in primary astrocytic cultures of the *dCAM x Gfap-Cre* line. As depicted in Figure 10 robust endogenous gene activation could be achieved for both combinations, paving the way for further *in vivo* experiments.

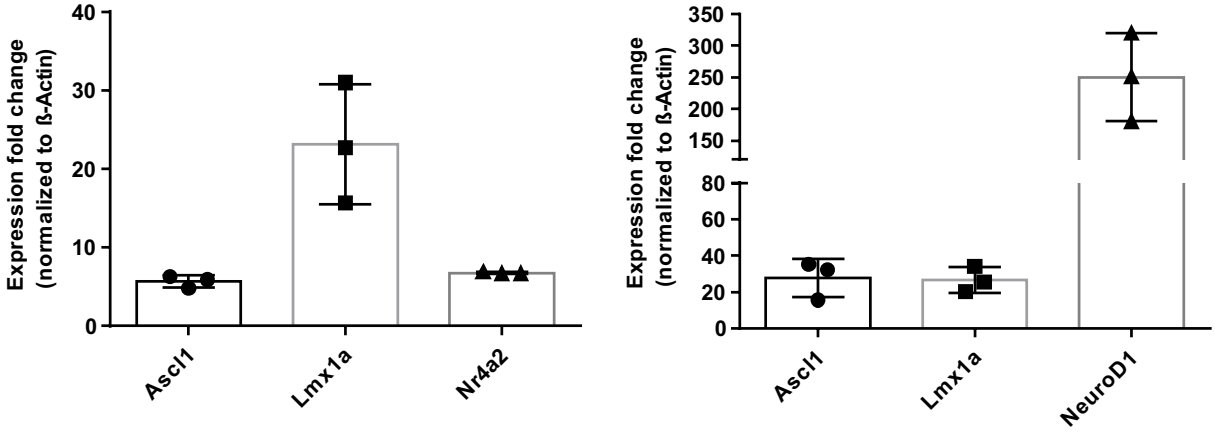

Figure 10: Evaluation of *dCAM* x *Gfap-Cre* primary astrocytes for their activation capacity.

Multiplexed activation of *Ascl1*, *Lmx1a*, *Nr4a2* (*Ascl1* 6 ± 1, *Lmx1a* 23 ± 8, *Nr4a2* 7 ± 0) and of *Ascl1*, *Lmx1a*, *NeuroD1* (*Ascl1* 28 ± 11, *Lmx1a* 27 ± 7, *NeuroD1* 250 ± 70) in primary astrocytic cultures. n=2-3, one representative run is shown, additional data in Supplementary Figure 1. Activation levels are depicted as fold change between cells transfected with and without sgRNAs. All levels were normalized to β-Actin. Error bars represent mean ± SD between technical replicates.

5.1.3 Dopamine denervation using a toxin-induced Parkinson´s disease model and *in vivo* experimental setup

A unilateral 6-hydroxydopamine (6-OHDA) PD model was used to degenerate the dopaminergic neurons in the ipsilateral SN*pc*. The neurotoxin was unilateral injected into the medium forebrain bundle (MFB) (coordinates in mm relative to bregma: AP -1.2, ML +1, DV -4.9) of 12-16 weeks old mice, resulting in an efficient and reproducible lesion of the dopaminergic neurons primarily in the ipsilateral SN*pc* and their projections into the striatum [88]. The injury promotes reactive gliosis in the striatum, increasing the number of reprogrammable astrocytes, while avoiding extensive scar formation [56, 89, 90]. The efficiency of the lesion was assessed 6 and 14 days after the induction of the lesion by tyrosine hydroxylase (TH) staining, and striatal reactive gliosis was evaluated by staining for the astrocytic marker GFAP. A strong upregulation of the GFAP marker could be observed already

6 days after the toxin injection in the ipsilateral striatum, this level remained stable, with a slight decreasing trend over the time period of 14 days until the AAV was injected (Figure 11).

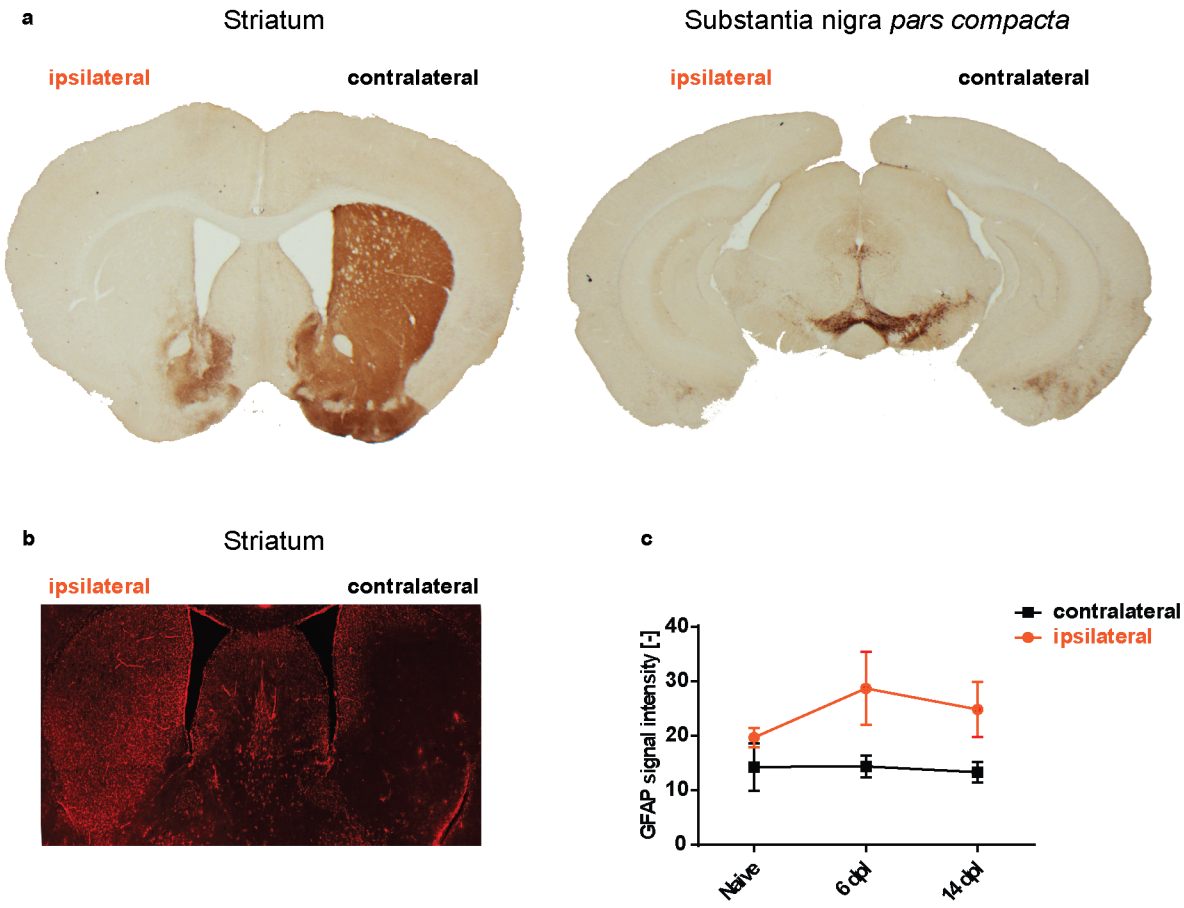

Figure 11: Evaluation of 6-OHDA induced lesion.

a, b, Stainings of an animal 14 days after the 6-OHDA injection into the medium forebrain bundle. **a,** Staining of dopaminergic lesion using the marker tyrosine hydroxylase (TH). **b,** Staining with the astrocytic marker GFAP to assess the reactive gliosis. **c,** Reactive gliosis was assessed via the signal intensity of GFAP stained striata. Naïve, 6 days post lesion (dpl) and 14 dpl animals were analyzed. Per condition data was collected from two animals, from each animal ten images were analyzed, randomly taken in striatal regions. Ipsilateral: Naïve 19.7 ± 1.8, 6 dpl 28.7 ± 6.7, 14 dpl 24.9 ± 6.0; contralateral: Naïve 14.3 ± 4.4, 6 dpl 14.4 ± 2.0, 14 dpl 13.3 ± 1.9.

In conclusion, the 6-OHDA injection led to a strong unilateral depletion of TH^+ somata in the SN*pc* and their dopaminergic projections into the striatum [91]. At the same time, an upregulation of GFAP was observed within the striatum, indicating reactive astrogliosis, rendering the astrocytes into a more plastic state [48, 92].

The *dCAM* line was crossed with a transgenic *Gfap-Cre* line, leading to astrocyte-specific aCRISPR expression [88]. Due to the low immunogenicity, the sgRNAs and the reporter gene *GFP* were delivered via AAVs [84, 85]. AAVs were injected into the dorsal striatum (coordinates

in mm relative to bregma: AP +1, ML +2.1, DV -3.5). To ensure specific reporter gene expression, the so-called FLEx-system (Cre-ON) was used, in which the *GFP* is inverted and flanked by two different *LoxP* sites and solely inverted and expressed in Cre-expressing cells [62]. To address reprogramming efficiencies two time points, 5 weeks and 13 weeks post injection of AAVs (wpi), were examined. Additionally, to the immunohistochemical analysis, neuronal functionality and integrity was addressed by measuring the electrophysiological properties of the reprogrammed neurons and the motor behavior of the mice (Figure 12).

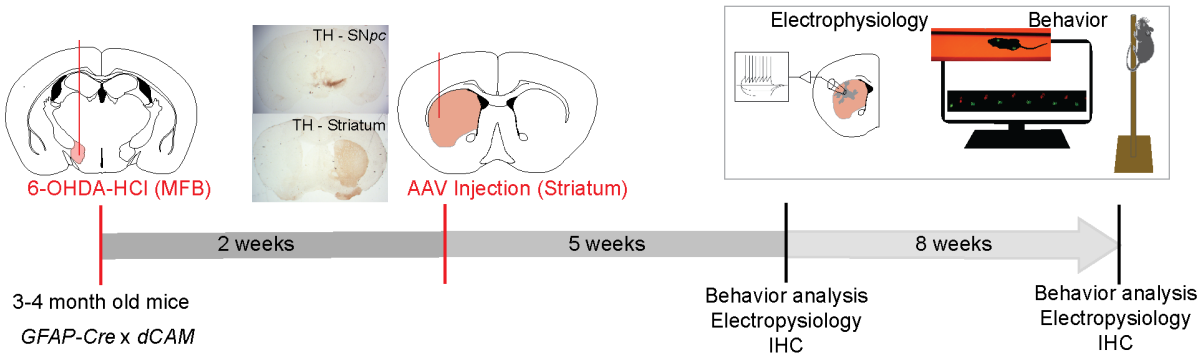

Figure 12: Experimental *in vivo* workflow.

A toxin-induced neurodegeneration model (6-OHDA) was used to induce Parkinson´s disease. Two weeks after the unilateral toxin injection into the medium forebrain bundle most dopaminergic neurons in the substantia nigra *pars compacta* were degraded and the striatal projections disappeared, as shown by tyrosine hydroxylase (TH) staining. The AAV was injected into the dorsal striatum, after a five weeks period the first analysis was performed. After another eight weeks period animals again underwent behavior tests, functionality of neurons was assessed via electrophysiological measurements and brains were analyzed by immunohistochemistry.

5.1.4 Endogenous activation of *ALN* and *ALNe-218* is sufficient to reprogram astrocytes into induced neurons

In the double-transgenic mouse line *dCAM x Gfap-Cre* the expression of the aCRISPR components was endogenously activated in astrocytes. Different sets of sgRNAs targeting the promotor regions of the transcription factors *Ascl1*, *Lmx1a*, *Nr4a2* (*ALN*) and *Ascl1*, *Lmx1a*, *NeuroD1* and ectopically expressing miRNA218 (*ALNe-218*) and mock FLEx-GFP (GFP-control) respectively, were delivered via stereotactic injection of 1 µl high titer AAV2/5 (3 x 10^{14} to 5 x 10^{15} GC/ml) into the dorsal striatum [61-63]. The AAV-FLEx-*GFP* was used to express the *GFP* marker specifically in astrocytes. No significant difference in the number of infected GFP^+ cells could be observed between the different conditions (*GFP*, *ALN* and *ALNe-218*) (Supplementary Figure 2). Injection of AAV-FLEx-*GFP* two weeks after the 6-OHDA lesion resulted in 97.13 ± 0.45% of astrocytes, that were GFP positive indicated by *Gfap* expression

(Figure 13 b). Accordingly, less than 4% (3.9 ± 0.53%) were positive for the neuronal marker NeuN (RBFOX3, Figure 13 d). Next, we determined the efficiency of reprogramming achieved by different sgRNA combinations. At five weeks post AAV injection both transcription factor combinations (*ALN* and *ALNe-218*) still showed a high proportion of $GFAP^+/GFP^+$ double positive cells (Figure 13 a, b), with an increased percentage of $NeuN^+/GFP^+$ cells to 14.77 ± 3.09% for *ALN* and 15.67 ± 0.96% for *ALNe-218* (Figure 13 c, d). After additional 8 weeks (13 wpi), the amount of $GFAP^+/GFP^+$ cells significantly decreased to 66.57 ± 2.35% for *ALN* and 78.45 ± 5.63% for *ALNe-218* (Figure 13 e, f). Inversely, the proportion of $NeuN^+$ neurons amongst GFP^+ transduced cells further increased to 17.87 ± 0.50% in striata treated with the *ALN*-inducing sgRNA combination. Interestingly, such marked increase was not observed for the *ALNe-218* sgRNAs ($NeuN^+/GFP^+$ 13.17 ± 1.36%) (Figure 13 g, h). Accordingly, the *ALN* combination is more efficient to induce neuronal conversion of striatal astrocytes after 6-OHDA lesion.

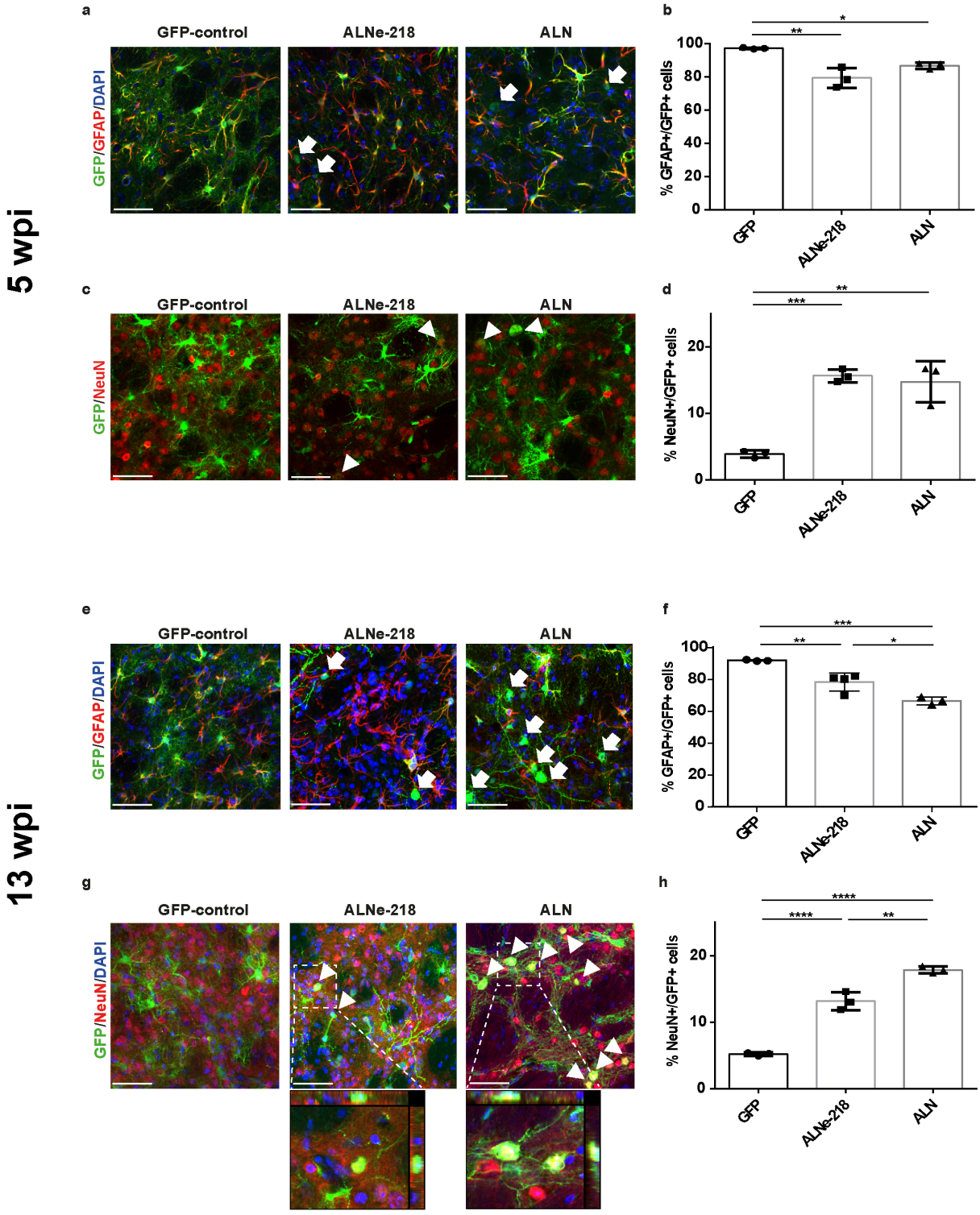

Figure 13: Rosa26 knock-in dCas9 Activator Mouse *(dCAM)* based reprogramming of astrocytes.

a, Photomicrographs showing GFP$^+$/GFAP$^+$ cells 5 wpi. Arrows indicating GFP$^+$/GFAP$^-$ cells. **b,** Quantification GFAP$^+$/GFP$^+$ cells. *GFP* 97.13 ± 0.45%, *ALNe-218* 79.33 ± 6.05%, and *ALN* 86.70 ± 1.90%. *GFP* vs. *ALNe-218* P=0.0025, *GFP* vs. *ALN* P=0.03. Multiple comparison ANOVA F(2,6)=17.78. **c,** Photomicrographs showing GFP$^+$/NeuN$^+$ neurons 5 wpi. Arrow heads indicating GFP$^+$/NeuN$^+$ cells. **d,** Quantification NeuN$^+$/GFP$^+$ cells. *GFP* 3.9 ± 0.53%, *ALNe-218* 15.67 ± 0.96% and *ALN* 14.77 ±

3.09%. *GFP* vs. *ALNe-218* P=0.0007, *GFP* vs. *ALN* P=0.001. Multiple comparison ANOVA F(2,6)=35-85. **e,** Photomicrographs showing $GFP^+/GFAP^+$ cells 13 wpi. Arrows indicating $GFP^+/GFAP^-$ cells. **f,** Quantification of $GFAP^+/GFP^+$ cells. *GFP* 92.3 ± 0.42%, *ALNe-218* 78.45 ± 5.63% and *ALN* 66.57 ± 2.35%. *GFP* vs. *ALNe-218* P=0.0064, *GFP* vs. *ALN* P=0.0002 and *ALN* vs. *ALNe-218* P=0.0127. Multiple comparison ANOVA F(2,7)=32.06. **g,** Photomicrographs showing $GFP^+/NeuN^+$ neurons 13 wpi. Arrow heads indicating $GFP^+/NeuN^+$ cells. **h,** Quantification of $NeuN^+/GFP^+$ cells. *GFP* 5.2 ± 0.26%, *ALNe-218* 13.17 ± 1.36% and *ALN* 17.87 ± 0.50%. *GFP* vs. *ALNe-218* P<0.0001, *GFP* vs. *ALN* P<0.0001 and *ALN* vs. *ALNe-218* P=0.0012. Multiple comparison ANOVA F(2,6)=170.3.
Scale bars indicate 50 µm.
Tukey's multiple comparisons test * P<0.05, **P<0.01, ***P<0.001, ****P<0.0001.
Error bars represent mean ± SD.

With the new knock-in mouse model cellular identity could efficiently be modulated *in vivo*. This transgenic line offers great value for basic research, in conditions when multiplexed gene activation is required, as the unsteadiness of viral coinfections can be circumvented, leading to controllable, uniform and reliable results.
As seen, aCRISPR operates as a potent tool to manipulate cellular status *in vivo*. To make it applicable to a broader scientific field, for example in other model organisms, like non-human primates or ultimately applicable for gene therapeutic usage, the system was adapted by delivering the complete activation machinery via AAVs.

5.2 AAV-based split-dCas9-Activator System (*AAV-dCAS*)

5.2.1 Design of the AAV-based split-dCas9-Activator System (*AAV-dCAS*)

AAVs are used as vehicles for gene therapy, as they exhibit low immunogenicity and stay as episomes, without genomic integration, within the infected cells [93]. One limitation of the AAV-based delivery system is its low packaging capacity of approximately 4.7 kb, which makes it unsuitable to package large constructs such as the aCRISPR system for gene activation.
To circumvent this shortcoming a split-dCas9 system was applied, in which the N-terminal, respectively the C-terminal part of the dCas9-VP64 was fused to the corresponding split-intein moiety (AAV-$N^{aa1-573}$-dCas9-N-intein and AAV-$C^{aa574-1368}$-dCas9-VP64-C-intein) [94]. Upon co-expression, intein-mediated trans-splicing leads to a reconstitution of the full-length dCas9 protein (Figure 14 a). Ultimately, the split-dCas9-VP64 (4x VP16, herpes simplex virus protein vmw65), together with the SAM activator, the reporter gene *GFP* and 10 sgRNAs can be

packaged onto four AAVs, whereby up to ten genes can be activated simultaneously *in vitro* and *in vivo* (Figure 14 b).

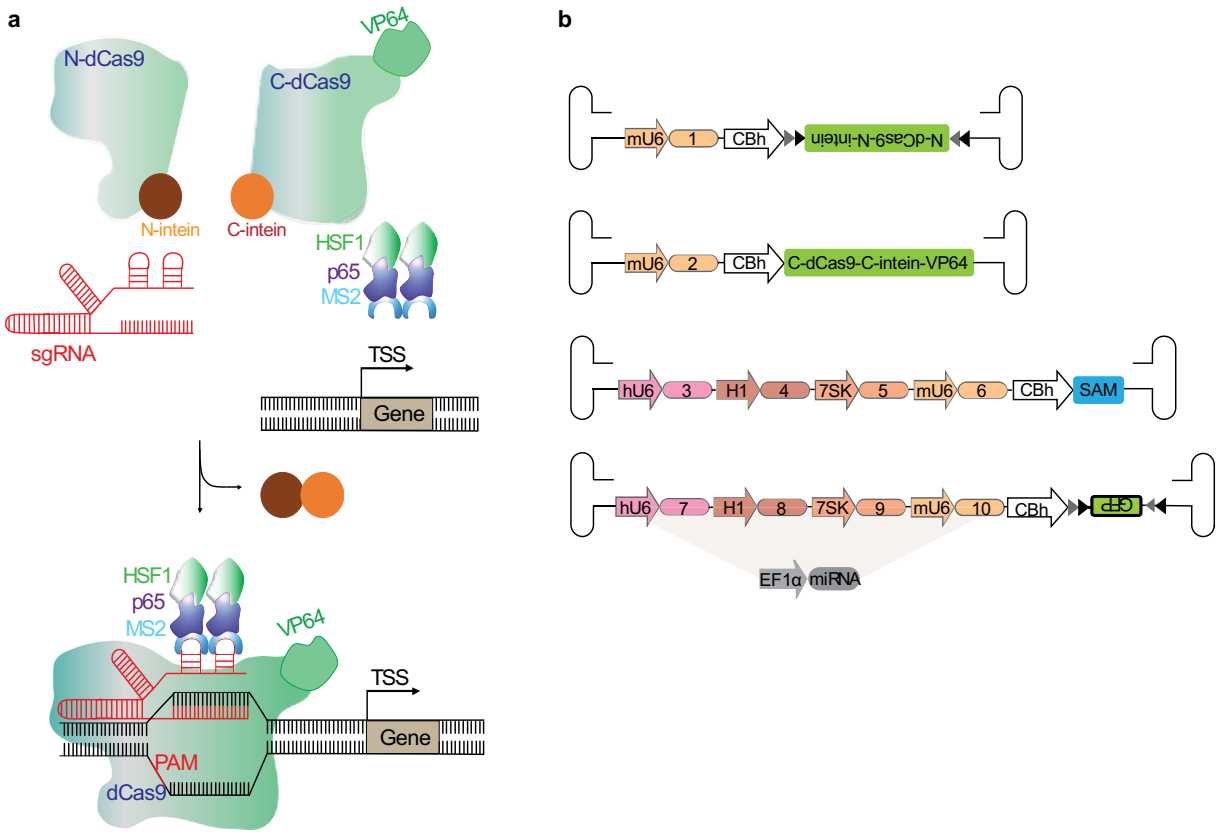

Figure 14: Schematic illustration of the AAV-based split-dCas9-Activator System (*AAV-dCAS*).

a, dCas9 was separated into a N- and a C-terminal part (AAV-N$^{aa1-573}$-dCas9-N-intein and AAV-C$^{aa574-1368}$-dCas9-VP64-C-intein), both portions were fused to the corresponding intein-moieties. Upon co-expression intein-mediated trans-splicing leads to a reconstitution of the protein. **b,** Based on the splitting of the large dCas9 gene, the system can be packed into AAVs. To ensure cell-type specificity upon Cre expression, the *N-dCas9* and the *GFP* were inverted and flanked by two different *LoxP* sites (*LoxX* and *Lox511*). dCas9 is delivered by two AAVs, a third AAV is needed for the delivery of the SAM activator. On a forth virus the reporter gene is delivered, sgRNAs are distributed between the vectors. Abbreviations: C-dCas9 - C-terminal dCas9 residues 574-1368; C-intein - C-terminal part of DNA polymerase III subunit alpha; N-dCas9 - N-terminal dCas9-residues 1-573; N-intein - N-terminal part of DNA polymerase III subunit alpha; VP64 – 4x VP16 herpes simplex virus protein vmw65; p65 - p65 subunit of human NF-κB; HSF1 – heat shock factor 1; MS2 - MS2 bacteriophage coat protein; PAM – protospacer adjacent motif; TSS – transcriptional start site. sgRNA expression is driven by the different Pol III promoters (H1, hU6, mU6 and 7SK).

For the AAV-based system, the SAM activator system alone was selected, as in *in vitro* studies for most endogenous genes comparable activation levels to the dual activator system (VPR and SAM) could be measured (Figure 15).

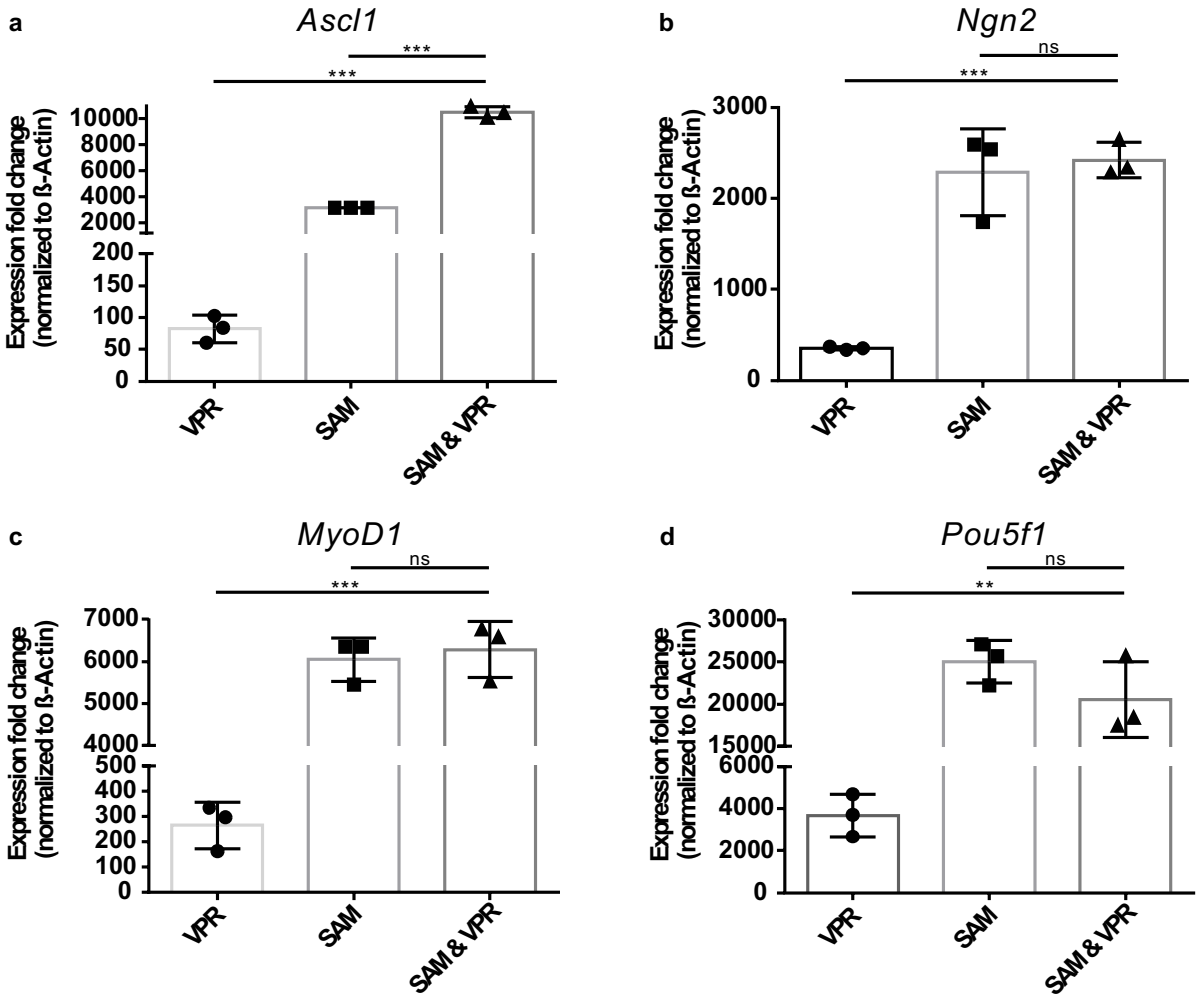

Figure 15: Comparison of the aCRISPR systems with the split-dCas9.

a, Activation of *Ascl1.* (VPR 82 ± 21, SAM 3158 ± 10, SAM&VPR 10493 ± 432) **b,** Activation of *Ngn2.* (VPR 355 ± 17, SAM 2290 ± 476, SAM&VPR 2422 ± 195) **c,** Activation of *MyoD1.* (VPR 264 ± 91, SAM 6047 ± 517, SAM&VPR 6285 ± 669) **d,** Activation of *Pou5F1*. (VPR 3682 ± 1003, SAM 25041 ± 2507, SAM&VPR 20534 ± 4521). Experiments were performed in Neuro2A cells. Each gene was activated by two sgRNAs targeting the 200 bp prior to the transcriptional start site. Activation levels are depicted as fold change between cells transfected with and without sgRNAs. All levels were normalized to β-Actin. n=1, with three technical replicates.
Error bars represent mean ± SD.

To achieve cell-type specificity the FLEx system was used, whereas the N-dCas9 and the *GFP* reporter gene were flexed. As seen in western blot analysis, the FLEx-*N-dCas9* was correctly inverted/expressed and reconstituted with the C-terminal part (Figure 16 a). As astrocytes shall

be targeted the *Gfap-Cre* (*B6.Cg-Tg(Gfap-Cre)77.6Mvs/2J*) mouse line was deployed. Simultaneously, FLEx-*N-dCas9* and the FLEx-*GFP* reporter are inverted and expressed in astrocytes.

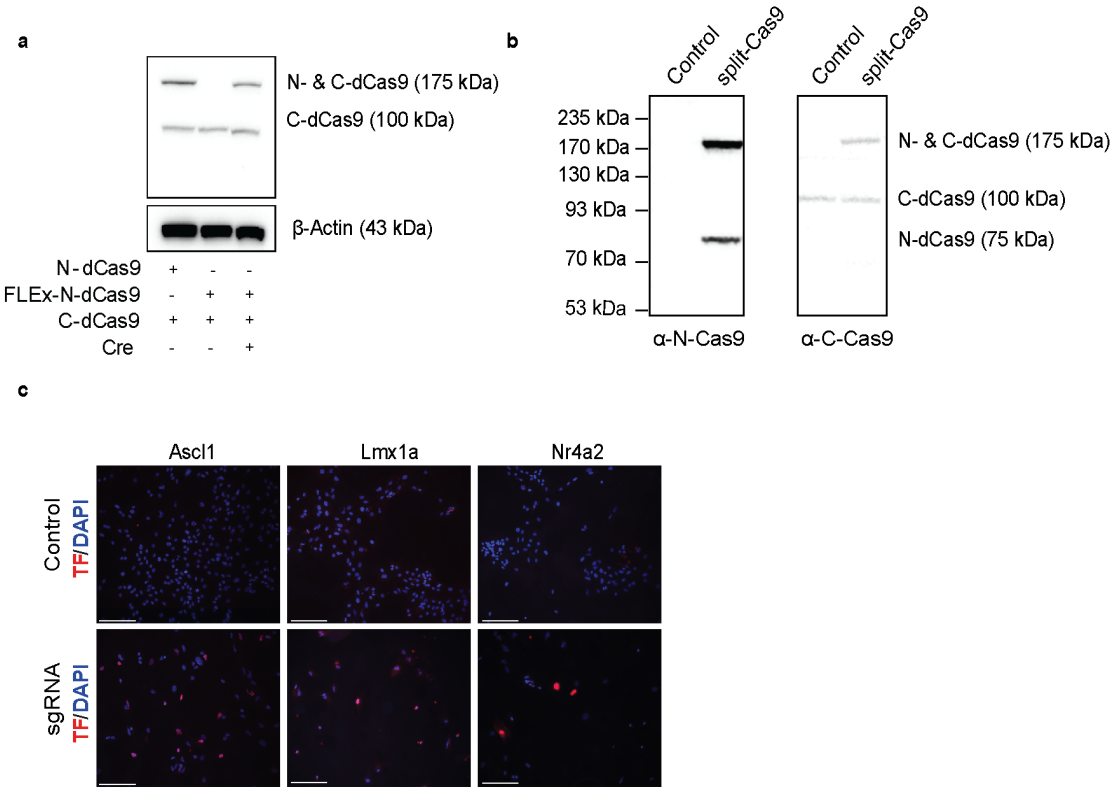

Figure 16: Evaluation of the *AAV-dCAS* and multiplexed endogenous gene activation in primary astrocytes of the *Gfap-Cre* line.

a, Western blot analysis evaluating the FLEx-N-dCas9 system in Neuro2A cells, using a C-Cas9 antibody. **b,** Western blot analysis evaluating the split-dCas9 system in Neuro2A cells, left blot – N-Cas9 antibody, right blot – C-Cas9 antibody. Correct fusion of the split-dCas9 parts at 175 kDa. **c,** Immunocytochemistry analysis on primary astrocytic cultures. Activation of *Ascl1*, *Lmx1a* and *Nr4a2*. Upper lane – Transfection of dCas9-activators without sgRNAs. Lower lane - Transfection of dCas9-activators with sgRNAs. Red channel staining for the respective protein. Scale bars indicate 20 µm.

5.2.2 Evaluation of the *AAV-dCAS* and multiplexed gene activation in primary astrocyte cultures

The correct assembly of the split-dCas9 system was assessed by western blot analysis using antibodies specific for the N-terminal, respectively C-terminal part of the Cas9 (Figure 16 b). To compare the efficiency of the split-system with the full-length version of the dCas9, *Ascl1* was activated endogenously (Figure 17 a). No significant difference could be observed between the two versions, making the spilt variant a valuable tool for gene activation (this

experiment was performed by Benedict Rauser). As depicted in Figure 17 b the two transcription factor combinations *ALN* and *ALNe-218* could robustly be activated in primary astrocyte cultures of the *Gfap-Cre* line. For the activation of *Ascl1*, *Lmx1a* and *Nr4a2* the activation capacity was also checked on protein level (Figure 16 c) and increased amounts of the protein in comparison to the control could be confirmed. Furthermore, up to five endogenous genes were activated in parallel (Figure 17 c). All five genes showed robust activation and it is not doubted that a further increase in gene number will be possible.

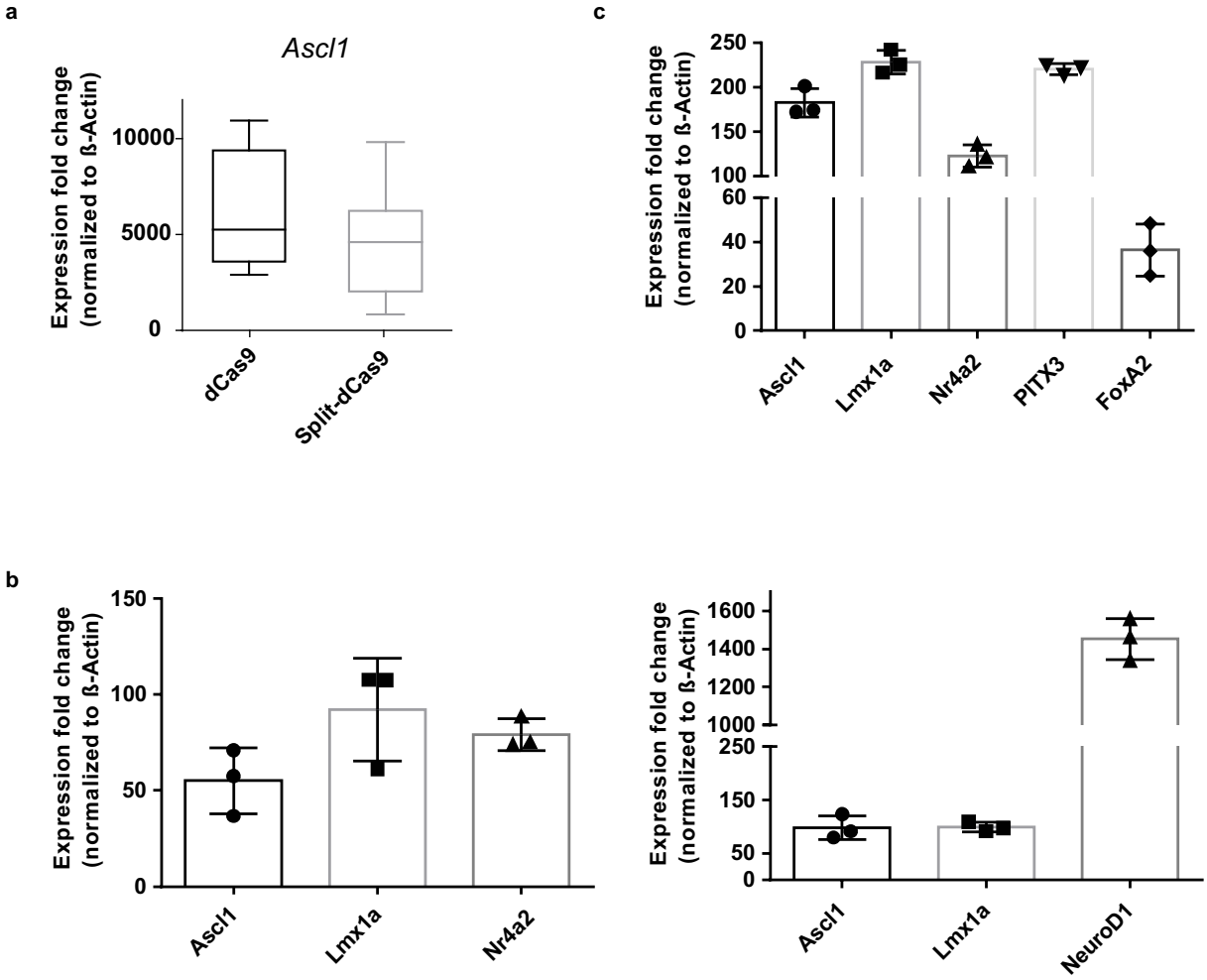

Figure 17: Evaluation of the *AAV-dCAS* and the multiplexed gene activation in primary astrocytes of the *GFAP-Cre* line.

a, RT-qPCR analysis of *Ascl1* endogenous induction in Neuro2A cells for the comparison of activation capacity of full-length versus split-dCas9. Data in fold change normalized to non-activated control: dCas9 6116 ± 847.3, split-dCas9 4415 ± 748.8, n=3, activation levels are depicted as fold change between cells transfected with and without sgRNAs. **b,** Multiplexed activation of *Ascl1*, *Lmx1a*, *Nr4a2* (*Ascl1* 55 ± 17, *Lmx1a* 92 ± 27, *Nr4a2* 79 ± 8) and *Ascl1*, *Lmx1a*, *NeuroD1* (*Ascl1* 98 ± 23, *Lmx1a* 99 ± 9, *NeuroD1* 1452 ± 109) in primary astrocytic cells. **c,** Multiplexed activation of *Ascl1*, *Lmx1a*, *Nr4a2*, *PITX3*, *FoxA2* (*Ascl1* 183 ± 16, *Lmx1a* 228 ± 13, *Nr4a2* 122 ± 12, *PITX3* 220 ± 6, *FoxA2* 36 ± 12) in

primary astrocytic cells. n=2-3, one representative run is shown, additional data in Supplementary Figure 3. Activation levels are depicted as fold change between cells transfected with and without sgRNAs. All levels were normalized to β-Actin. Error bars represent mean ± SD between technical replicates.

5.2.3 The *AAV-dCAS* efficiently activates *ALN* and *ALNe-218* leading to reprogramming of astrocytes into induced neurons

Analog to the *dCAM*-based reprogramming experiment, a transgenic *Gfap-Cre* line was utilized to ensure astrocyte-specific expression of the tools. Experimental setup and timeframe were identical to the *dCAM* setting; for delivering dCas9, a FLEx-N-dCas9 and a C-dCas9-VP64 AAV virus were used [61-63]. Also, with this setup both combinations were sufficient to convert astrocytes into induced neurons. At 5 wpi, the proportion of different infected cell types was comparable to the results in the *dCAM* approach (Figure 18 a, b). Interestingly, less than 5% (4.23 ± 1.55%) of the of GFP positive cells were also NeuN positive in GFP control injected mice, while percentage increased in both reprogramming conditions, *ALN* (14.67 ± 1.21%) and *ALNe-218* (14.10 ± 0.89%) to about 14% (Figure 18 c, d). At 13 wpi the percentage of $GFAP^+/GFP^+$ cells decrease to 48.0 ± 6.65% for *ALN* and 76.23 ± 3.27% for *ALNe-218* (Figure 18 e, f), whereas the proportion of $NeuN^+/GFP^+$ reprogrammed cells increased to 25.47 ± 6.85% upon *ALN* activation, but not under the *ALNe-218* condition (11.67 ± 0.35%) (Figure 18 g, h). Thus, the *AAV-dCAS* validates the results obtained with the *dCAM* model, highlighting a higher efficiency of the *ALN* combination over time. None of the treated animals developed tumors during the period of the experiment.

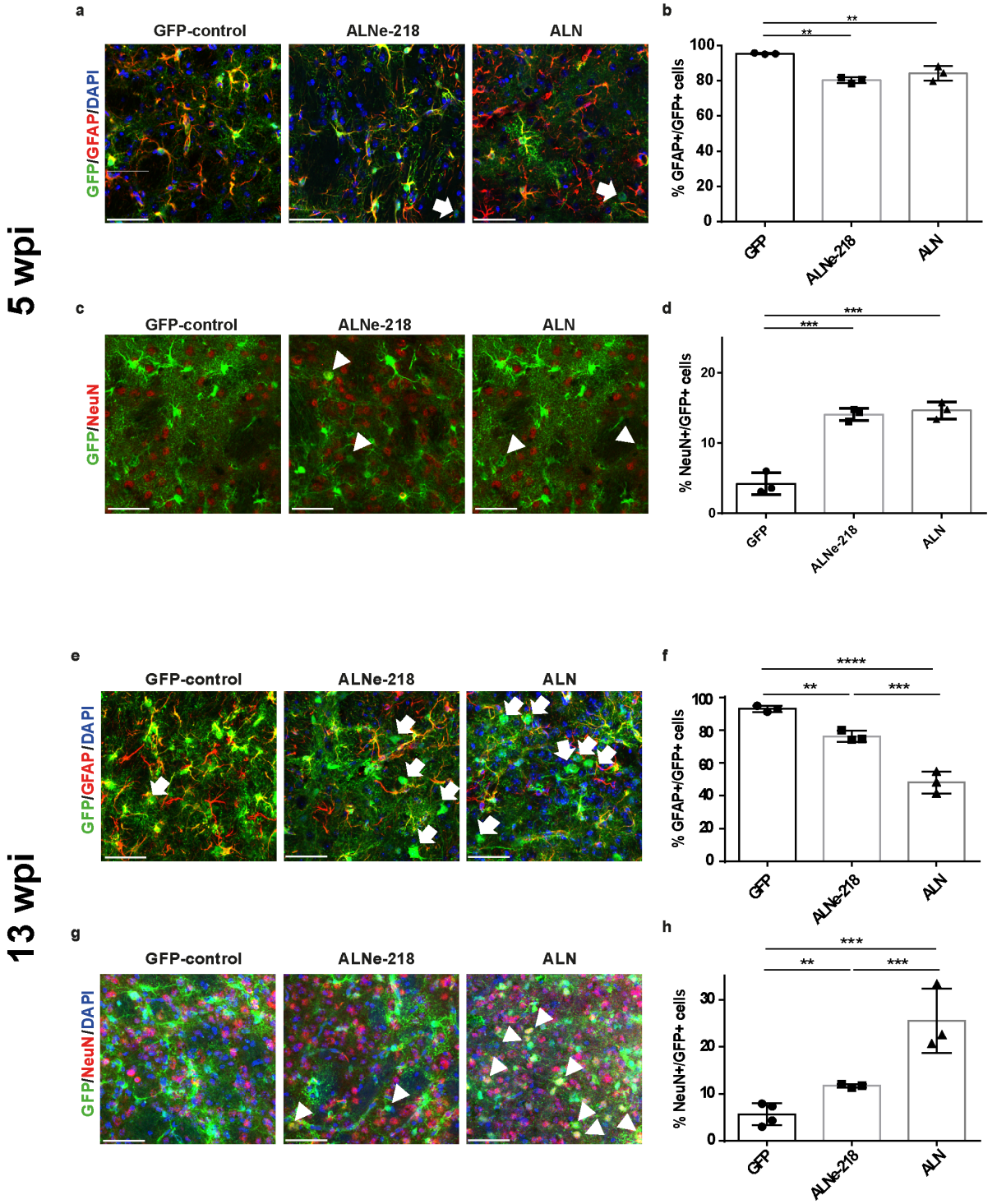

Figure 18: AAV-based split-dCas9-Activator System (*AAV-dCAS*) based reprogramming of astrocytes.

a, Photomicrographs showing GFP$^+$/GFAP$^+$ cells 5 wpi. Arrows indicating GFP$^+$/GFAP$^-$ cells. **b,** Quantification GFAP$^+$/GFP$^+$ cells. *GFP* 95.37 ± 0.40%, *ALNe-218* 80.33 ± 1.75% and *ALN* 84.10 ± 4.16%. *GFP* vs. *ALNe-218* P=0.001, *GFP* vs. *ALN* P=0.0045. Multiple comparison ANOVA F(2,6)=26.85. **c,** Photomicrographs showing GFP$^+$/NeuN$^+$ neurons 5 wpi. Arrow heads indicating GFP$^+$/NeuN$^+$ cells. **d,** Quantification NeuN$^+$/GFP$^+$ cells. *GFP* 4.23 ± 1.55%, *ALNe-218* 14.10 ± 0.89%, *ALN* 14.67 ± 1.21%. *GFP* vs. *ALNe-218* P=0.0002, *GFP* vs. *ALN* P=0.001. Multiple comparison ANOVA

F(2,6)=66.67. **e,** Photomicrographs showing $GFP^+/GFAP^+$ cells 13 wpi. Arrows indicating $GFP^+/GFAP^-$ cells. **f,** Quantification $GFAP^+/GFP^+$ cells. *GFP* 93.0 ± 1.85%, *ALNe-218* 76.23 ± 3.27% and *ALN* 48.0 ± 6.65%. *GFP* vs. *ALNe-218* P=0.0083, *GFP* vs. *ALN* P<0.0001 and *ALN* vs. *ALNe-218* P=0.0006. Multiple comparison ANOVA F(2,6)=79.76. **g,** Photomicrographs showing $GFP^+/NeuN^+$ neurons 13 wpi. Arrow heads indicating $GFP^+/NeuN^+$ cells. **h,** Quantification $NeuN^+/GFP^+$ cells. *GFP* 5.6 ± 2.35%, *ALNe-218* 11.67 ± 0.35% and *ALN* 25.47 ± 6.85%. *GFP* vs. *ALN* P=0.0008, *ALN* vs. *ALNe-218* P=0.0092. Multiple comparison ANOVA F(2,7)=21.74.
Scale bars indicate 50 µm.
Tukey's multiple comparisons test * P<0.05, **P<0.01, ***P<0.001, ****P<0.0001.
Error bars represent mean ± SD.

5.3 Characterization of cell identity of induced neurons

To characterize the induced neurons, immunohistochemical (IHC) analysis on striatal sections of mice 13 wpi was performed. Data is shown for the *AAV-dCAS* system, the analysis for the *dCAM* approach revealed similar results (data not shown). In particular, the expression of cell-type specific neurotransmitters was evaluated, including tyrosine hydroxylase (TH) for dopaminergic neurons or noradrenergic, GAD65/67 for GABAergic neurons and vGLUT1 for glutamatergic neurons. Neurons were positive for the GABAergic marker Gad65/67 (Figure 19).

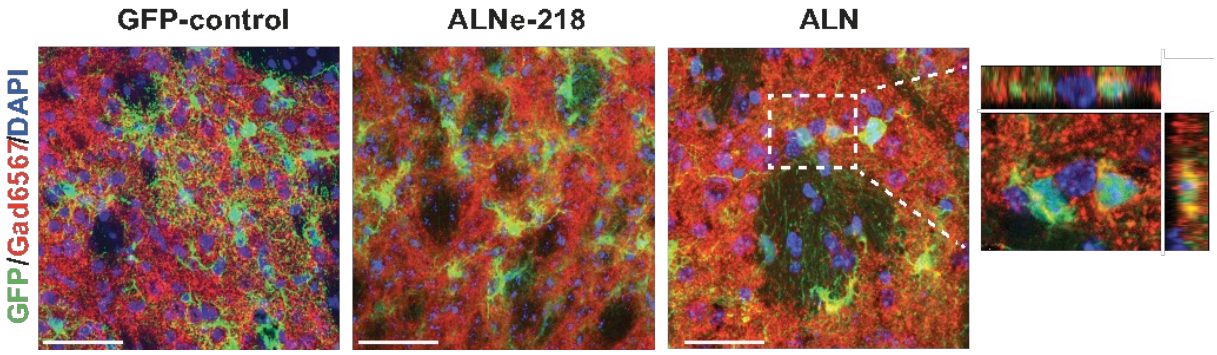

Figure 19: Characterization of AAV-split-dCas9 Activator System (*AAV-dCAS*) reprogrammed neurons reveals GABAergic identity.

Confocal images showing co-localization of GFP and glutamic acid decarboxylase, a marker specific for GABAergic neurons. Scale bar indicates 50 µm.

No converted neurons expressing TH could be found, even though some TH^+ neurons could be detected in the striatum, which however are also observed in the 6-OHDA treated control animals. Additionally, cells were not positive for the glutamatergic marker vGLUT1 (Figure 20).

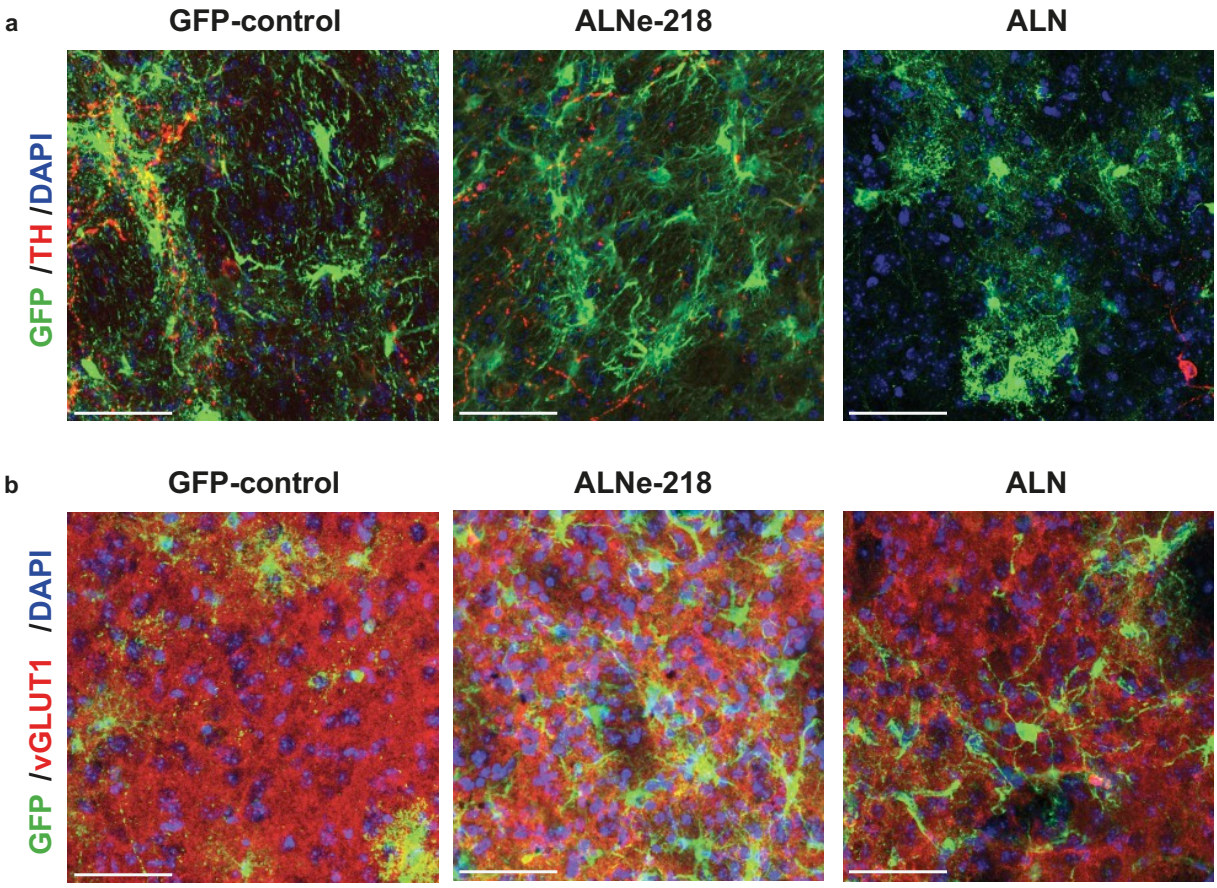

Figure 20: Neurotransmitter identities of reprogrammed neurons using *AAV-dCAS*.

a, b, Confocal images showing co-localization of GFP and markers specific for neurotransmitter subtype neurons. **a,** Tyrosine hydroxylase – dopaminergic neurons, **b,** Vesicular glutamate transporter 1 – glutamatergic neurons. Scale bars indicate 50 µm.

Staining was performed for striatum-specific markers such as DARPP32 for striatal medium spiny neurons and the classical interneuron-specific markers, namely parvalbumin, calretinin, NPY and CHAT. Most *in vivo* induced neurons were not positive for the broad striatal marker DARPP32 (*dCAM*: *ALNe-218* 4.7%, *ALN* 5.7%; dCAS: *ALNe-218* 4%, *ALN* 6.4%) (Figure 21).

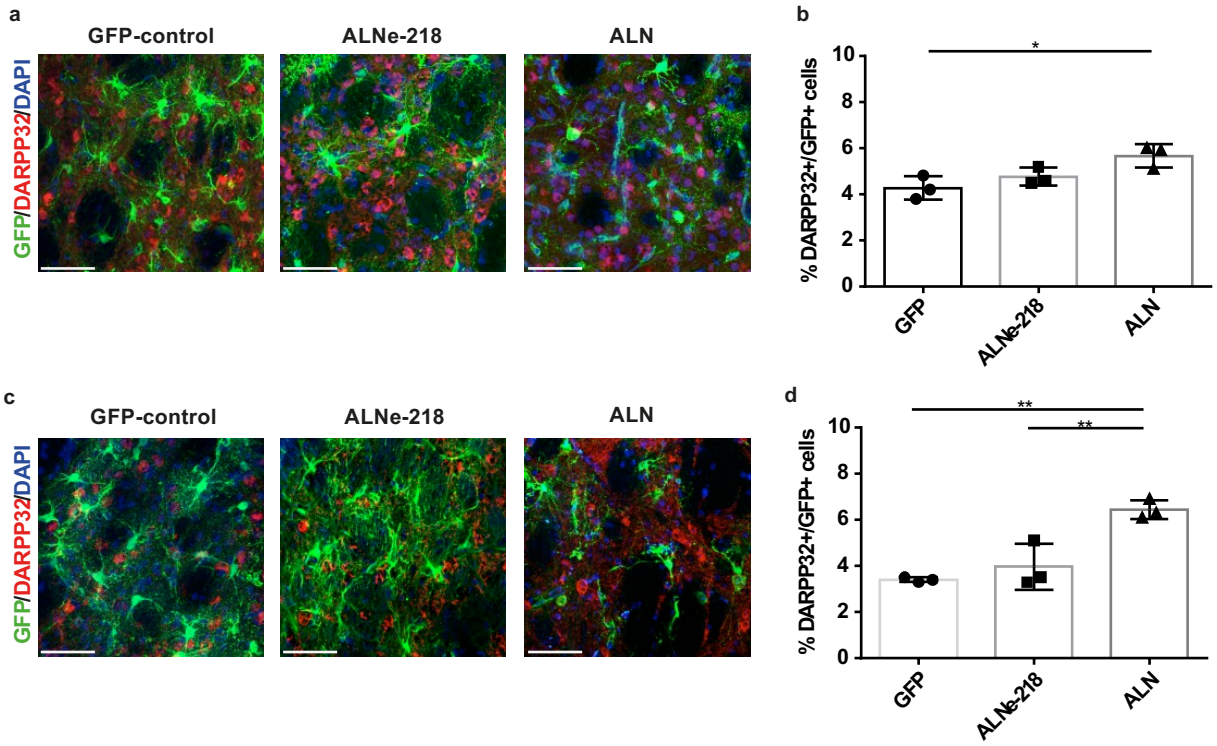

Figure 21: DARPP32 staining and quantification 13 wpi.

a, b, Evaluation DARPP32 staining in *dCAM* model. **a,** Confocal images showing co-localization of GFP and DARPP32. **b,** Quantification DARPP32+/GFP+ cells. *GFP* 4.3 ± 0.5%, *ALNe-218* 4.76 ± 0.38% and *ALN* 5.67 ± 0.49%. *GFP* vs. *ALN* P=0.023. Multiple comparison ANOVA F(2,6)=7.078. **c, d,** Evaluation DARPP32 staining in *AAV-dCAS* model. **c,** Confocal images showing co-localization of GFP and DARPP32. **d,** Quantification DARPP32+/GFP+ cells. *GFP* 3.4 ± 0.1%, *ALNe-218* 3.97 ± 0.99% and *ALN* 6.43 ± 0.42%. *GFP* vs. *ALN* P=0.0024, *ALN* vs. *ALNe-218* P=0.0067. Multiple comparison ANOVA F(2,6)=20.24. Scale bars indicate 50 µm.
Tukey's multiple comparisons test * P<0.05, **P<0.01, ***P<0.001.
Error bars represent mean ± SD.

Furthermore, they were not positive for interneuron markers like parvalbumin, neuropeptide Y, calretinin and CHAT (Figure 22).

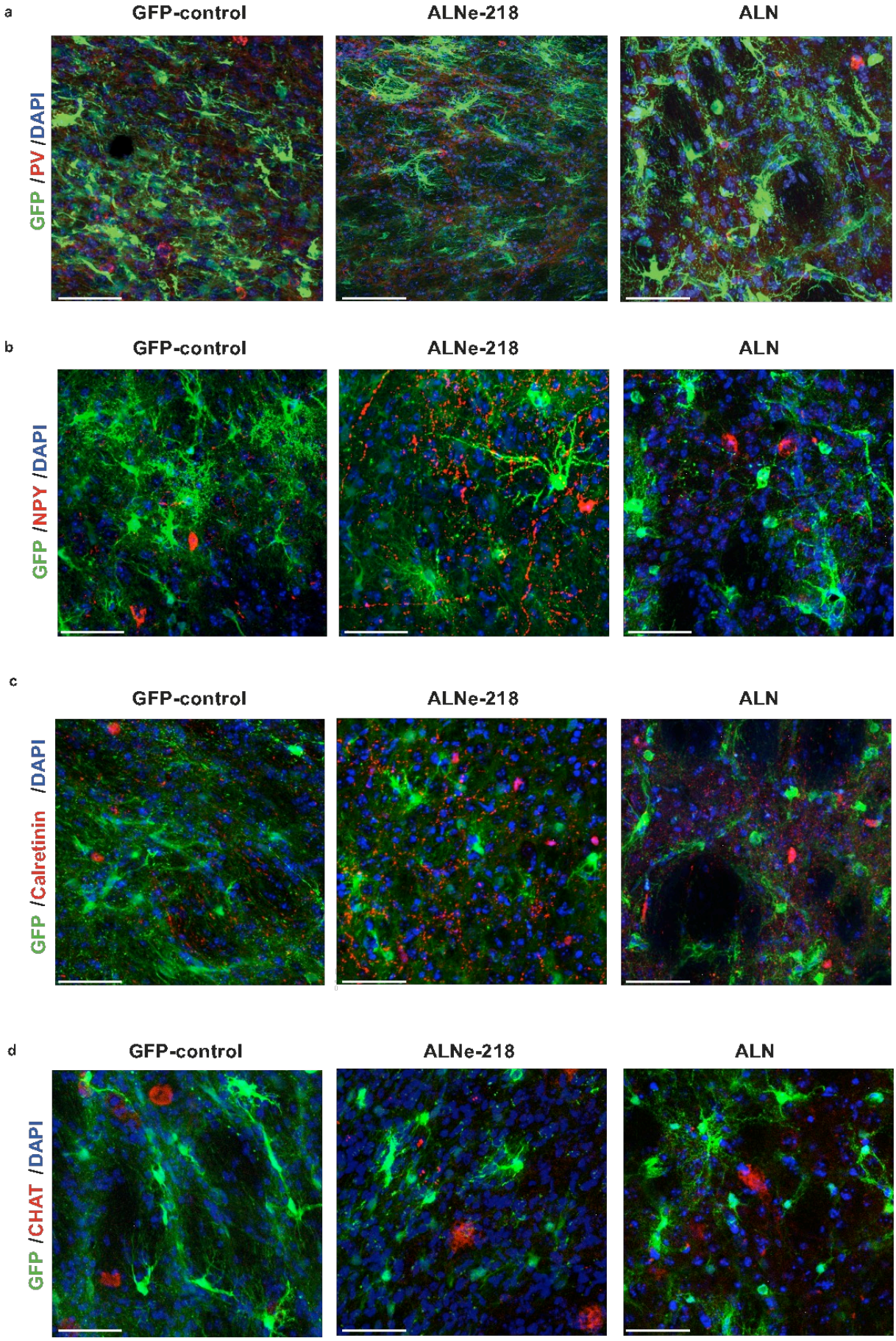

Figure 22: Phenotypical identities of reprogrammed neurons using *AAV-dCAS*.

a-d, Confocal images showing co-localization of GFP and the interneuron markers: **a,** parvalbumin, **b,** neuropeptide Y, **c,** calretinin and **d,** choline acetyl transferase. Scale bars indicate 50 µm.

5.4 Single cell RNA-seq analysis reveals the GABAergic fate of induced neurons in *dCAM* approach

To further distinguish the induced neurons, scRNA-seq experiments were performed using striatal tissue 13 wpi from *GFP* control and *ALN* reprogrammed animals (n=2). The *dCAM* approach was used, as low number of AAVs ensures high consistency within the data. Batch integration of single cell data using Scanorama [95] unsupervised clustering and marker gene annotation of all 3,899 QC-controlled cells (Supplementary Figure 4) exhibited grouping into main expected striatal cell types such as oligodendrocytes (n=733), astrocytes (n=646), neurons (n=464) and monocytes (n=1,453) (Figure 23 a, Supplementary Figure 5) [96]. *Cre* expression could be ascribed to the astrocytic cluster (Supplementary Figure 6 b). The astrocytic and neuronal cells (n=1,110) were further subclustered, uncovering a total of four cell groups. Selection of marker genes based on cluster-specific up-regulation allowed unsupervised separation of neurons and astrocytes into four subclusters and uncovered their cell identities (Figure 23 b, Supplementary Figure 6 a). GFP positive cells were detected in both *GFP* control and *ALN* reprogrammed astrocytic subclusters, but solely for the *ALN* condition GFP positive cells were detected in neuronal cells as well (n=21, Figure 23 c). Despite the low number of neurons recovered in the scRNA-seq experiment versus other cell types (11.2%), expression of all endogenously activated genes (*Ascl1*, *Lmx1a*, *Nr4a2*) co-expressed with GFP could be detected in the astrocytic-neuronal subclusters (Figure 23 c, Supplementary Figure 6 b). *Ascl1* expression was enriched in one of the neuronal subcluster, however in the *ALN* condition, expression could also be detected in one of the astrocytic subclusters (11 out of 17 cells are GFP^+ and $Ascl1^+$). These $Ascl1^+$ cells may represent astrocytes with forced expression of endogenous *Ascl1*, locked in the astrocytic fate or in directly conversion process. The two neuronal subclusters are characterized by either high *Ascl1* or *Myt1l* expression (Figure 23 c). The analysis for neurotransmitter subtypes revealed no glutamatergic and dopaminergic neurons in the samples, though, the reprogrammed neurons were positive for *Gad1/Gad2* confirming a GABAergic fate (14 out of 21 GFP^+ cells in neuronal cluster are $Gad1/2^+$) (Figure 23 c, Supplementary Figure 6 c). Complete bioinformatic analysis of the scRNA-seq data war performed by Dr. Ignacio Ibarra Del Río.

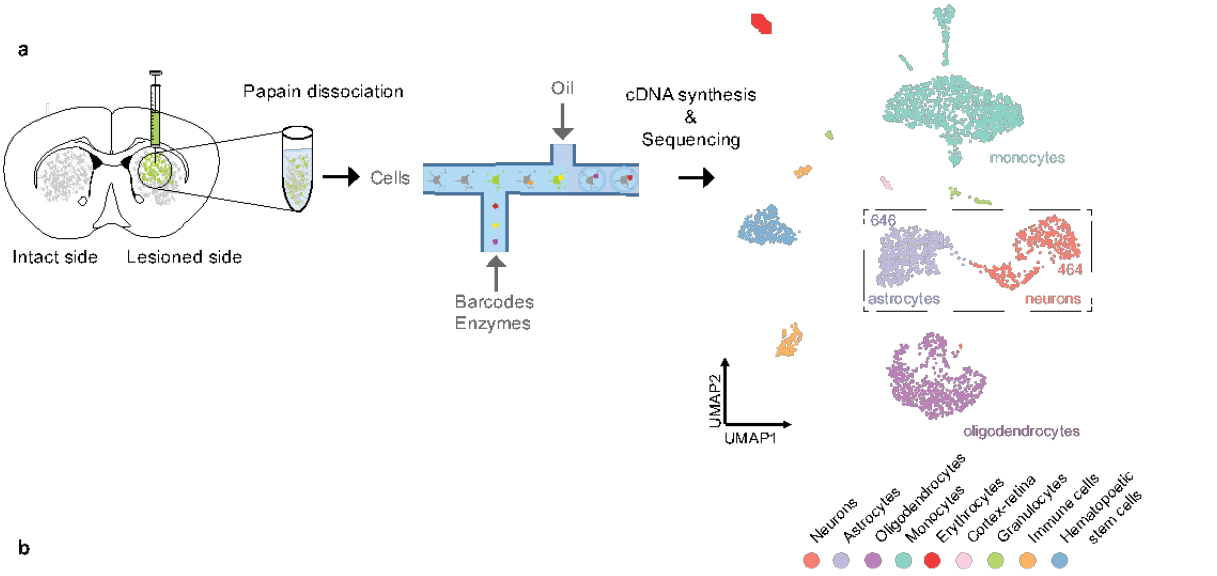
a
Papain dissociation
Intact side
Lesioned side
Cells
Oil
Barcodes
Enzymes
cDNA synthesis
&
Sequencing
monocytes
646
464
astrocytes
neurons
oligodendrocytes
UMAP2
UMAP1
Neurons
Astrocytes
Oligodendrocytes
Monocytes
Erythrocytes
Cortex-retina
Granulocytes
Immune cells
Hematopoetic
stem cells

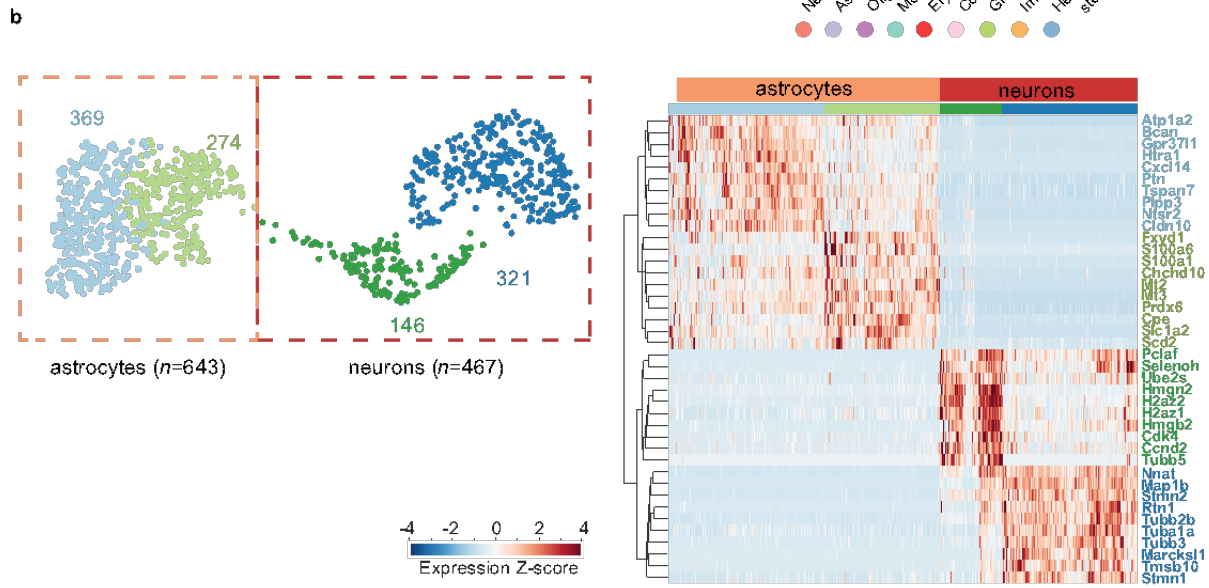
b
369
274
321
146
astrocytes (n=643)
neurons (n=467)
astrocytes
neurons
Atp1a2
Bcan
Gpr37l1
Htra1
Cxcl14
Ptn
Tspan7
Plpp3
Nfasr2
Cldn10
Fxyd1
S100a6
S100a1
Chchd10
Mt2
Mt3
Prdx6
Cpe
Slc1a2
Scd2
Pclaf
Selenoh
Ube2s
Hmgn2
H2az2
H2az1
Hmgb2
Cdk4
Ccnd2
Tubb5
Nnat
Map1b
Stmn2
Rtn1
Tubb2b
Tuba1a
Tubb3
Marcksl1
Tmsb10
Stmn1
-4 -2 0 2 4
Expression Z-score

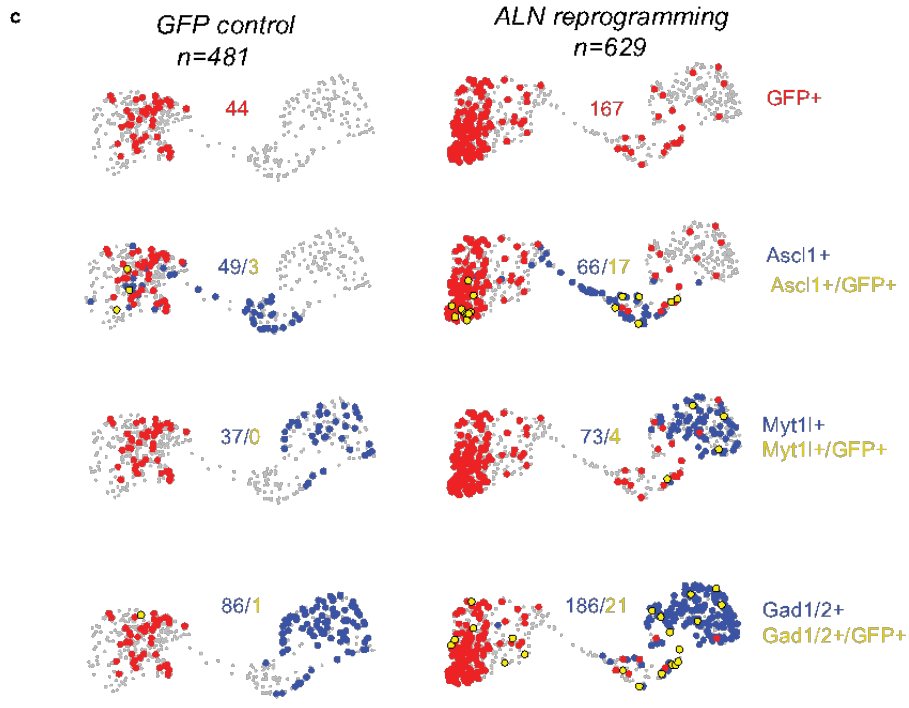
c
GFP control
n=481
ALN reprogramming
n=629
44
167
GFP+
49/3
66/17
Ascl1+
Ascl1+/GFP+
37/0
73/4
Myt1l+
Myt1l+/GFP+
86/1
186/21
Gad1/2+
Gad1/2+/GFP+

Figure 23 Analysis of striatal tissue from *ALN* reprogrammed *dCAM* mice by single cell RNA-seq.

a, Scheme depicting experimental preparation of cells of 13 wpi mice striatal regions (n=2, one technical replicate). Papain dissociated cells are prepared for scRNA-seq using droplet-based separation and barcoding. Uniform Manifold Approximation and Projection (UMAP) visualization of QC-selected cells for *GFP* and *ALN* (n=3,899). Color labeling highlights nine main cell groups based on Leiden clustering and identification based on marker genes. Rectangle highlights astrocytic and neuronal cell clusters. 4,273 highly variable genes (HVG) were detected. **b,** Subclustering of 1,110 cells identified four groups of astrocytic and neuronal identity. Layout is based on UMAP visualization presented in **a**. Clustering of markers genes selected based on expression levels between clusters. Expression Z-scores are hierarchically clustered by rows. **c,** *GFP control* and *ALN reprogrammed* cells selected from the neuronal and astrocytic clusters are visualized based on detection of GFP (red cells), marker gene *Ascl1*, *Myt1l* and *Gad1/Gad2* (*Gad1/2*) (blue cells), and the co-detection of both (yellow cells).

5.5 Electrophysiological properties of *AAV-dCAS* induced neurons

All electrophysiological measurements were performed by Dr. Sandrine Lefort using acute slices from mice treated with the *AAV-dCAS* setting. 13 weeks after the initiation of the reprogramming process the reprogrammed neurons exhibited mature electrophysiological properties characterized by depolarization-induced action potentials (APs) (Figure 24 a, AP threshold= -33.49 ± 2.09 mV; n=14). Further, induced neurons also integrated within the striatal circuits, as shown by the synaptic inputs they receive (Figure 24 a, bottom right). Conversely, *ALNe-218*-induced neurons displayed properties similar to immature neurons, i.e. the inability to produce APs even with a somatic injection of a strong depolarizing current (>1500pA) leading to a resting membrane potential above the normal AP threshold observed with the *ALN* condition at 13 wpi (Figure 24 b), and reminiscent of characteristics seen at 5 wpi with the *ALN* condition (Supplementary Figure 7). No significant difference in the resting membrane potential could be observed between both reprogramming approaches (ALN_{Vm}= -64.55 ± 1.53 mV vs $ALNe\text{-}218_{Vm}$= -63.8 ± 2.99 mV; n=15 and n=10 respectively; p=0.85, Kruskall-Wallis test). However, the input resistance (R_{in}) exhibited significant differences between the two reprogramming conditions, with a R_{in} for *ALN*-induced neurons of 314.69 ± 41.2 mΩ vs a R_{in} for *ALNe-218* neurons of 105.39 ± 52.27 mΩ (n=15 and n=10 respectively; p=0.002; Kruskall-Wallis test – Figure 24 c).

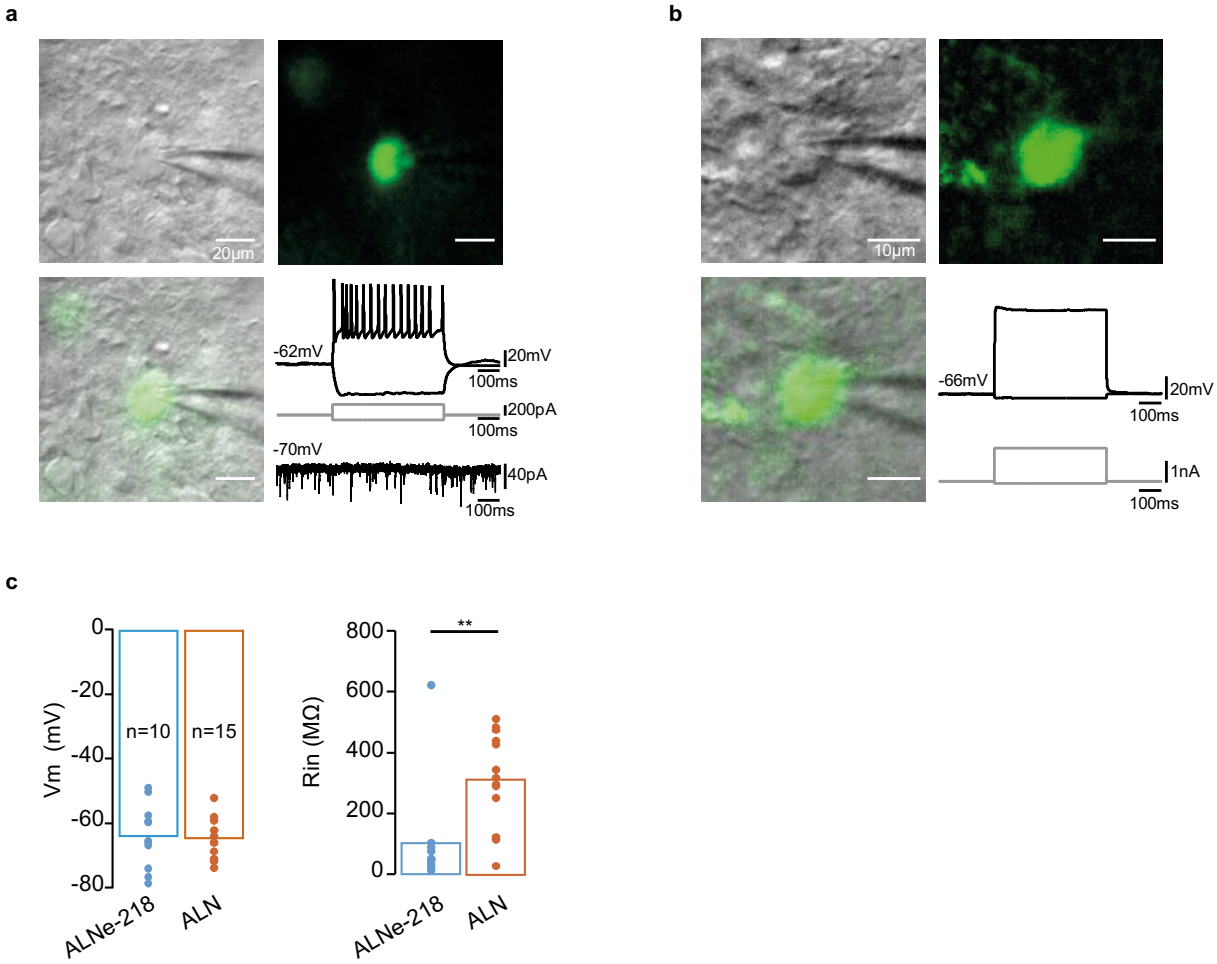

Figure 24: Electrophysiological measurements of induced neurons reprogrammed using the *AAV-dCAS* technology.

a, Firing pattern of a neuron reprogrammed by the endogenous activation of *Ascl1*, *Lmx1a*, *Nr4a2 (ALN).* 14/15 cells exhibit action potentials, 1/15 showed electrophysiological properties of of immature neuron/glia-like cells (i.e. lack of APs and a relatively low R_{in}). Bottom right: Example of spontaneous synaptic events recorded from a different reprogrammed neuron, therefore showing the integration within striatal neuronal network. **b,** Firing pattern of a neuron reprogrammed by the endogenous activation of *Ascl1*, *Lmx1a*, *NeuroD1* and expression of miRNA218 (*ALNe-218*). 10/10 cells showed electrophysiological properties of immature neuron/glia-like cells (i.e lack of APs and a relatively low R_{in}). **c,** Left panel – the resting membrane potential (Vm in mV) is similar between different reprogramming conditions. Right panel – Input resistance (R_{in} in mΩ) is significantly different between the different conditions (p=0.002, Kruskall-Wallis test). The input resistance of cells measured in the *ALNe-218* condition are similar to immature neurons/glia-like cells, whereas *ALN* reprogrammed cells exhibit an input resistance within the range of endogenous neurons. Kruskall-Wallis test **P<0.01. Error bars represent mean ± SEM.

5.6 Parkinsonian mice receiving the reprogramming combination *ALN* exhibit phenotypical rescue in their voluntary motor behavior

The ultimate proof for the functionality and integration of the induced neurons in this approach consists in the phenotypic rescue of toxin-induced phenotypes.

After the examination of the functionality of the *in vivo* produced induced neurons (iNs), it was tested, whether they were also capable to impact the toxin-induced motor behavior in the unilateral PD mouse model.

In PD patients gait alteration have been excessively studied, it has been shown that several of these parameters also hold true in the 6-OHDA toxin-induced degeneration mouse model [97]. To study the voluntary, coordinated limb usage of mice the computer-based analysis CatWalk XT system was deployed [98]. To correlate the immunohistochemical data with the behavior tests, the animals were analyzed at 5 and 13 wpi. At 5 wpi, we did not observe obvious differences in spontaneous motor behavior between lesioned animals injected with GFP control virus or sgRNA combinations. The parameter average speed exhibits hereby a representative measurement for the gait alteration due to the neuron loss. The disruption of the dopaminergic system led to drastic decrease in the average speed, whereas reprogramming conditions did not exhibit ameliorated values compared to controls (Figure 25 a, data of *dCAM* transgenic model). However, at 13 wpi the reprogramming combination *ALN* induced a significant rescue, represented by the average speed of the animal (Figure 25 c). This pattern of improvement was confirmed when analyzing the stride length, a measurement for the parkinsonian gait associated small shuffling steps, with naïve and *ALN* treated animals executing larger steps, depicted in Figure 25 d. A significant decrease of this parameter could be observed due to the 6-ODHA lesion, whereby the *ALN* reprogramming condition indicated levels similar to naïve animals. Also arm swing is a parameter altered in PD patients, so front paw usage was examined in detail [99]. Ipsilateral to the lesion we observe a strong improvement in the duty cycle of the front paw (Figure 25 e). Intriguingly, these very same findings were observed to a similar extent in both systems – using the *dCAM* model or the *AAV-dCAS* approach. Based on these results the *dCAM* group was additionally analyzed by the vertical pole test, investigating striatum-dependent motor coordination, also here a trend towards improved behavior was observed for the *ALN* combination (Figure 25 b) [100]. Another meaningful parameter to estimate PD-related gait alteration is the phase dispersion of the paws, which represents the movement of the paws relative to each other. As PD is often accompanied with anomalies in axial symmetry, the phase dispersion between the left hind and the right hind paw exhibits a suitable parameter to address this abnormality. As depicted in Figure 25 g, a significant change in phase dispersion could be observed between naïve and

6-ODHA-lesioned animals, this change converged back to naïve level in the *ALN* treated animals.

Modifications in axial symmetry and gait are typical for PD patients and are also present in MPTP-based PD mouse models [101, 102]. These results demonstrate that the same motor deficits can also be mimicked in a 6-ODHA PD mouse model. Due to *in vivo* reprogramming of astrocytes into induced neurons it was possible to alleviate voluntary motor behavior in the *ALN* reprogramming condition, in both the *dCAM*, as well as the *AAV-dCAS* setting.

Further characterizing the unilateral model, the dopamine-dependent drug-induced circling behavior was addressed, which is typically used in unilateral PD models to assess the severity of the dopaminergic lesion [103]. By the application of the dopamine releaser substance amphetamine, the unilateral lesioned animals exhibited a specific rotation pattern towards the ipsilateral site [104]. This pattern could be observed between naïve vs. 6-OHDA treated animals (Figure 25 f), however no rescue in rotation behavior was observed in neither condition nor reprogramming setup. These results confirm that the induced neurons reprogrammed by *ALN* exhibit functional output leading to a rescue in 6-OHDA motor behavior deficits independent of the dopaminergic system.

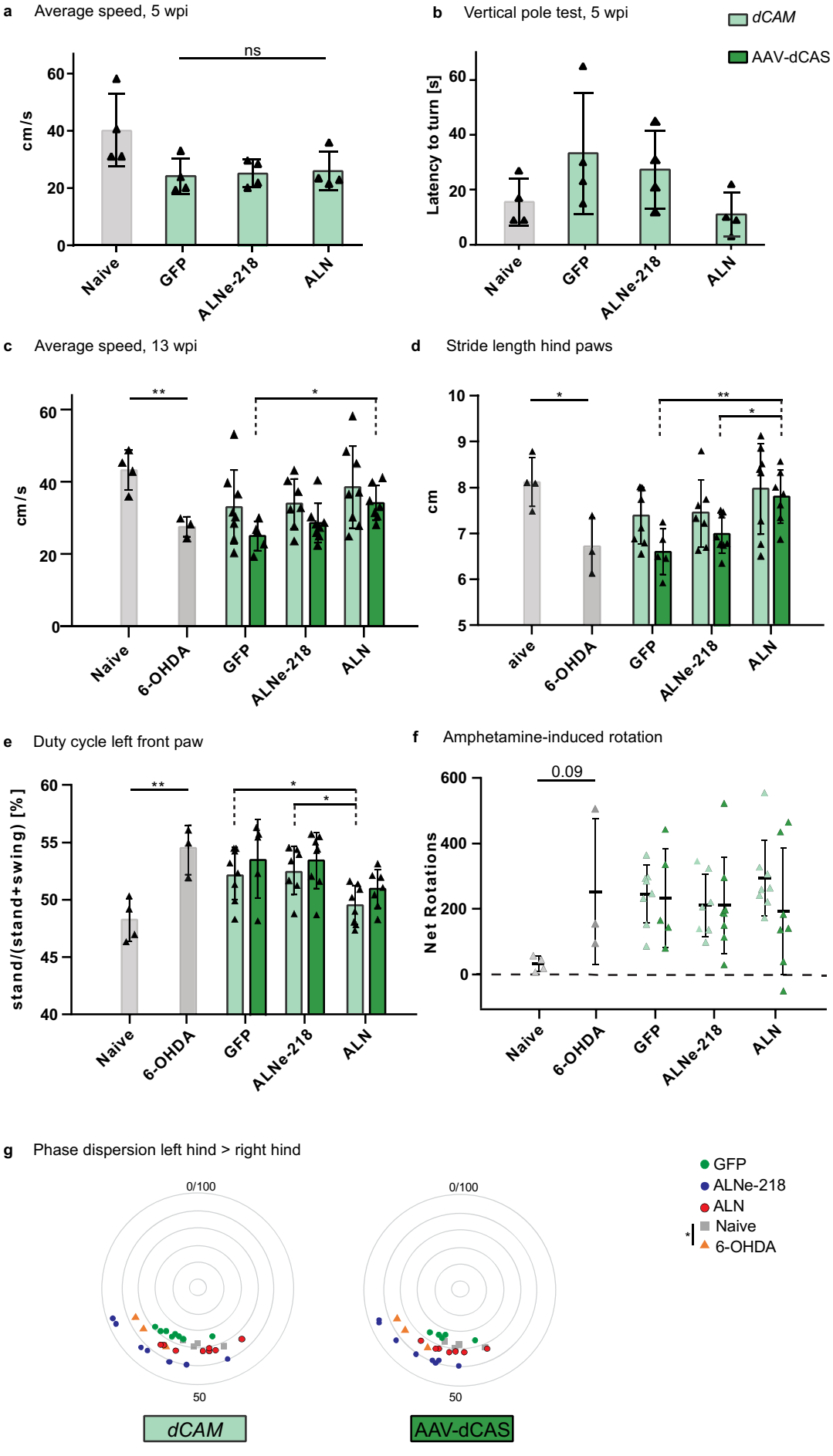
a Average speed, 5 wpi
ns
cm/s
Naive
GFP
ALNe-218
ALN
b Vertical pole test, 5 wpi
dCAM
AAV-dCAS
Latency to turn [s]
c Average speed, 13 wpi
6-OHDA
d Stride length hind paws
cm
e Duty cycle left front paw
stand/(stand+swing) [%]
f Amphetamine-induced rotation
0.09
Net Rotations
g Phase dispersion left hind > right hind
0/100
50
GFP
ALNe-218
ALN
Naive
6-OHDA
dCAM
AAV-dCAS

Figure 25: Motor behavior analysis 5 and 13 weeks after AAV injection.

a, Gait analysis using the CatWalk XT system. Average speed of tread. *dCAM* animals 5 wpi, n=4. Data in cm/s: Naïve 40.30 ± 12.78, *GFP* 24.19 ± 6.25, *ALNe-218* 25.14 ± 4.74, *ALN* 26.03 ± 6.69. **b,** Vertical pole test for *dCAM* animals. Latency time to turn, n=4. Data in s: Naïve 15.50 ± 8.54, *GFP* 33.25 ± 22.04, *ALNe-218* 27.25 ± 14.15, *ALN* 11.00 ± 7.96. *GFP* vs *ALN* P=0.17.**c,** Gait analysis using the CatWalk XT system. Average speed of tread 13 wpi. Data in cm/s: Naïve 43.52 ± 5.48, 6-OHDA 27.66 ± 2.78, *dCAM*: *GFP* 33.22 ± 10.30, *ALNe-218* 34.09 ± 6.94, *ALN* 38.76 ± 11.45, *AAV-dCAS*: *GFP* 25.14 ± 4.10, *ALNe-218* 28.70 ± 5.44, *ALN* 34.31 ± 4.87. Significant decrease in speed due to 6-OHDA lesion (13 wpi). Naïve vs. 6-OHDA P=0.0063. *AAV-dCAS*: *GFP* vs. *ALN* P=0.015 multiple comparison ANOVA F(2,17)=12.81. **d,** Stride length of front paws, 13 wpi. Data in cm. Naïve 8.32 ± 0.46, 6-OHDA 6.83 ± 0.66, *dCAM: GFP* 7.39 ± 0.67, *ALNe-218* 7.58 ± 0.66, *ALN* 8.02 ± 0.99. *AAV-dCAS*: *GFP* 6.73 ± 0.47, *ALNe-218* 7.12 ± 0.43, *ALN* 7.56 ± 0.43. Naïve vs. 6-OHDA P=0.0164. *AAV-dCAS*: *GFP* vs. *ALN* P=0.005, *ALN* vs. *ALNe-218* P=0.0042, multiple comparison ANOVA F(4,22)=9.9. **e,** Duty cycle of left front paw, 13 wpi. Data in%: Naïve 48.24 ± 1.86, 6-OHDA 54.42 ± 2.15, *dCAM*: *GFP* 52.29 ± 2.29, *ALNe-218* 52.57 ± 2.10, *ALN* 49.55 ± 1.70, *AAV-dCAS*: *GFP* 53.59 ± 3.40, *ALNe-218* 53.42 ± 2.44, *ALN* 50.93 ± 1.67. Naïve vs. 6-OHDA P=0.0096. *dCAM*: *GFP* vs. *ALN* P=0.036 and *ALN* vs. *ALNe-218* P=0.0252, multiple comparison ANOVA F(2,20)=5.199. **f,** Amphetamine-induced rotation analysis, 13 wpi. Change in rotational behavior in lesioned animals upon treatment with dopamine releaser substance. Net rotation = ipsilateral rotation-contralateral rotation. Naïve 32.0 ± 11.42, 6-OHDA 252.0 ± 128.2, *dCAM*: *GFP* 244.9 ± 31.16, *ALNe-218* 191.4 ± 36.68, *ALN* 293.8 ± 40.84, dCAS: *GFP* 233.8 ± 67.21, *ALNe-218* 210.6 ± 51.94, *ALN* 192.9 ± 72.66. Naïve vs. 6-OHDA P=0.09. **g,** Phase dispersion left hind paw to right hind paw (LH>RH), 13 wpi. Controls Grey – naïve, orange – 6-OHDA treated animals. Data in%: Naïve 52.42 ± 3.58, 6-OHDA 62.53 ± 4.08. Naïve vs. 6-OHDA P=0.0174. Treatments. Green – *GFP*, blue – *ALNe-218*, red – *ALN*. *dCAM*: *GFP* 54.47 ± 3.66, *ALNe-218* 56.84 ± 7.28, *ALN* 49.82 ± 5.14. *ALN* vs. *ALNe-218* P=0.0549, multiple comparison ANOVA F(2,20)=3.250. dCAS: *GFP* 53.77 ± 3.56, *ALNe-218* 58.04 ± 5.42, *ALN* 52.38 ± 3.84. *ALN* vs. *ALNe-218* P=0.0653, multiple comparison ANOVA F(2,17)=3.193.

Naïve vs. 6-OHDA unpaired t-test (two-tailed) * P<0.05, ** P<0.01.

GFP vs *ALN*, *GFP* vs *ALNe-218* and *ALN* vs *ALNe-218* Tukey's multiple comparisons test * P<0.05, ** P<0.01.

CatWalk error bars represent mean ± SD. Rotation analysis error bars represent mean ± SEM.

6 Discussion

6.1 Development of a versatile transgenic platform for multiplexed gene activation *in vivo* and *in vitro* - *dCAM*

A versatile platform for simultaneous activation of multiple endogenous genes *in vitro* and *in vivo* was deployed. The conventional reprogramming approaches use the ectopic expression of the gene coding sequences (cDNA), making multiplexing of divers genes difficult if not impossible - particularly when large genes have to be expressed. In contrast, the aCRISPR platform allows the multiplexed activation of many endogenous genes simply by introducing sgRNAs, with a fixed cargo size for each gene, whereby the usage of multiple constructs can be circumvented, and such that the endogenous transcriptional machinery can be co-opted to conduct complex genetic splicing patterns [46, 62, 105]. Furthermore, using the aCRISPR system for cellular reprograming potentially reflects a more natural mechanism of dedifferentiation, as endogenous activation accompanies chromatin remodeling of target loci [106]. The introduced *dCAM* mouse line is the first targeted Rosa26 knock-in of a specific dual activator system harboring the VPR and SAM activator complexes, which, due a floxed stop cassette and SAM activator flanked by *FRT* sites, can be used as a conditional dual activator system. The defined integration and the optional twofold mode of activation are prominent features differentiating our line from the recently published SPH transgenic mouse line, as well as the absence of the reporter in the transgenic mouse line, which allows the identification of the sgRNAs targeted cells, rather than the cells expressing SPH transgene [107].

By crossing the *dCAM* line with any Cre reporter line, specific aCRISPR expression can be achieved, making it a universal scientific tool. As the focus was the reprogramming of astrocytes into neurons the *Gfap-Cre* reporter line was used. In the double-transgenic *dCAM x Gfap-Cre* line the combinations *Ascl1*, *Lmx1a*, *Nr4a2* and *Ascl1*, *Lmx1a*, *NeuroD1* could robustly be activated in primary astrocytes. Activation levels between different genes exhibited huge variability, which may be explained due to chromatin accessibility, baseline gene expression and different gene regulatory elements [81, 82, 107]. Furthermore, it was reported that depending on the position and number of sgRNAs used, the level of activation can be titrated. [108]. This is in line with experiences made in our laboratory, based on these results two sgRNAs per gene were used.

6.2 Advancement of the aCRISPR system to a universal species-independent AAV-based tool – *AAV-dCAS*

After confirming the technical and biological functionality of the aCRISPR approach, we expanded the toolbox by developing an AAV-based split-dCas9/SAM system (*AAV-dCAS*), making it versatile and applicable across species barriers by minimal modifications [94]. The N- and the C-terminal part were packed into two different AAVs, to ensure cell-type specific expression, a FLEx-N-dCas9 was used [62]. Most aCRISPR systems consist of activators directly coupled to the dCas9, as this necessarily results in a coding sequence exceeding the packaging limit of the AAV, the synergistic activation mediator (SAM) system was used, in which activators are separated from the dCas9 and can be packed in a separate AAV [81]. When comparing full-length versus split-version no difference in efficiency of endogenous gene activation was noticed. In primary astrocytic cultures it was possible to efficiently activate up to five endogenous genes, while the maximum limit of genes possible to be activated was not tested, it could be demonstrated that already complex gene combinations are feasible. Compared to the *dCAM* system, less activator domains are included, as the AAV packaging limit did not enable the additional fusion of the VPR activators. However, *in vitro* experiments confirmed that for most genes activation levels did not differ between the usages of the SAM system only or in combination with the VPR activators.

With this system, up to four AAVs are necessary to co-transduce *in vivo*, which might lower efficiencies, however when comparing *in vivo* data from the *dCAM* and the *AAV-dCAS* model, results were reproducible and consistent. Furthermore, in a recently published paper using the same split-intein mediated Cas9 system, but for base editing, high *in vivo* editing efficiencies suggest high rates of co-transductions and effective intein-mediated trans-splicing [109].

So far, with this aCRISPR system the dCas9 is constitutively expressed using the CBh promoter. However, fast and easy adaptions, for example by using different promoters, might enable transient expression and further flexibility and temporal control of gene activation, as well as an adaption of the system for gene therapeutic usage.

6.3 Toxin-induced (6-OHDA) mouse model

In the *in vivo* setup a toxin-induced acute PD model was used. 6-Hydroxydopamine was unilaterally injected into the medium forebrain bundle to achieve fast and irreversible dopaminergic neuron depletion in the ventral midbrain accompanied with the degeneration of the ipsilateral dopaminergic projections to the striatum. Due to structural similarities to dopamine, the toxin is specifically uptaken by the dopaminergic neurons, which then degrade due to the formation of excessive reactive oxygen species and toxic quinines [110]. The

degradation of the dopaminergic neurons by the axonal toxin administration leads to increased reactive gliosis in the striatum [111, 112]. The enhanced astrogliosis pushes the astrocytes into a more immature state, in which they acquire stem-cell-like properties and are more susceptible to be reprogrammed into another cell type [56, 92, 113, 114].
The toxin-induced model was favored over the published PD mouse models, which are based on the genetic alterations observed in PD patients, as none of them recapitulate full disease symptoms, like loss of dopaminergic neurons [115]. However, to test our system also in a chronic PD model and to circumvent the problematic of genetic PD models, it is also worked on a new artificial PD model, in which *Caspase8-ERT2* is knocked-in into the *PITX3* locus, whereupon administration of tamoxifen, degeneration can be induced over time. However, so far, the mouse line is not characterized in detail [116].

6.4 Starter cell population and reprogramming environment

During development different neuronal subtypes are established from radial glia cells, due to the specific expression of transcription factors [117, 118]. The *Gfap-Cre* mouse line was choosen, which expresses *Cre* rebombinase under the murine promoter of GFAP, to target astrocytes for the cellular conversion. As they maintain some original patterning from the radial glia ancestors, they are an appropriate candidate for reprogramming.
Additionally, in a recently published paper from Rivetti di Val Cervo *et al.* it was shown that astrocytes can be reprogrammed into dopaminergic neurons *in vivo* [63]. In a different publication, in which $NG2^+$ oligodendrocyte precursor cells were chosen as starter cell population, reprogramming into dopaminergic neurons was not possible by forced expression of *Ascl1*, *Lmx1a* and *Nr4a2* [119]. Based on this data the *Gfap-Cre* reporter line was applied in this study.
Surprisingly, despite applying the dopaminergic neuron specifying factors *ALN*, immunohistochemistry and scRNA-seq data revealed a GABAergic identity of the induced neurons. This data suggest that the reprogramming of striatal glial cells into striatal, functional and integrated GABAergic neurons, may be a consequence of region-specific induction of reprogramming factors. Though, the striatal niche-specific environment might impinge on reprogramming mechanisms and thus influence the outcome of the reprogramming process [120].

6.5 *In vivo* activation of endogenous genes and direct astrocyte to neuron conversion

Degenerative diseases are correlated to the loss of a specific cell population, restoring these populations by direct cellular reprogramming requires the expression of several transcription factors. Although efficient conversion has been reported in cell culture experiments, *in vivo* studies remain challenging [46, 62, 121]. AAVs are used as vehicles for *in vivo* experiments, as they exhibit low immunogenicity and are already applied in clinical studies, however its low packaging capacity hinders multiplexed transgene expression [93]. With the two newly introduced systems it is possible to easily activate several endogenous genes *in vivo* by using a small number of AAVs.

Notably both aCRISPR systems led to successful reprogramming of astrocyte into induced neuron, with comparable efficiencies. Two cocktails of pro-neuronal transcription factors were used, known to convert somatic cells into dopaminergic neurons [61, 63]. At 5 wpi both combinations showed similar levels of conversion, with time an increase in reprogrammed neurons was observed for the transcription factor combination *Ascl1*, *Lmx1a* and *Nr4a2.* For this approach, not only cell number, but also functional properties matured, as indicated by electrophysiological measurements. However, the combination *Ascl1*, *Lmx1a*, *NeuroD1* and miRNA218 even at 13 wpi exhibited electrophysiological properties of astrocytes or immature neurons, with stagnated numbers of converted neurons.

The divergent results achieved for both transcription factor combinations, might be explained by the different pathways stimulated by the activation of *Nr4a2*, respectively *NeuroD1* and the expression of miRNA218 [122-124]. A recently published paper from Mattugini *et al*. showed a strong increase in reprogramming efficiency when *Nr4a2* was co-expressed in addition to other pro-neuronal factors [85]. As during reprogramming cells undergo a metabolic switch, accompanied with high levels of reactive oxygen species, the high conversion efficiency could be explained due to the anti-inflammatory effects mediated by NR4A2 [49, 59, 125]. However, the different efficiencies might also be explained due to different reprogramming kinetics, eventually the *ALNe-218* condition promotes a slower conversion and later time points need to be examined.

6.6 Induced neurons display a GABAergic subtype specification

Characterization of reprogrammed neurons was performed using scRNA-seq and immunohistochemical analysis, both techniques revealed a GABAergic identity of the induced neurons. To further specify the GABAergic subtype, immunohistochemical stainings were performed, as the low capture efficiency of the scRNA-seq experiment did not reveal further

inside into neuronal characteristics. Reprogramming was performed within the striatum, where about 95% of existing neurons are medium spiny neurons, therefore the influence of the direct microenvironment on the cellular reprogramming was investigated. Reprogrammed neurons were stained with the medium spiny neuron marker DARPP32. When comparing the control condition to both reprogramming conditions, only a minor fraction reprogrammed into DARPP32$^+$ neurons, excluding a transdifferentiation into the main neuronal population [48, 126].

Staining was performed for all classical GABAergic interneuron subtypes, such as parvalbumin, neuropeptide Y and calretinin, and for the cholinergic CHAT$^+$ interneurons. However, reprogrammed neurons were not positive for any of these markers. In a recently published paper from Pereira *et al*., NG2$^+$ oligodendrocyte precursors were successfully reprogrammed into PV$^+$ interneurons, when using the same reprogramming factors *ALN*. The distinct starter cell population, as well as the different reprogramming method (aCRISPR vs. transgene overexpression) might explain these differences [119]. Different neurotransmitter markers were addressed as well, by staining TH for dopaminergic and noradrenergic neurons, and vGLUT1 for glutamatergic neurons. In treatment, as well as in control groups, some spontaneously arising exogenous TH$^+$ neurons in the striatum were detected, which might emerge due to toxin-induced DA-denervation, or represent naturally occurring TH$^+$ interneurons within the striatum, however none of the reprogrammed neurons expressed the dopaminergic marker [119, 127, 128]. In a previously reported study, the factor combination *ALNe-218* led to high amounts of TH$^+$ reprogrammed neurons [63]. In this report forced overexpression of factors was used to initiate reprogramming, dynamics and timing might be different from the aCRISPR induced transdifferentiation, thus eventually different time point need to be examined. However, in contrast to the published data in the present study the FLEx-GFP marker was employed, to allow the definite identification of induced neurons and its demarcation from reprogramming independent TH$^+$ neurons. Whereas in the publication the original fate of the reported TH$^+$ neurons was not addressed, leaving their emergence in uncertainty.

To further clarify the GABAergic subtype identity a scRNA-seq experiment with higher solution will be performed.

6.7 Reprogrammed neurons exhibit mature electrophysiological properties with the *ALN* reprogramming condition

Electrophysiological analysis revealed the different stages of neuronal maturation between the two reprogramming conditions *ALN* and *ALNe-218*. Whereas *ALNe-218* induced neurons at 13 wpi still showed patterns of glial cells/immature neurons, showed *ALN* induced neurons

properties of mature neurons, integrated within the striatal network, as shown by the synaptic inputs. This difference may be explained due to the different reprogramming kinetics executed by the various reprogramming factor combinations. Over time *ALN*-induced neurons acquired a decreased input resistance indicating that the cells achieve more ion channels and gain a more mature morphology [45, 119].

To further characterize the *de novo* generated neurons their electrophysiological characteristics are compared to endogenous neurons. The measured electrophysiological properties, like firing pattern, resting membrane potential and input resistance are rather different from endogenous medium spiny neurons and do not exhibit standard electrophysiological properties of this particular neuronal subtype. This indicates that the reprogrammed neurons presumably differentiate into a distinct GABAergic interneuron population, capable of modulating striatal circuits [129-132].

6.8 *ALN* induced GABAergic neurons lead to measurable phenotypical changes and amelioration of disease symptoms

The difference in the ability for cell-fate conversion at 13 wpi, detected between the two reprogramming conditions, was even reflected in the direct phenotypical output. An improvement in voluntary movement, as well as a balancing in axial symmetry could be observed with the *ALN* condition. In an independent PD test, the vertical pole test, motor coordination was examined and repeatedly a trend for the improvement of motor behavior for *ALN* treated animals was observed, whereas *ALNe-218* treated animals showed patterns similar to *GFP* controls. To investigate the dopamine-dependent motor phenotype, the drug-induced circling behavior was accessed, a standard test for unilateral 6-OHDA mouse models [103]. Lesion-induced specific rotation behavior was measured for the dopamine agonist apomorphine (data not shown), as well as for the dopamine releaser substance amphetamine, however, for both reprogramming conditions no phenotypical rescue was achieved, suggesting a rescue in voluntary motor behavior independent of the dopaminergic system. These behavioral changes could be confirmed in both aCRISPR approaches. Our results are contradictory to a study from Rivetti di Val Cervo *et al*. showing a behavior improvement with the *ALNe-218* condition, by a rescue in dopamine-dependent circling behavior, which we do not observe, and an amelioration in motor behavior. In this study, gait was assessed using a treadmill setup, in which movement of animals in enforced, in our study the voluntary movement of the mice was analyzed, a parameter far more affected in PD patients [63]. Differences in results might be explained due to the different setups.

The striatum is the central input structure of the basal ganglia, implicated in motor planning and behavior [133]. In a very simplified depiction, the main output is mediated by the

striatonigral (direct, D1-MSN mediated) and the striatopallidal (indirect, D2-MSN) pathway. The assumption, that in PD, dopamine denervation leads to an imbalance between the two pathways, with increased striatopallidal output and associated disrupted gait, is widely accepted [134, 135]. In a study from Kravitz *et al.* optogenetic activation of the striatonigral D1-MSN mediated pathway led to ameliorated gait alterations in a 6-OHDA treated mouse model, comparable to the observations made in this study [31]. This indicates that by balancing the D1- and D2-mediated output signals DA-denervation induced behavior can be rescued.

Additionally, it has been reported that dopamine depletion in 6-OHDA treated rodent models has a strong effect on striatal circuits. Specifically, increased excitatory cholinergic and reduced inhibitory GABAergic signals have been noticed [136]. Furthermore, most of the basal striatal excitatory drive arising from cholinergic interneurons is balanced by a concomitant GABAergic inhibition, whereat this signaling is impaired by dopamine deprivation [137]. Another study showed, that integrity of the fast spiking striatal GABAergic interneurons depends on the dopaminergic input from the SN*pc,* and dopamine deprivation leads to their degradation [138]. Altogether, these reports, as well as findings revealed in this study, suggest, that the imbalance in striatal microcircuitry - including impaired GABAergic signaling - contribute to the altered motor behavior in parkinsonian state. Therefore, restoration or reinforcing of GABAergic inhibition in the striatum represents an attractive, novel therapeutic concept for PD.

However, still much of the complex striatal circuits is unknown, leaving open questions about the definite action of the *de novo* generated neurons. This might be further addressed by retro- and anterograde tracing, as well as optogenetic manipulation of the reprogrammed cells.

7 Conclusion and Future Perspectives

Using the aCRISPR platform was sufficient to activate multiple endogenous genes, leading to adequate overexpression of functional protein to provide the basis for astrocyte to induced neuron conversion. The newly generated GABAergic neurons exhibit functionality and integrity, leading to a measurable phenotypical change and amelioration of disease symptoms. Two independent aCRISPR settings were developed, leading to consistent results. The generated *dCAM* mouse line, serves as an excellent screening tool to find new gene combinations to transdifferentiate any cell into another specific cell type. As up to six endogenous genes can be activated simultaneously by using only one AAV, the results are highly standardized and uniform, excluding influences dependent on viral co-transductions. With the *AAV-dCAS* setting, a higher flexibility is achieved, as the AAV-based system can easily be used in other model organisms, as non-human primates, and as an ultimate goal also in human therapy. With the *AAV-dCAS* system, also the transgenic dCas9 expression could be silenced by using cell-type specific promoters, as feasible for our setup the *Gfap* promoter. In further studies this possibility shall be elucidated.
With the reprogramming condition *ALN* it was possible to generate a sufficient amount of *de novo* generated neurons, which are able to ameliorate 6-OHDA associated gait alterations. Interestingly, these induced neurons exhibited a GABAergic identity, suggesting a possible dopamine-independent rescue of parkinsonian motor behavior by interfering into striatal circuits downstream of dopamine. Using retro- and anterograde tracing methods neuronal connectivity will be elucidated, to identify the specific striatal circuits altered by the reprogrammed neurons.

Altogether this thesis provides new genetic tools able to create new functional neurons *in situ*, evaluating the aCRISPR system as a potent technology for *in vivo* usage. Furthermore, a novel GABAergic neuron-based treatment strategy was discovered, possibly applicable in PD therapy.

8 Material and Methods

8.1 Material

Table 1 Chemicals

Description	Catalogue Number	Supplier
2-Mercaptoethanol	M7522	Sigma-Aldrich
3,3´-Diaminobenzidine tetrahydrochloride	D5637	Sigma-Aldrich
4´,6-Diamidin-2-phenylindol	62248	Thermo Fisher Scientific
Acetic acid	71251	Sigma-Aldrich
Agar	05040	Sigma-Aldrich
Agarose	870055	Biozym
Ampicilline	11593-027	Thermo Fisher Scientific
Bovine serum albumin	A7906	Sigma-Aldrich
D-(+)-Glucose	G8270	Sigma-Aldrich
dCTP, [α-32P]- 3000Ci/mmol 10mCi/ml EasyTide Lead, 250 µCi	NEG513H250UC	PerkinElmer
Rapid-hyb Buffer	RPN1636	Merck Millipore
Dimethyl sulfoxide	A994.1	Carl Roth
Ethanol	1.00983.2500	Merck Millipore
Ethidium bromide	2218.2	Carl Roth
Ethylene glycol	2441	Carl Roth
Ethylenediaminetetraacetic acid	798681	Sigma-Aldrich
Glycerol	G9012	Sigma-Aldrich
Hydrochloric acid	435570	Sigma-Aldrich
Hydrogen peroxide solution	H1009	Sigma-Aldrich
Isopropanol	109634	Merck Millipore
Kanamycin sulfate	11815024	Thermo Fisher Scientific
Methanol	1.06009.2500	Merck Millipore
Milk powder	70166	Sigma-Aldrich
Paraformaldehyd	158127	Sigma-Aldrich
Sodium chloride	S7653	Sigma-Aldrich
Sodium citrate	1613859	Sigma-Aldrich
Sodium Deoxycholate	D6750	Sigma-Aldrich
Sodium dodecyl sulfate	L3771	Sigma-Aldrich
Sodium hydroxide	221465	Sigma-Aldrich
Sucrose	S7903	Sigma-Aldrich
Triton X-100	T9284	Sigma-Aldrich
Trizma® base	T1503	Sigma-Aldrich
Trizma® hydrochloride	T5941	Sigma-Aldrich
Tryptone	T7293	Sigma-Aldrich
Tween 20	P1379	Sigma-Aldrich
Water for embryo transfer	W1503	Sigma-Aldrich
Xylol	9713.1	Carl Roth
Yeast extract	Y1625	Sigma-Aldrich

Table 2 Cell culture media and supplements

Description	Catalogue number	Supplier
B27 serum-free supplement	17504044	Thermo Fisher Scientific
BDNF	203702	Merck Millipore

FGF-Basic Recombinant Mouse Protein-10 µg	PMG0034	Thermo Fisher Scientific
DMEM/F12, GlutaMAX supplement	31331	Thermo Fisher Scientific
Dulbecco´s Modified Eagle Medium	21969	Thermo Fisher Scientific
Dulbecco´s phosphate-buffered saline	14190169	Thermo Fisher Scientific
EGF	E4127	Sigma-Aldrich
Fetal bovine serum	A2153	Thermo Fisher Scientific
Forskolin	F3917	Sigma-Aldrich
GlutaMAX supplement	35050061	Thermo Fisher Scientific
Hank´s Balanced Salt Solution, Mg^{2+}/Ca^{2+} free (HBSS)	14175-053	Thermo Fisher Scientific
Horse serum	16050-122	Thermo Fisher Scientific
Lipofectamine 2000	11668-019	Thermo Fisher Scientific
Opti-MEM I	31985-047	Thermo Fisher Scientific
Penicillin-Streptomycin	15140122	Thermo Fisher Scientific
Poly-D-lysine hydrobromide	P7886	Sigma-Aldrich
Trypsin-EDTA (0,05%), phenol red	25300054	Thermo Fisher Scientific
Trypsin-EDTA (0.25%), phenol red	25200056	Thermo Fisher Scientific

Table 3 Surgery materials

Description	Catalogue number	Supplier
Detaisodona® Lösung (Povidon-Jod)		Mundipharma
2% Lidocainhydrochlorid	6357796.00.00	Bela-pharm
6-Hydroxydopamine hydrochloride	H4381	Sigma-Aldrich
Amphetamine sulfate		Th. Geyer
Apomorphine hydrochloride	1041008	Sigma-Aldrich
Atipazole 5 mg/ml (Atipamezol)		Prodivet
Bepanthen Augen- und Nasensalbe		Bayer
L-Ascorbic acid	A92902	Sigma-Aldrich
Sedin® 1 mg/ml (Medetomidinhydrochlorid)		Alvetra GmbH
Metamizol 500 mg/ml		WDT
Dormicum® 5 mg/ml (Midazolam)		Roche Pharma AG
Chirlac (Nahtmaterial)	PG0203	Chirmax GmbH
Glass capillaries	504949	World Precision Instruments
Rotilabo®-Wattestäbchen	272-EH11.1	Karl Roth
Absorption Triangles - Unmounted / Sterile	18105-03	Fine Science Tools
Paraffin oil	18512	Sigma-Aldrich
Injekt®-F 1 ml Einmalspritzen	5000754	Braun
Flumazenil 0.1 mg/ml		Hexal AG
0.9% NaCl solution	04499344	Braun
Melosus 1.5 mg/ml	126	CP-Pharma
Fentanyl Piramal 0,1 mg, Injektionslösung		Piramal

WS-Kugelfräser, grobe Verzahnung Ø 0,3 mm	329586	Flume Technik

Table 4 Cell lines

Description	Catalogue number	Supplier
HEK293	CRL-1573	ATCC
Neuro2A	CCL-131	ATCC

Table 5 Primary antibodies

Description	Dilution	Catalogue number	Supplier
Ascl1	ICC 1:1000	556604	BD Bioscience
Calretinin	IHC 1:1000	CR7697	Swant
C-Cas9	WB: 1:1000	NBP2-52398SS	Novus biologicals
CHAT	IHC 1:100	AB144P	Merck Millipore
DARPP32	IHC 1:500	ab40801	Abcam
GAD65/67	IHC 1:500	ab49832	Abcam
GFAP	IHC 1:1000	ab7260	Abcam
GFP	IHC 1:1000	ab13970	Abcam
HA tag (C29F4)	WB 1:500	3724	Cell Signaling
Lmx1a	ICC 1:2000	ab10533	Merck Millipore
MAP2	IHC 1:500 ICC 1:500	ab5622	Abcam
N-Cas9	WB: 1:500	A-9000	Epigentek
NeuN	IHC 1:1000	ab104224	Abcam
Neuropeptide Y	IHC 1:1000	ab30914	Abcam
Nr4a2	ICC 1:2000	sc-376984	Santa Cruz
P2A	WB 1:1000	ABS31	Sigma
Parvalbumin	IHC 1:1000	P3088	Sigma
TUJ1	IHC 1:500 ICC 1:500	ab18207	Abcam
Tyrosine hydroxylase	IHC 1:500 DAB 1:10000	P40101	PelFreeze
vGLUT1	IHC 1:1000	AMAb91041	Atlas
B-Actin	WB 1:10000	GTX26276	GeneTex

Table 6 Secondary antibodies

Description	Conjugate	Dilution	Catalogue number	Supplier
Donkey anti-guineapig	Alexa 594	IHC 1:500	11076	Thermo Fisher Scientific
Donkey-anti-chicken	Alexa 488	IHC 1:250 ICC 1:250	703-546-155	Dianova
Donkey-anti-mouse	Alexa 594	IHC 1:500 ICC 1:500	A-21203	Thermo Fisher Scientific
Donkey-anti-rabbit	Alexa 594	IHC 1:500 ICC 1:500	A-21207	Thermo Fisher Scientific
Goat-anti-mouse	HRPO	WB 1:5000	115-035-003	Dianova
Goat-anti-rabbit	HRPO	WB 1:5000	111-035-003	Dianova
Goat-anti-rabbit	Biotin-SP	DAB 1:300	303-225-003	Dianove

Table 7 Enzymes

Description	Catalogue Number	Supplier
BamHI	R3136	New England Biolabs
BbsI	R0539	New England Biolabs
BsiWI	R0553	New England Biolabs
BsmBI	R0580	New England Biolabs
EcoRI-HF	R3103	New England Biolabs
NotI-HF	R3189	New England Biolabs
RsrII	R06501	New England Biolabs
SbfII	R3642	New England Biolabs
AgeI	R0552	New England Biolabs
DpnI	R0176	New England Biolabs
EcoRV-HF	R3195	New England Biolabs
PmeI	R0560	New England Biolabs
PmlI	R0532	New England Biolabs
Proteinase K	A3830	AppliChem
T4 DNA Ligase	M0202	New England Biolabs
XhoI	R0146	New England Biolabs

Table 8 Kits

Description	Catalogue numbers	Supplier
ABC Peroxidase Standard Staining Kit	32020	Thermo Fisher Scientific
Adult Brain Dissociation Kit, mouse and rat	130-107-677	Miltenyi Biotec
Anti-ACSA-2 MicroBead Kit, mouse	130-097-678	Miltenyi Biotec
cOmplete™, EDTA-free Protease Inhibitor Cocktail	04693132001	Roche
KAPA HiFi HotStart PCR Kit	KR0369	KAPA Biosystems
mirVana™ miRNA Isolation Kit, with phenol	AM1560	Thermo Fisher Scientific
NEBuilder HiFi DNA Assembly Cloning Kit	E5520	New England Biolabs
N-Per™ Neuronal Protein Extraction Reagent	87792	Thermo Fisher Scientific
Phusion High-Fidelity PCR Master Mix	F531S	Thermo Fisher Scientific
Pico Pure RNA Isolation Kit	KIT0204	Thermo Fisher Scientific
Pierce BCA Protein Assay Kit	23225	Thermo Fisher Scientific
Q5 High-Fidelity 2x Master Mix	M0492	New England Biolabs
QIAprep Spin EndoFree Maxiprep Kit	12362	Qiagen
QIAprep Spin Miniprep Kit	27104	Qiagen
QIAquick Gel Extraction Kit	28704	Qiagen
QIAquick PCR Purification Kit	28104	Qiagen
QuickChange Lightning Site-Directed Mutagenesis Kit	210518	Agilent
Rediprime II DNA Labeling System	RPN1633	GE Healthcare
RNeasy Plus Mini Kit	74134	Qiagen
Single Cell 3´Library & Gel Bead Kit v2	PN-120237	10x Genomics
SuperScript® VILO cDNA Synthesis Kit	11755050	Thermo Fisher Scientific

TaqMan Gene Expression Assay	4331182	Thermo Fisher Scientific
TaqMan™ Universal Master Mix II, no UNG	4440043	Thermo Fisher Scientific
TOPO TA Cloning Kit	45-0640	Thermo Fisher Scientific
VWR Taq DNA Pol. 2x Master Mix, 1.5 mM MgCl2	733-1316	VWR
Wizard Genomic DNA Purification Kit	A1125	Promega
Papain Dissociation System	LK003150	Worthington

Table 9 Composition of buffers and solutions

Description	Constituents
10x TBS	100 mM Tris base 1.4 M NaCl Add water to 1 l Adjust pH to 8
1x MOPS Running buffer	50 ml MOPS Buffer (20x, BioRad) Add water to 1 l
1x TBS-T	100 ml 10x TBS 1 mL Tween20 Add water to 1 l
Agar plates	10 g Tryptone 5 g Yeast extract 10 g NaCl 15 g Agar Add water to 1 l Adjust to pH 7
Astrocyte medium	DMEM/F-12, GlutaMAX supplement 10% FBS 5% Horse serum 45 mg/ml Glucose 1x B27 supplement 10 ng/ml FGF 10 ng/ml EGF 1% Penicillin/Streptomycin
Astrocyte reprogramming medium	DMEM/F-12, GlutaMAX supplement 45 mg/ml Glucose 1x B27 supplement 1% Penicillin/Streptomycin 25 µM Forskolin 20 ng/ml BDNF, every fourth day
Blocking buffer (IHC)	0.1 M PBS pH 7.4 1% BSA 0.5% Triton X-100
Blocking buffer (WB)	1x TBS-T 5% Milk powder
Cell culture freezing medium	50% FBS 10% DMSO 40% DMEM/F-12, GlutaMAX supplement
Cryo protection solution	125 ml Glycerol 125 ml Ethylene glycol 250 ml 0.1 M PBS pH 7.4
DAB working solution	0.1M Tris-HCl 0.02% H_2O_2 0.05% DAB
Denaturation solution (Southern Blot)	0.5 M NaOH

	1.5 M NaCl
Fibroblast medium	DMEM/F-12, GlutaMAX supplement 10% FBS 1% Penicillin/Streptomycin
Growth medium HEK293, Neuro2a cells	DMEM/F-12, GlutaMAX supplement 10% FBS
LB medium	10 g Tryptone 5 g Yeast extract 10 g NaCl Add water to 1 l Adjust pH to 7
Neutralization solution (Southern Blot)	0.1 M Tris-HCl pH 7.5 0.5 M NaCl
RIPA buffer	50 mM Tris-HCl 150 mM NaCl 1% Triton X-100 0.5% Sodium deoxycholate 0.1% Sodium dodecyl sulfate 3 mM EDTA Freshly add phosphatase/protease inhibitors
20x SSC	3 M NaCl 0.3 M sodium citrate pH 7.0
TAE buffer	40 mM Tris base 20 mM Acetic acid 1 mM EDTA
TE buffer	10 mM Tris HCl 1 mM EDTA Adjust to pH 8
Wash solution I,II,III (Southern Blot)	2 x SSC, 0.5 x SSC, 0.1 x SSC, 0.1% SDS

Table 10 Consumables

Description	Catalogue Number	Supplier
10x Tris/Glycine Buffer	1610771	BioRad
Amersham ECL Western Blotting Detection Reagent	RPN2106OL/AF	GE Healthcare
Aqua-Poly/Mount	10606	Polysciences
Cell scraper	83.1830	Sarstedt
Cover slips	1001/14	Karl Hecht
Criterion XT 4-12% Bis-Tris Gel	3450124	BioRad
DNA Gel Loading Dye (6X)	R0611	Thermo Fisher Scientific
EasYFlask 225 cm²	159934	Thermo Fisher Scientific
EasYFlask 25 cm²	156367	Thermo Fisher Scientific
EasYFlask 75 cm²	156499	Thermo Fisher Scientific
Framestar 384	4ti-0384/C	4Titude
GeneRuler 1 kb DNA Ladder	SM0311	Thermo Fisher Scientific
GeneRuler 100 bp DNA Ladder	SM0243	Thermo Fisher Scientific
HBSS - Hank's Balanced Salt Solution	14025092	Thermo Fisher Scientific
Immobilion-P PVDF Membrane	IPVH00010	Merck Millipore
MACS SmartStrainers (70 µm)	130-098-462	Miltenyi Biotec
MS Columns	130-042-201	Miltenyi Biotec
Multi-well plate, 24 well	353047	Corning

Multi-well plate, 6 well	353046	Corning
Neg-50 medium	6502	Thermo Fisher Scientific
NuPAGE™ LDS Sample Buffer (4X)	NP0007	Thermo Fisher Scientific
Pertex	41-4010-00	Medite
Protein Marker VI	A8889	AppliChem
Skim milk powder	1153630500	Merck Millipore
S.O.C. medium	15544034	Thermo Fisher Scientific
Whatman cellulose chromatography papers	101085004	Agilent
XT MOPS Running Buffer	1610788	BioRad

Table 11 Bacterial strains

Description	Catalogue number	Supplier
DH5α	18265017	Thermo Fisher Scientific
NEB stable	C3040I	New England BioLabs
One Shot® TOP10	C404010	Thermo Fisher Scientific
XL10-Gold Ultracompetent Cells	200315	Agilent Technologies

Table 12 Mouse lines

Description	Supplier
B6.Cg-Tg(Gfap-Cre)77.6Mvs/2J	Jackson Laboratories
C57Bl6/N	Charles River
dCAM/N	Generated at Helmholtz Zentrum München (IDG) by author of this thesis

Table 13 gRNA sequences

Name	Gene	Sequence 5´- 3´
Ascl1-1	Ascl1/Mash1	GGGAGCCGCTCGCTGCAGCAGCG
Ascl1-2	Ascl1/Mash1	GGGGCTGAATGGAGAGTTTGCA
Ascl1-3	Ascl1/Mash1	GAGTTTGCAAGGAGCGGGCG
Lmx1a-1	Lmx1a	GGGAGCAAAGGAGTCGCCTTG
Lmx1a-2	Lmx1a	GAATGCATCCAAGAGTGAACC
Nr4a2-1	Nr4a2/NR4A2	GGCGGTGGGTCATTGTTTCCG
Nr4a2-2	Nr4a2/NR4A2	GTGCCAGTGACGCCGGCCTGG
NeuroD1-1	NeuroD1	GGTTCTGGGAGGGGTGAATGA
NeuroD1-2	NeuroD1	GGCCATATGGCGCATGCCGGGG
Neurog2-1	Neurog2/Ngn2	ATAAGCTGGGGAGGGAGAGC
Neurog2-2	Neurog2/Ngn2	AAACAATCAGATCTGCCCCG
Neurog2-3	Neurog2/Ngn2	GGGAGAGGGACTAAAGAAA
PITX3-1	PITX3	ATTCACTTTATGGCAACCCA
PITX3-2	PITX3	GCTAGCCTGGGAGAGCCCAG
FoxA2-1	FoxA2	GAAAGTAACCTTGAAACACCG
FoxA2-2	FoxA2	GGGTAGCCAGAAAGAGGACTG
MyoD1-1	MyoD1	CCAATAGGAGTGTAGTAGGG
MyoD1-2	MyoD1	GAGAGACTGGCAGCCATACG
Pou5f1-1	Pou5f1	ATCTGCCTGTGTCTTCCAGA
Pou5f1-2	Pou5f1	TGTCCGGTGACCCAAGGCAG

Table 14 Southern blot Rosa 5´probe

Sequence 5´- 3´
aaggatactggggcatacgccacagggagtccaagaatgtgaggtgggggtggcgaaggtaatgtctttggtgtggGaaaagcagcag ccatctgagataggaactggaaaaccagaggagaggcgttcaggaagattatggaggggaggactgggcccccacgagcgaccaga gttgtcacaaggccgcaagaacaggggaggtgggggctcagggacagaaaaaaaagtatgtgtattttgagagcagggttgggaggc ctctcctgaaaagggtataaacgtggagtaggcaatacccaggcaaaaaggggagaccagagtagggggaggggaagagtcctgac ccagggaagacattaaaaaggtagtggggtcgactagatgaaggagagcctttctctctgggcaagagcggtgcaatggtgtgtaaaggt agctgagaag

Table 15 TaqMan probes

Gene	TaqMan probe (Assay ID)
Ascl1/Mash1	Mm03058063_m1
Lmx1a	Mm00473947_m1
Nr4a2/NR4A2	Mm00443060_m1
NeuroD1	Mm01280117_m1
Ngn2	Mm00437603_g1
PITX3	Mm01194166_g1
FoxA2	Mm00839704_mH
MyoD1	Mm00440387_m1
Pou5f1	Mm00658129_gH
B-Actin	Mm00607939_s1

Table 16 Genotyping primers

Mouse line	Forward primer (5´-3´)	Reverse primer (5´-3´)	T_a [°C]	t_E [s]
B6.Cg-Tg(Gfap-Cre)77.6Mvs/2J	atcccaggagccagcaga	gttgcatcgaccggtaatg	54	30
dCAM/N	tcttcggcaacatcgtggacg	cggttcttgtcgcttctggtcagca	58	150

Table 17 DNA vectors

Description	Catalogue number	Supplier
pAAV-MB-Flex-NCas9(D10A-SpCas9$^{2-573}$)-sgRNA1-Ascl1	N/A	Available at IDG, generated for this thesis
pAAV-MB-CCas9-VP64 (N863A-Sp-Cas9$^{574-1368}$)-sgRNA2-Ascl1	N/A	Available at IDG, generated for this thesis
pAAV-SAM-sgRNA1/2-Lmx1a/Nr4a2	N/A	Available at IDG, generated for this thesis
pAAV-SAM-sgRNA1/2-Lmx1a/NeuroD1	N/A	Available at IDG, generated for this thesis
pAAV-SAM-sgRNA1/2-Neurog2/Nr4a2	N/A	Available at IDG, generated for this thesis
pAAV-SAM-EF1α-mir9/mir124	N/A	Available at IDG, generated for this thesis
pAAV-SAM	N/A	Available at IDG, generated for this thesis
pAAV-CBh-Flex-GFP (No.697)	N/A	Available at IDG, generated by Lao Chu Lan
pAAV-Syn-Flex-GFP (No.696)	N/A	Available at IDG, generated by Lao Chu Lan
pAAV-CBh-Flex-GFP-mir218	N/A	Available at IDG, generated for this thesis

pAAV-CBh-Flex-GFP-sgRNA1/2-PITX3/FoxA2	N/A	Available at IDG, generated for this thesis
pAAV-CBh-Flex-GFP-sgRNA1/2-Ascl1/Lmx1a/Nr4a2	N/A	Available at IDG, generated for this thesis
pAAV-CBh-Flex-N-GFP$^{1-642}$-sgRNA1/2-Ascl1/Lmx1a/NeuroD1	N/A	Available at IDG, generated for this thesis
pAAV-CBh-C-GFP$^{643-714}$-mir218	N/A	Available at IDG, generated for this thesis
pLenti-sgRNA(MS2)_zeo backbone (SAM)	61472	Addgene [81]
pLenti-MS2-p65-HSF1_Hygro (SAM)	61426	Addgene [81]
pLenti-CAG-dCas9 (D10A/H841A)-VPR	N/A	Available at IDG, generated by Jeffrey Truong
pRosa26-dCas9(D10A/H841A)-VPR-P2A-SAM	N/A	Available at IDG, generated for this thesis

Table 18 Equipment

Description	Supplier
ABI Prism 7900 HT Real-Time PCR System	Applied Biosystems
AxioCAm HRc camera	Zeiss
Axioplan2 microscope	Zeiss
CatWalk XT	Noldus
Centro LB 960 Luminometer	Berthold Technologies
ChemiDoc MP imaging system	BioRad
Confocal LSM880	Zeiss
Digital Just for Mouse Stereotaxic Instrument	Stoelting
Farbkamera acA1300-60gm	Basler
Gel-Documentation system E.A.S.Y Win32	Herolab
High Speed Rotary Micromotor Kit, K.1070 with 2.35mm (3/32") or K.107018 with 1/8" Collet	Laboratory Equipment
Microm HM 560 Cryostat	Thermo Fisher Scientific
NanoDrop® Spectrophotometer ND-1000	PeqLab
Nanoliter Injector with SMARTouch Controller	World Precision Instruments
NovaSeq6000	Illumina
PCR Gelelectrophoresis chambers	Peqlab
Rodent Warmer Control Box	Stoelting
Rotarod	Bioseb
Stereoinvestigator Zeiss Imager M2	Zeiss
Thermo cycler Mastercyler pro	Eppendorf
Transilluminator	Herolab
Western Blot Mini Trans-Blot® Cell	Thermo Fisher Scientific

Table 19 Software

Description	Supplier
Ethovision XT 14	Noldus
CatWalk XT	Noldus
GraphPad Prism 6	Graphpad Software, Inc.
SDS 2.4.1	Applichem
Vector NTI® Advance 11.5.2	Invitrogen
Stereoinvestigator Version 2019.1.3	MBF Bioscience
Image Lab 6.0	BioRad
Zen 2.3 SP1	Zeiss

8.2 Methods

8.2.1 Molecular methods

8.2.1.1 Cloning

miRNA218 construct was cloned according to Rivetti di Val Cervo *et al.* [63].

Polymerase Chain Reaction

PCRs are performed using the Q5 High-Fidelity 2x Master Mix. For the amplification of GC-rich regions the KAPA HiFi HotStart PCR Kit was used. For colony PCR and genotyping reactions VWR Red Taq DNA Polymerase Master Mix was deployed. Primer sequences, annealing temperatures and elongation times for mouse genotyping are listed in Table 16. For STAgR cloning the Phusion High-Fidelity DNA Polymerase was applied [139]. Site-directed mutagenesis was performed using QuikChange II Site Directed Mutagenesis Kit. All reactions were performed according to manufacturer´s instructions.

Purification of PCR products

If the PCR product was further employed in cloning steps it was either PCR purified using QIAquick PCR purification kit or gel purified followed by a gel purification step using QIAquick gel extraction kit, both reactions were performed according to manufacturer´s instructions.

Agarose gel electrophoresis

Agarose gel electrophoresis was performed to separate DNA fragments during cloning and for mouse genotyping. Agarose powder was boiled in 1x TAE buffer until dissolved, for DNA detection 1 µg/ml ethidium bromide was added. Agarose concentration was adjusted dependent of the size of the analyzed DNA fragments (0.8-1% agarose for DNA fragments > 0.4 kb, 1.5-2% agarose for DNA fragments < 0.4 kb). DNA was mixed with loading dye and added to the gel. Gel electrophoresis was performed in 1x TAE at 120 V. Pictures were taken using the E.A.S.Y Win32 gel documentation system.

Enzymatic digest

Restriction enyzmes from New England Biolabs were used according to manufacturer´s instructions. For plasmid digest 500 ng to 1 µg of DNA was digested and subsequently gel purified using QIAquick gel extraction kit. For the digest of PCR products 500 ng of DNA was used followed by a PCR purification using QIAquick PCR purification kit, both reactions were performed according to manufacturer´s instructions.

DNA ligation

DNA fragments were ligated using T4 DNA Ligase using 20 ng of vector DNA and a molar ratio of vector/insert of 1/3, reaction was performed for 20 minutes at room temperature. For the ligation of multiple PCR fragments Gibson assembly was performed using NEBuilder® HiFi DNA Assembly Master Mix, fragments were used in an equimolar ratio and reaction was performed for 1 h at 50°C.

sgRNA design and cloning

All sgRNAs were designed using the online tool benchling.com. sgRNAs were targeted to the region -250 bp to the transcriptional start site of the target gene. Two sgRNAs were used per gene. Multiplexed sgRNA cloning was performed using the string assembly sgRNA cloning strategy (STAgR) [139].

Transformation

Chemically competent bacteria were used for transformation. 40 µl of bacteria were mixed with 3 µl of ligation reaction or 1 ng of plasmid DNA. Cells were incubated of ice for 25 minutes, heat-shock was performed at 42°C for 45 seconds, followed by an immediate incubation on ice for two minutes. 500 µl of S.O.C. medium was added, and the mixture was shaked at 37°C and 180 rpm for 20 minutes. Bacteria were spread on agar plates containing the suitable selection marker. Plates were incubated over night at 37°C and single colonies were picked for further analysis.

Plasmid DNA preparation

For low quantity DNA isolation 5 ml LB medium containing the appropriate antibiotic selection was inoculated with a single bacterial colony and shaked over night at 37°C with 180 rpm. For high quantity DNA isolation 200 ml LB medium containing the appropriate antibiotic selection were inoculated with 100 µl Miniprep culture and shaked over night at 37°C with 180 rpm. For plasmid purification QIAprep Spin Miniprep Kit or QIAprep Spin EndoFree Maxiprep Kit was used according to manufacturer´s instructions.

Glycerol stock

For long-term storage of bacteria containing specific plasmids 600 µl of bacterial solution were mixed with 400 µl glycerol and immediately stored at -80°C.

8.2.1.2 Preparation of genomic DNA

Genomic DNA was isolated from mouse ear clips or cells using the Wizard Genomic DNA Purification Kit according to manufacturer´s instruction.

8.2.1.3 Southern Blot

For the genotyping of the founder animal of the *Rosa26-dCAM* mouse line the Rosa-5´probe was used, sequence information can be found in the supplement. Approximately 20 µg of gRNA was digested overnight at 37°C with 20 units of EcoRV. The digested DNA was run on a 0.8% agarose gel for 15 hours at 30 to 60 Volt. Afterwards the gel was rinsed with water and incubated in denaturalization solution for 1 hours at room temperature under gentle agitation. After rinsing the gel with water, it was incubated in neutralization solution for 1 hour. DNA was blotted overnight on nylon membranes using 20x SSC buffer. Membrane was briefly rinsed with 2x SSC and UV cross-linked. Afterwards membrane was pre-incubated at 65°C for 1 hour in 10 mL Rapid-Hyp™ buffer. The DNA probe was excised from the pCR™2.1-TOPO® vector using EcoRI and gel purified. 300 ng of the probe were labelled with α-^{32}P-CTP using Rediprime II Kit following the manufacturer´s instructions. For purification, the radioactive labelled probe was centrifuged through a Microspin S-300 column. For hybridization the labeled DNA probe was denatured at 95°C, chilled on ice and added to the hybridization buffer, following a hybridization overnight. The membrane was washed with each washing solution I.II and III at 65°C for approximately 20 minutes, depending on the amount of radiation left on the membrane. Subsequently, the mebrane was covered in transparent foil to keep it humid and exposed to an autoradiography film at -80°C for approximately 3 days. Finally, the film was developed using a developing machine.

8.2.1.4 Protein isolation and Western Blot

48 hours after transfection cells were lysed by using RIPA buffer for cell lines and N-Per™ Neuronal Protein Extraction Reagent for primary astrocyte cultures, both buffers were supplemented with fresh protease inhibitor. Lysis buffer was added to the cells (100 µl 24 well, 300 µl 6 well) and incubated on ice for 10 minutes. Cell lysate was centrifuged at maximum speed (21000 x g) for 10 minutes. Supernatant was used for further analysis. Protein concentration was determined using Pierce BCA protein assay kit according to manufacturer´s instructions. Protein was diluted to the appropriate concentration and mixed with LDS sample buffer supplemented with 2-mercaptoethanol. Samples were heated at 95°C for 5 minutes, followed by an incubation on ice for 5 minutes.

Samples were loaded on 4-12% Criterion XT gels, protein marker VI was used for size determination. Electrophoresis was performed at 180 V for 1.5 hours in XT MOPS buffer.

The protein was blotted on PVDF membranes that were previously activated in methanol. Blotting was performed in 1x Tris/Glycine buffer, with 20 V overnight at 4°C.

The membrane was blocked using 5% milk in TBS-T buffer for 1 hour at room temperature. Subsequently the membrane was incubated in 0.5% milk in TBS-T containing the appropriate primary antibody overnight at 4°C. Afterwards the membrane was washed three times for 15

minutes with TBS-T buffer and incubated in 5% milk in TBS-T containing the corresponding secondary antibody. The incubation was performed at room temperature for 1 hour. Washing was repeated and protein bands could be detected using ECL detection substrate and a transilluminator.
For normalization the housekeeping protein β-Actin was detected.

8.2.1.5 RNA isolation and cDNA synthesis

RNA isolation

The isolation of RNA from cell lines was performed using the RNeasy plus mini kit according to manufacturer´s instructions.
Due to the low transfection efficiency of primary cells they were cotransfected with GFP and in advance FACS sorted using the FACSARIA III with a 100 µm nozzle according to GFP signal, due to cotransfection. RNA was isolated using PicoPure RNA Isolation Kit according to manufacturer´s instructions.

miRNA isolation

miRNA was isolated using the mirVana™ miRNA Isolation Kit according to manufacturer´s instructions.

cDNA synthesis

Complementary DNA (cDNA) was produced using SuperScript VILO cDNA Synthesis Kit. 500 ng of total RNA was transcribed according to manufacturer´s instructions. For further processing the cDNA mixture was diluted 1:5 with RNase-free water.

8.2.1.6 Quantitative real-time PCR

The qRT-PCR was performed in FrameStar® 384 well PCR plates using TaqMan™ Universal Master Mix II (no UNG) according to manufacturer´s instructions. TaqMan probes are listed in Table 15. The fluorescence signal was measured using the ABI Prism 7900 HT analyzer. From each sample three technical replicates were measured, the mean of the threshold cycle (ct) values was used for further analysis. For normalization the signal of the housekeeping gene β-Actin was measures, fold change was calculated as follows:

$$\Delta ct = \frac{\text{ct gene of interest}}{\text{ct housekeeping gene}}$$

$$\Delta\Delta ct = \frac{\Delta ct \text{ treatment}}{\Delta ct \text{ control}}$$

$$\text{Fold change} = 2^{-\Delta\Delta ct}$$

8.2.2 Cell culture

All cell culture experiments were performed under sterile conditions. Cells were kept at 37°C and 7% CO_2.

8.2.2.1 Storage and culture of stable cell lines

HEK293 and Neuro2a cell lines were stored in liquid nitrogen in cell culture freezing medium. The cells were cultured in T75 cell culture flasks with 20 ml growth medium. Splitting was performed when confluency reached 90%. Cells were washed with DPBS and trypsinized for 5 minutes at 37°C using 0.25% Trypsin-EDTA. Centrifugation was executed with a maximum speed of 200 x g Seeding was performed in a 1:10 dilution. Composition of all media can be gleaned in Table 9.

8.2.2.2 Isolation and culture of primary astrocytes

Primary cortical astrocytes were obtained from postnatal p5 to p6 mice as described by Heinrich *et al.* [140]. Shortly, brains were abstracted and put into ice cold HBSS buffer, olfacotory bulbs and cerebellum were removed. Meninges were substracted and the two brain hemispheres were separated by a longitudinal cut. Diencephalon and hippocampal formation were abstracted. The cortices were transferred into buffer Z of the adult brain dissociation kit for mouse and rat from Myltenyi. Subsequently buffer Y, as well as the enzymes P and A were added and the protocol was followed according to manufacturer´s instructions. However, instead of using the gentleMACS Octo Dissociator the tissue was kept in the enzyme mixture for 30 minutes, every 10 minutes the mixture was pipetted up and down (5 times) using a 10 mL serological pipette for tissue dissociation. Afterwards the protocol was performed according to manufacturer´s instructions without conducting the red blood cell removal. For the purification of astrocytes the cortical cell mixture was separated using the Anti-ACSA-2 MicroMead Kit. As soon as the cells reach a confluency of ~80% (day 7-10), 300.000 cells were seeded per 6 well, respectively 60.000 cells in a 24 well.

8.2.2.3 Lipofection

Lipofection was performed using Lipofectamine 2000 according to manufacturer´s instructions. Plasmids were adjusted based on their molar ratio, amount of DNA was equalized using the empty plasmid pcDNA3.

For primary cells 600 ng of DNA was applied to a 24 well and 3.6 µg to a 6 well plate. The ration of DNA to lipofectamine was 1:1.25, lipofection was performed in Opti-MEM I medium, 4 hours after application of the lipofection mix, and medium was changed to growth medium. In case the cells were used for reprogramming experiments the medium was changed after 24 hours to reprogramming medium. If cells were further processed for qRT-PCR, they were lysed 48 hours after lipofection.

For cell lines 500 ng of DNA was applied to a 24 well, DNA to lipofectamine ratio was 1:3. Lipofection mix was prepared in Opti-MEM I, but cells were kept in growth medium for lipofection. 24 hours after the addition of the lipofection mix, medium was changed to growth medium. Additional 24 hours later cells were further processed for qRT-PCR.

8.2.2.4 Reprogramming

For reprogramming primary cortical astrocytes were seeded on PDL-coated coverslips. 24 hours prior to transfection 60.000 cells were seeded per 24 well. Transfection was performed as described above. As soon as cells were cultured in reprogramming medium, BDNF was added in a concentration of 20 ng/ml every fourth day, until cells were fixed after 14 days using 4% PFA.

8.2.2.5 Immunocytochemistry

Cells were fixed using 4% paraformaldehyde. Primary and secondary antibodies were diluted in PBS containing 1% bovine serum albumin and 0.5% Triton X-100. Primary antibody was incubated overnight at 4°C, followed by three washing steps with PBS. Secondary antibody was incubated for one hour at room temperature in the dark, subsequently cells were washed with 100 ng/mL DAPI-PBS solution for 5 minutes, followed by three 15 minutes washes with PBS. Coverslips were mounted onto glass slides using Aqua-Poly/Mount. Pictures of the fluorescent stainings were analyzed using an Axioplan 2 microscope.

8.2.3 AAV production

rAAVs were produced by Chu Lan Lao. The protocol will just shortly be introduced.
High-titer preparations of rAAV2/5 were produced based on the protocol of Zolotukhin *et al.* [141] with minor modifications. In brief, HEK 293T cells were transfected with the $CaPO_4$ precipitation method, the plasmids pRC5, Ad helper and pAAV were applied in an equimolar ratio. After 72 hours, cell pellet was harvested with AAV release solution, 50 U/ml benzonase was added, solution was incubated for 2 hours at 37°C. Cells were frozen and thawed in liquid nitrogen to allow rAAV release. Purification of rAAV vector was done with iodixanol densities gradient (consisting of 15, 25, 40 and 56% iodixanol), followed by gradient spinning at 50.000 rpm for 2 hours 17 min at 22°C in a Ti70 rotor from Beckman. rAAV was collected at 40% iodixanol with a 5 ml syringe. Virus was dialyzed (Slide-A-Lyzer 10.000 MWCO 5 ml) in buffer A overnight to remove iodixanol. Anion exchange chromatography column HiTrap Q FF sepharose column and superloop were connected with the ÄKTAprime plus chromatography system to collect the eluted fraction. To measure rAAV concentration, the eluted fraction was spun and washed once in PBS-MK Pluronic-F68 buffer with a Millipore 30K MWCO 6 ml filter

unit. rAAVs were stored in a glass vial tube at 4°C. rAAVs were titered by SYBR Green qPCR with GFP or SV40 primer [142]. Usual titer was 3 x 10^{14} to 5 x 10^{15} GC/ml.

8.2.4 Mouse handling and treatment

8.2.4.1 Animal housing

Animal housing and handling protocols were approved by the committee for the Care and Use of Laboratory animals of the Government of Upper Bavaria (Germany) and were carried out in accordance with the European Communities' Council Directive 2010/63/EU. During the work, all efforts were made to minimize animal suffering. All mouse lines were kept in a controlled pathogen free (SPF) hygiene standard environment on a 12 h light/dark cycle. The mice had access to ad libitum standard feed and water always. All tests were approved for the ethical treatment of animals by the Government of Upper Bavaria.

8.2.4.2 Generation of CRISPR-Activator mouse line *dCAM*

The mouse line was produced by the Transgenic Unit of the IDG, Helmholtz Zentrum München. The method will just shortly be introduced.

The Rosa26-dCas-activator mouse line was generated using CRISPR/Cas9-based gene editing by microinjection into one cell embryos. For this, a gene specific guide RNA (Rosa26_gRNA 5'- ACTCCAGTCTTTCTAGAAGA-3') was used as *in vitro* transcribed single gRNA using the EnGen® sgRNA Synthesis Kit. Prior to pronuclear injection, gRNA (25 ng/µl) and targeting vector (50 ng/µl) were diluted in microinjection buffer (10 mM Tris, 0.1 mM EDTA, pH 7.2) together with recombinant Cas9 protein from IDT (50ng/µl) and incubated for 10 min at room temperature and 10 minutes at 37°C to form the active ribonucleoprotein (RNP) complex. One-cell embryos were obtained by mating of C57BL/6N males (obtained from Charles River, Sulzbach, Germany) with C57BL/6N females superovulated with 5 units PMSG (Pregnant Mare`s Serum Gonadotropin) and 5 units HCG (Human Chorionic Gonadotropin). For microinjections, one-cell embryos were injected into the larger pronucleus. Following injection, zygotes were transferred into pseudopregnant CD1 female mice to obtain live pups. All mice showed normal development and appeared healthy. Handling of the animals was performed in accordance to institutional guidelines and approved by the animal welfare committee of the government of upper Bavaria. The mice were housed in standard cages in a specific pathogen-free facility on a 12 h light/dark cycle with ad libitum access to food and water. Analysis of gene editing events was performed on genomic DNA isolated from ear biopsies of founder mice and F1 progeny, using the Wizard Genomic DNA Purification Kit following the manufacturer's instructions.

8.2.4.3 Stereotactic surgery

For the stereotactic experiments animals from B6.Cg-Tg(Gfap-Cre)77.6Mvs/2J x wildtype/N breedings and from B6.Cg-Tg(Gfap-Cre)77.6Mvs/2J x dCAM breedings were used. When crossing the B6.Cg-Tg(Gfap-Cre)77.6Mvs/2J line with transgenic animal carrying *LoxP* cassettes, it was payed attention to only breed female Cre mice, as it is known for this line to have *Cre* expression in the male germline.

6-OHDA lesion

Adult (3-4 months) mice were chosen for dopamine depletion of the left striatum, mice received a unilateral injection of 6-hydroxydopamine-HCl (6-OHDA-HCl) into the left medial forebrain bundle (MFB). All animals receive intraperitoneal injection of Medetomidin (0.5 mg/kg), Midazolam (5 mg/kg), Fentanyl (0.05 mg/kg) (MMF) as anesthesia. The mouse received pre-emptive Metamizol (200 mg/kg s.c.) and a local subcutaneous injection of 2% Lidocain. The animal was positioned into the stereotactic frame containing an integrated warming base to maintain normothermia. 6-OHDA-HCl was dissolved in 0.2% ascorbic acid in saline at a concentration of 2 µg/µl of free-base 6-OHDA-HCl. Each mouse was injected 1.5 µl (0.2 µl/min) of solution into the left MFB according to the following coordinates: anteroposterior (AP) -1.2, mediolateral (ML) +1, dorsoventral (DV) -4.9 (all millimeters relative to bregma) with flat skull position. The needle was left in place for 3 minutes after the injection to allow the toxin to diffuse before slow withdrawal of the capillary. Mice were woken up from anesthesia by the subcutaneous injection of Atipamezol (2.5 mg/kg) and Flumazenil (0.5 mg/kg). Mice were left for recovery for 2 weeks before experimentation.

rAAV injection

The dopamine depleted animals were injected into the left striatum with high titer recombinant adeno-associated virus (rAAV). Mice were anesthetized with MMF and received pre-emptive pain treatment as for the 6-OHDA-HCl injection, subsequently they were positioned into the stereotactic frame with flat skull position. Each mouse received 1 µl rAAV2/5 (0.2 µl/min) into the left dorsal striatum according to the following coordinates: AP +1, ML +2.1, DV -3.5 (all millimeters relative to bregma). The needle was left in place for 3 minutes after the injection to allow the virus to diffuse before slow withdrawal of the capillary. Mice were woken up from anesthesia by the subcutaneous injection of Atipamezol (2.5 mg/kg) and Flumazenil (0.5 mg/kg).

8.2.5 Behavior phenotyping

All tests were performed in the German Mouse Clinic under controlled conditions. All test protocols were run during a 12h/12h dark/light cycle. The operated animals were tested for

spontaneous rotation 5 weeks after rAAV injection. Additional 8 weeks later the injected animals were tested for spontaneous rotation, as well as drug-induced rotation. Furthermore, a gait analysis was performed using CatWalk as well as rotarod measurements.

8.2.5.1 Rotation tests

The mice were placed in transparent plexiglas cylinders (diameter 12.5 cm, height 30 cm). Experiments were recorded from a ventral plane view, videos were analyzed with the automated 90° body rotation counts using the Ethovision XT14 software. Rotations in drug-free condition were monitored for 15 min. For drug-induced rotations the mice were allowed to habituate for 15 min before monitoring for 45 min. Apomorphine hydrochloride was dissolved in 0.1% ascorbic acid in saline at a concentration of 0.5 mg/mL, each mouse received a subcutaneous injection of 5 mg/kg before placed into the cylinder. To allow drug wash out the animals were tested for amphetamine induced rotation not until 5 days later. Amphetamine was dissolved in saline at a concentration of 0.5 mg/mL, each mouse received an intraperitoneal injection of 5 mg/kg before placed into the cylinder.

8.2.5.2 Catwalk

Mice were tested on an automated, video-based gait analysis system, the CatWalk XT. The animals walk over an elevated glass walkway (width 8 cm, length 100 cm) enclosed by plexiglas walls (height 14 cm) in a dark room. A camera (Pulnix Camera RM-765) situated below the middle of the walkway tracked the illuminated footprints, which were later analyzed with the CatWalk software Version 7.1. The software automatically calculates a wide number of parameters in several categories which describe gait in spatial and temporal aspects. For a more detailed description see Hölter *et al*. and Zimprich *et al.* [143, 144].

8.2.5.3 Vertical pole test

Mice were placed facing upwards onto a wooden, rough-surfaced pole (length 50 cm, diameter 1 cm) with a square base plate. Mice were tested for the time they need to turn downwards (latency time) and the total time they need to reach the base of the pole (total time). Right before the test trials, the mice were trained in small groups with less than ten animals. Each mouse was coached three to five times before moving on to the next one. Then three test trials were performed with each mouse in the same sequential order, so that the time interval between training and testing was the same for each individual.

8.2.6 Histology

8.2.6.1 Perfusion and dissection of mice

For histological analysis the mice were asphyxiated with CO_2 and perfused transcardially with 4% ice-cold paraformaldehyde (PFA) in 0.1 M PBS with pH 7.4. After dissection the brain was post-fixed in PFA overnight at 4°C followed by storage in 30% sucrose for minimum 24 hours at 4°C.

8.2.6.2 Preparation of frozen sections

Brains were embedded in Neg-50 freezing medium and cut coronal into 40 µm thick 12 serial sections on a Microm HM 560 cryostat. Free floating sections were stored at 4°C in cyroprotection solution until further processing.

8.2.6.3 Immunohistochemistry

Firstly, sections were washed for at least 4 hours in PBS to remove the cryo protection solution.

Fluorescence staining

Sections were blocked in PBS pH 7.4 with 2% fetal bovine serum and 0.1% Triton X-100 for 2 hours. Subsequently, brain slices were incubated over night at 4°C in primary antibody diluted in blocking solution. Sections were washed three times for 15 minutes with PBS before incubated with secondary antibody diluted in PBS pH 7.4 containing 0.1% Triton X-100 for one hour at room temperature. Slices were washed with 100 ng/mL DAPI-PBS solution pH 7.4 for 5 minutes, followed by three 15 minutes washes with PBS. Slices were mounted on coverslips using Aqua-Poly/Mount. For the NeuN staining the sections were undertaken an antigen retrieval protocol. In short, the sections were incubated in 0.01 M Na-citrate buffer pH 6 at 80°C for 45 minutes and allowed to cool down to room temperature per se. Subsequently, brain slices were blocked in 3% milk solution containing 0.3% Triton X-100 for 2 hours. Sections are incubated overnight at 4°C in primary antibody diluted in blocking solution. Slices are washed three times for 1 hour in PBS pH 7.4 containing 0.3% Triton X-100 and incubated overnight at 4°C in secondary antibody diluted in blocking solution. Sections were washed with 100 ng/mL DAPI-PBS solution pH 7.4 (Sigma-Aldrich, D8417, USA) for 5 minutes, followed by three 15 minutes washes with PBS pH 7.4. Slices were mounted on coverslips using Aqua-Poly/Mount (Polysciences, 18606, USA).

DAB staining

Sections were incubated with 0.1% H_2O_2 PBS pH 7.4 solution for 10 minutes, followed by two 10 minutes washing steps with PBS. Sections were blocked in PBS pH 7.4 with 2% fetal bovine serum and 0.1% Triton X-100 for 2 hours. Subsequently, brain slices were incubated over night

at 4°C in primary antibody diluted in blocking solution. Sections were washed three times for 15 minutes with PBS before incubated with secondary antibody diluted in PBS pH 7.4 containing 0.1% Triton X-100 for one hour at room temperature. Sections were washed three times for 15 minutes with PBS. Signal intensity amplification was performed using the ABC Peroxidase Standard Staining Kit according to manufacturer´s instructions. Shortly, sections were incubated in ABC-solution, which was prepared 30 minutes in advance, for 45 minutes, followed by two washing steps for 15 minutes with PBS. Subsequently sections were incubated two times for 15 minutes with 0.1M Tris-HCl. DAB working solution (
Table 9) was added to the slices and incubated until a good staining could be recognized. Reaction was stopped by washing with PBS three times for 15 minutes. Sections were mounted onto glass slides and subsequently dehydrated using ascending ethanol concentration each for 2 minutes (2 x 70%, 2 x 96%, 2 x 100% ethanol) and xylol two times for 5 minutes. Afterwards slices were mounted using Pertex.

8.2.6.4 Image acquisition

If not differently indicated all images were acquired on a confocal laser scanning (Zeiss LSM880) microscope.

8.2.6.5 Stereological quantification

All stereological quantifications were performed using the stereoinvestigator software Version 2019.1.3. The dorsal striatum of at least three animals was analyzed for quantification. Regions close to the subventricular zone were excluded form counting.

8.2.7 Electrophysiological measurements

Preparation of brain slices

Acute 220 µm thick brain coronal slices containing the dorsal striatum were cut on a vibratome (Leica VT1200, Germany) in a bubbled (95% O_2 / 5% CO_2) standard ice-cold artificial cerebrospinal fluid (ACSF) containing (in mM): 126 NaCl, 2.5 KCl, 1.2 $MgCl_2$, 2.4 $CaCl_2$, 1.2 NaH_2PO_4, 21.4 $NaHCO_3$, 11.1 glucose, complemented from slicing only with (in mM): 3 kynurenic acid, 26.2 $NaHCO_3$, 225 sucrose, 1.25 glucose and 4.9 $MgCl_2$. Slices were then transferred to a chamber containing standard ACSF oxygenated with 95% O_2 / 5% CO_2 at 35°C for 15 min and subsequently maintained at room temperature for at least another 15 min prior to use.

Whole-cell recordings

Dorsal striatal “reprogrammed” cells (either neurons or glia) were visualized with a 20x/1.0NA WI objective, 4x post-magnification, under video microscope (Olympus BX51WI, Germany) coupled with infrared gradient contrast and epifluorescence. Whole-cell patch-clamp recordings in current clamp mode were acquired from the somata of fluorescent cells with a Multiclamp 700B amplifier (Molecular Devices, Foster City, CA), digitized at 10 kHz and Bessel filtered at 4kHz. Pipettes (4-6 mΩ) were filled with an intracellular solution containing (in mM): 100 K-gluconate, 20 KCl, 4 Mg-ATP, 0.3 Na-GTP, 10 Na_2-Phosphocreatine, 10 Hepes, (pH 7.3, 290 mOsm). All recordings were carried out at 35°C and slices continually superfused with oxygenated (95% O_2/5% CO_2) ACSF. Passive membrane properties were assessed by injecting 500 ms depolarizing current steps. Putative spontaneous postsynaptic potential was recorded with the same internal solution in voltage clamp mode while the cell being held at -70 mV. Data were analyzed with custom-written routines in IgorPro.

8.2.8 Single cell RNA sequencing

8.2.8.1 Tissue preparation

Cells were dissected from mouse striatum (n=2) and dissociated into single cell suspension using the papain kit (Worthington) according to manufacturer´s instructions. Incubation with dissociating enzyme was performed for 90 min.

8.2.8.2 Library preparation and sequencing

Single cell suspensions were loaded onto 10x Genomics Single Cell 3´Chips together with the reverse transcription mastermix according to manufacturer´s instructions for the Chromium Single Cell 3´Library & Gel Bead Kit v2 (PN-120237, 10xGenomics) to generate single cell gel beads in emulsion (GEMs). cDNA synthesis was done according to 10x Genomics guidelines. Libraries were pooled and sequenced on a NovaSeq6000 (Illumina) according to the Chromium Single Cell v.2 specifications and with an average read depth of 50,000 aligned reads per cell. Sequencing was performed in the genome analysis center of the Helmholtz Center Munich.

8.2.8.3 Alignment and data analysis

Transcriptome alignment of single cell data was done using Cell Ranger 3.1.0 against a modified version of the mouse transcriptome GrCm38 (Ensembl Release 99) that included both GFP and Cre sequences. Quality Control (QC) of mapped cells was done using recommendations by Luecken *et al.* [145], selecting 3,899 cells with at least 800 reads and 250 detected genes. Normalization and log transformation was performed using the counts

per million (CPM) strategy with a target count depth of 10,000 using SCANPY´s [146] normalize_total and log1p functions. Highly variable gene selection was performed via the function highly_variable_genes using the Seurat [147] flavour with default parametrization, obtaining 4,274 HVGs in at least one experimental group. Following cell count normalization experimental groups were integrated with Scanorama [95]. Unsupervised clustering of cells was done using the Leiden algorithm [148] as implemented in SCANPY and with resolution parameter of 0.05. This allowed classification and counting of nine main cell types based on marker genes selected using *t*-test between the normalized counts of each marker gene in a cell type against all others (function *rank_genes_groups* in SCANPY). 1,110 cells assigned to astrocytic and neuronal cell types were subclustered into four groups using Leiden with a resolution of 0.30. Marker genes in these four groups were detected using *t*-test between each group against the other three. Detection of cells positive for GFP, Cre and other marker genes was done using as criteria any cell with normalized counts greater than zero. Visualization of cell groups is done using Uniform Manifold Approximation and Projection (UMAP) [149], as implemented in SCANPY.

8.2.9 Statistical analysis

Statistical analysis was performed using Graphpad Prism 7 software. If not differently indicated, at least three biological replicates were analyzed. The normality of the distribution of data points was verified using Shapiro-Wilk test. Data was analyzed using either an unpaired t-test or a multiple comparison ANOVA, followed by a posthoc Tukey's multiple comparisons test. When normality tests did not indicate normal distribution, non-parametric Kruskall-Wallis test was performed.

Asterixis are assigned as followed * $p<0.5$, ** $p<0.01$, *** $p<0.001$, **** $p<0.0001$.

9 Appendix

9.1 Supplementary Data

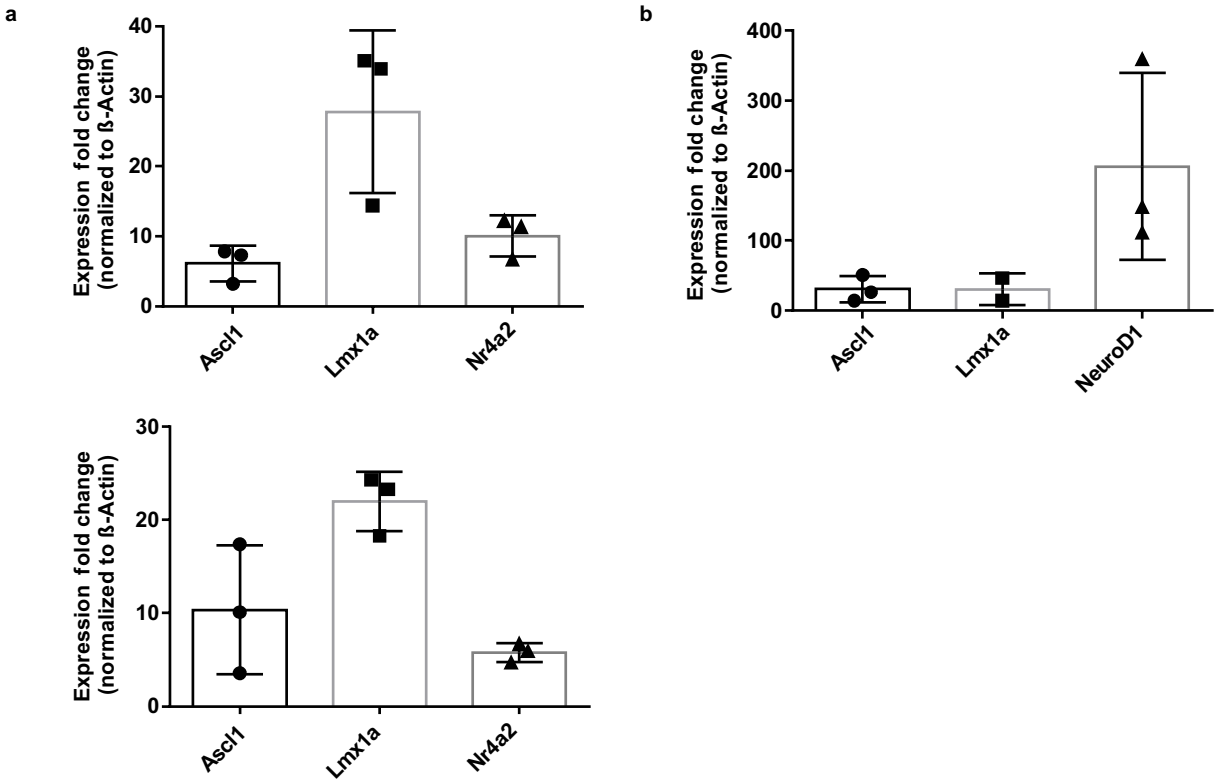

Supplementary Figure 1: Evaluation of the *dCAM* approach for the activation capacity in primary *dCAM x Gfap-Cre* astrocytes.

a, Multiplexed activation of *Ascl1*, *Lmx1a* and *Nr4a2*. (top: *Ascl1* 6 ± 3, *Lmx1a* 28 ± 12, *Nr4a2* 10 ± 3, bottom: *Ascl1* 10 ± 7, *Lmx1a* 22 ± 3, *Nr4a2* 6 ± 1) **b,** Multiplexed activation of *Ascl1*, *Lmx1a* and *NeuroD1*. (*Ascl1* 31 ± 19, *Lmx1a* 30 ± 23, *NeuroD1* 206 ± 134). Activation levels are depicted as fold change between cells transfected with and without sgRNAs. All levels were normalized to β-Actin.
Error bars represent mean ± SD.

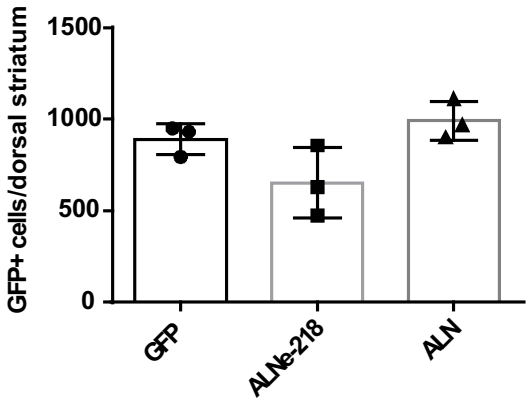

Supplementary Figure 2: Total amount of GFP$^+$ cells *in vivo* in *dCAM x Gfap-Cre* mice injected with FLEx-GFP reporter from different viruses.

GFP$^+$ cells in the ipsilateral dorsal striatum of one slide after five weeks of injection. No significant difference could be observed between the different reprogramming conditions and the GFP control. *GFP* 892.0 ± 85.4, *ALNe-218* 652.7 ± 193.6, *ALN* 993.3 ± 106.6.

Error bars represent mean ± SD.

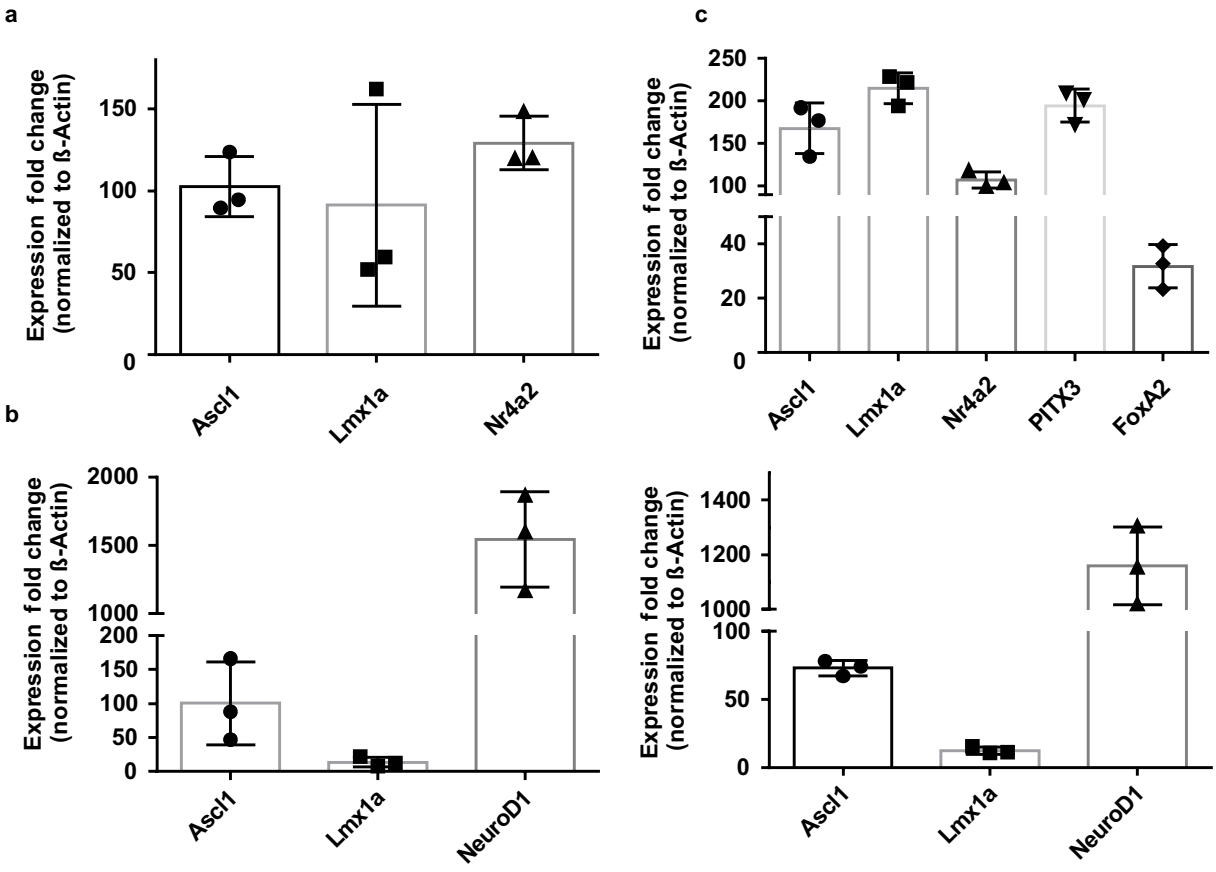

Supplementary Figure 3: Evaluation of *the AAV-dCAS approach for the* activation capacity in primary astrocytes.

Multiplexed activation of **a,** *Ascl1*, *Lmx1a*, *Nr4a2* (*Ascl1* 103 ± 19, *Lmx1a* 91 ± 62, *Nr4a2* 129 ± 16) **b,** *Ascl1, Lmx1a,* and *NeuroD1* (left: *Ascl1* 100 ± 61, *Lmx1a* 14 ± 7.5, *NeuroD1* 1542 ± 352, right: *Ascl1* 73 ± 6, *Lmx1a* 12 ± 3, *NeuroD1* 1160 ± 142) and **c,** *Ascl1*, *Lmx1a*, *Nr4a2, PITX3, FoxA2* (Ascl1 167 ± 30, Lmx1a 215 ± 18, Nr4a2 107 ± 10, PITX3 195 ± 19, FoxA2 32 ± 8) in primary astrocytic cultures. Activation levels are depicted as fold change between cells transfected with and without sgRNAs. All levels were normalized to β-Actin.

Error bars represent mean ± SD.

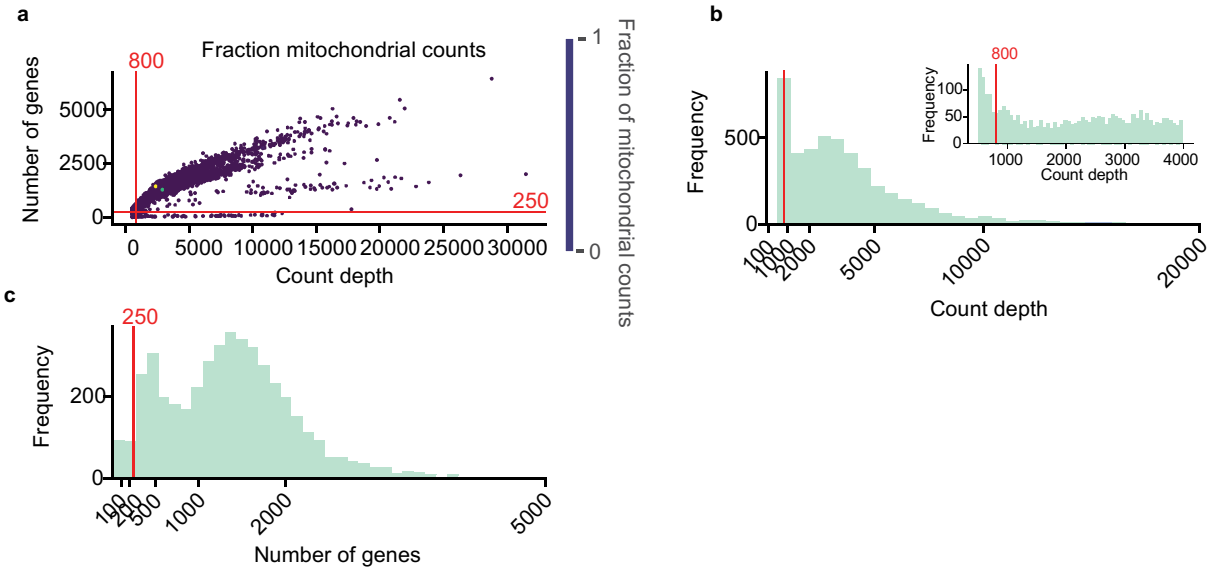

Supplementary Figure 4: Quality control of single cell RNA-seq at 13 wpi of AAVs in *dCAM x GFAP-Cre* mice striatal tissue.

a, Number of genes (y-axis) versus count depth (x-axis) per cell. Color highlights fraction of mitochondrial reads. Quality control thresholds of 800 and 250 for number of genes and minimum cell depth are defined, respectively, obtaining 3,899 cells. **b,** Distributions of count depth for all cells. Inset shows count depth distribution from for all cells with fewer than 4000 counts. The count depth threshold of 800 is shown as a red, vertical line. **c,** Distribution of number of genes detected per cell. Red line indicates thresholds as in **a**.

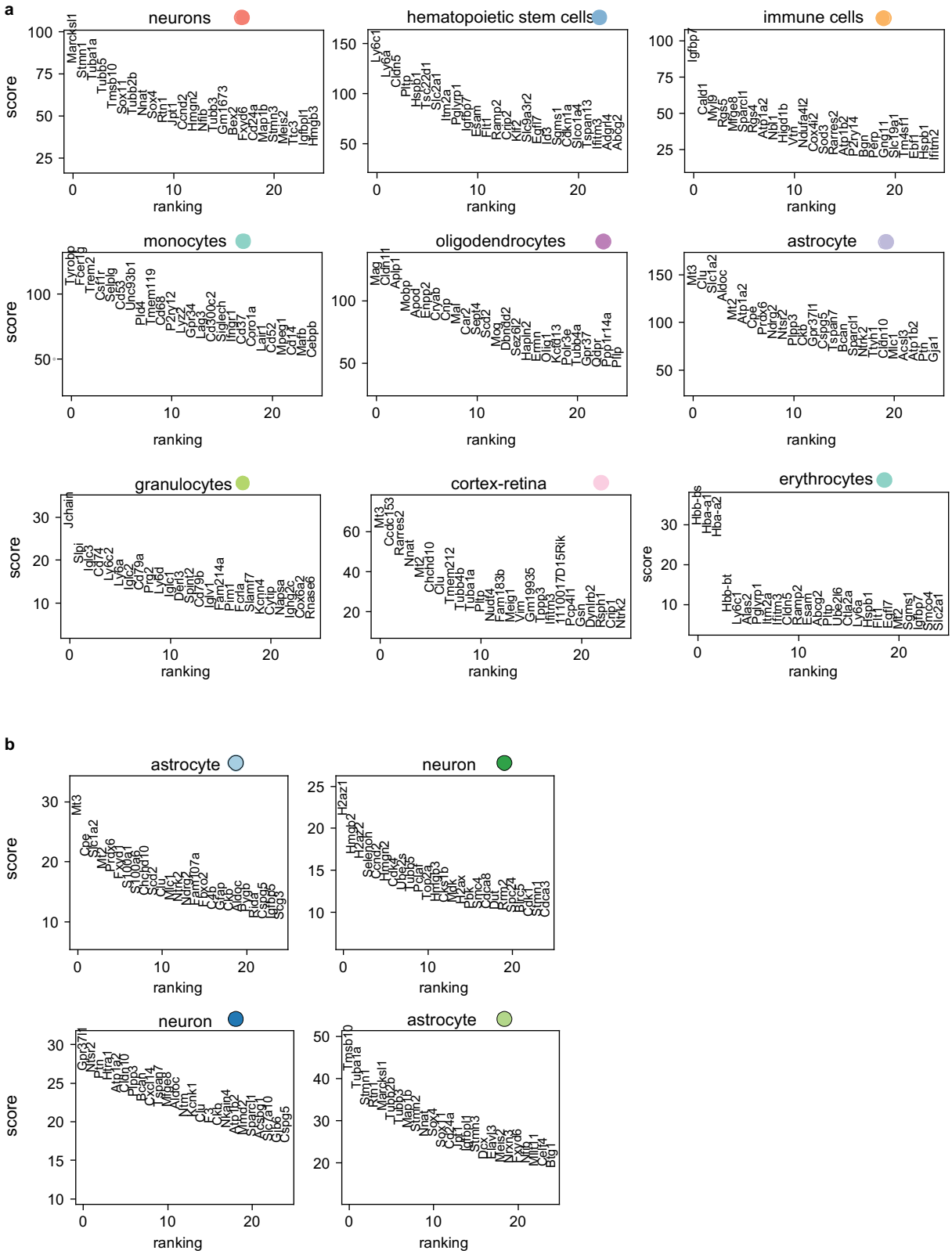

Supplementary Figure 5: Rank_genes_groups plots from Scanpy showing the top 25 marker genes using a t-test between log-normalized expression values.

a, Top 25 marker genes ranked by their using *t*-test statistic when comparing normalized cell counts between annotated group against all other groups. **b,** Same as in **a** but using four astrocytic-neuronal subclusters (n=1,110 cells). Colors as in Figure 4 a, b.

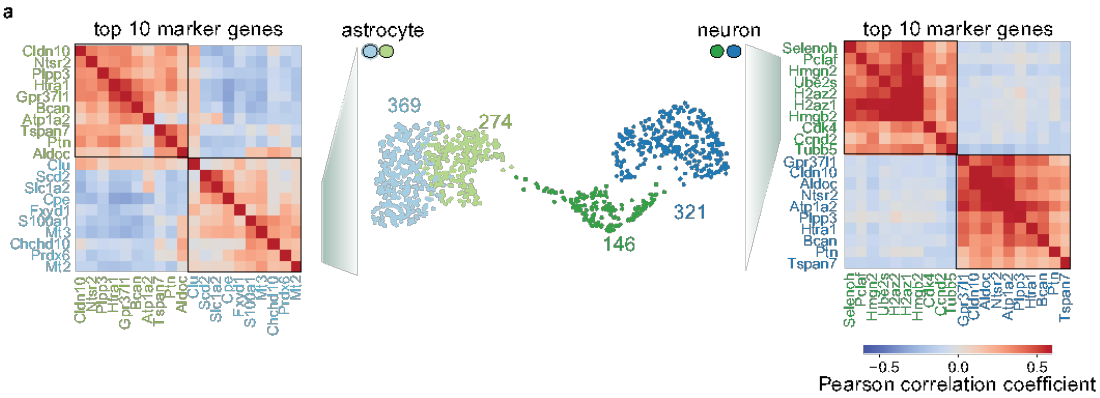
a
top 10 marker genes
astrocyte
neuron
top 10 marker genes
369
274
321
146
Cldn10
Ntsr2
Plpp3
Htra1
Gpr37l1
Bcan
Atp1a2
Tspan7
Ptn
Aldoc
Clu
Scd2
Slc1a2
Cpe
Fxyd1
S100a1
Mt3
Chchd10
Prdx6
Mt2
Selench
Pclaf
Hmgn2
Ube2s
H2az2
H2az1
Hmgb2
Cdk4
Ccnd2
Tubb5
−0.5
0.0
0.5
Pearson correlation coefficient

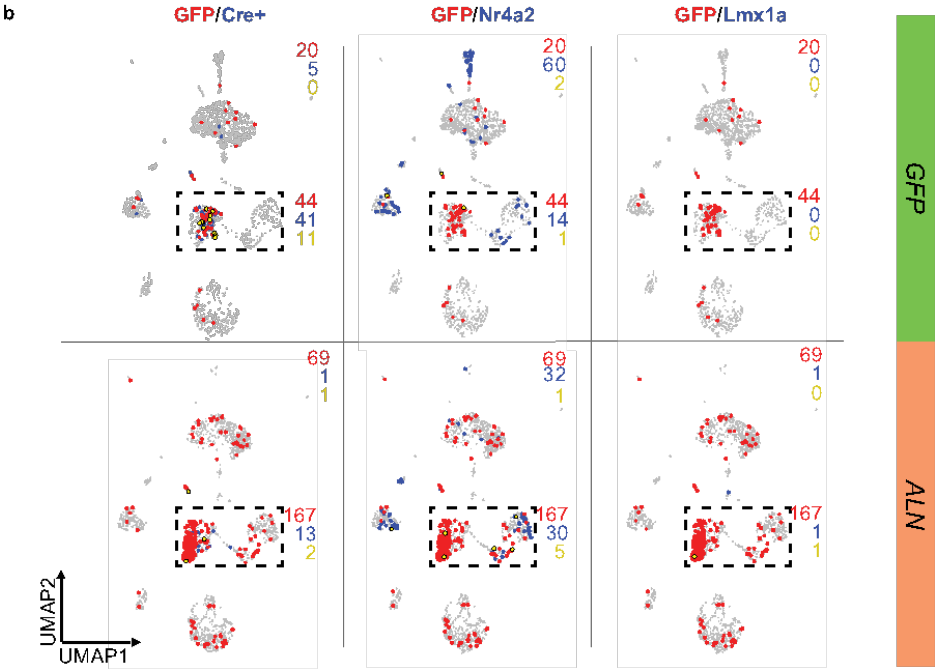
b
GFP/Cre+
GFP/Nr4a2
GFP/Lmx1a
GFP
ALN
UMAP2
UMAP1

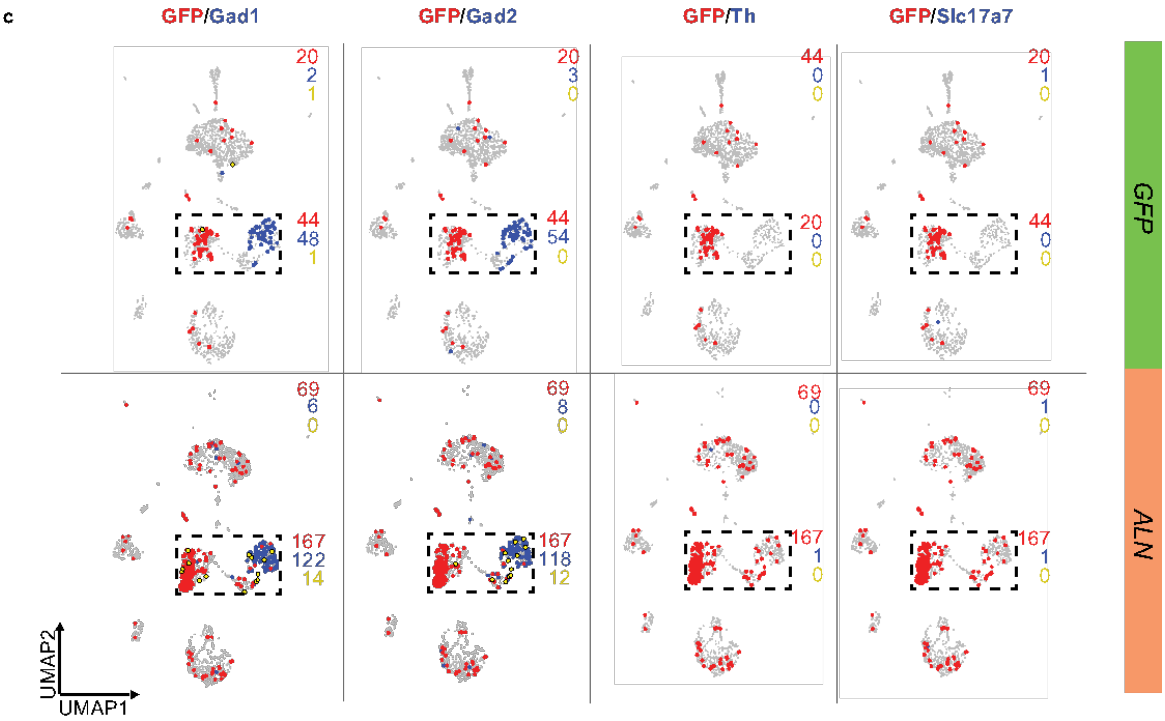
c
GFP/Gad1
GFP/Gad2
GFP/Th
GFP/Slc17a7
GFP
ALN
UMAP2
UMAP1

Supplementary Figure 6: scRNA-seq analysis 13 wpi in *dCAM x GFAP-Cre* mice.

a, Pearson´s correlation coefficient of top-10 marker gene expression levels of cells in astrocytic subgroups (n=643) and in neuronal cell subgroups (n=467). **b,** Counts for GFP$^+$ cells (red), markers *Cre*, *Nr4a2*, and *Lmx1a* (blue) and co-detection of cell with both markers (yellow) in *GFP control* and *ALN* reprogramming. **c,** Same as in **b** but showing *Gad1*, *Gad2*, *Th* and *Slc17a7* as markers genes.

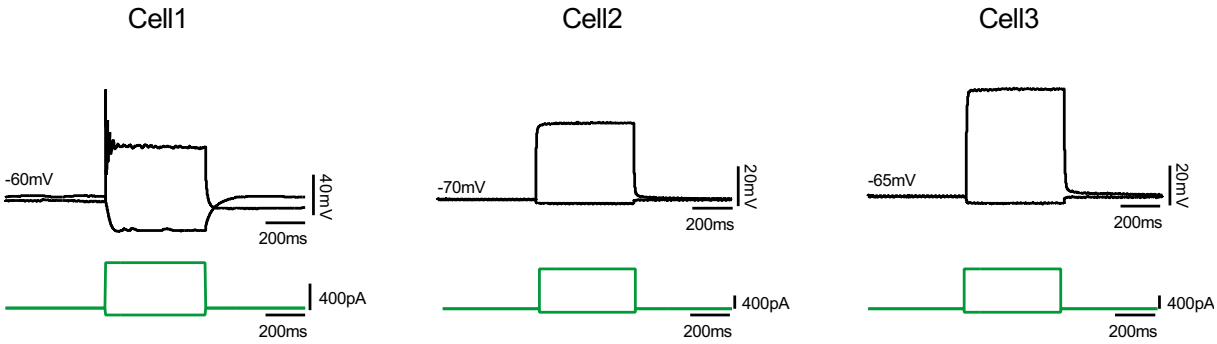

Supplementary Figure 7: Electrophysiological measurements 5 wpi of AAVs to induce the factors *Ascl1*, *Lmx1a*, *Nr4a2*.

Firing pattern of induced neurons 5 weeks after sgRNA injection. Neurons exhibit electrophysiological properties of immature neurons (cell 1 exhibited one action potential) respectively of glial cells (cell 2 and 3).

9.2 List of Figures

9.3 List of Supplementary Figures

9.4 List of Tables

9.5 Bibliography

1. Niccoli, T. and L. Partridge, *Ageing as a risk factor for disease.* Curr Biol, 2012. **22**(17): p. R741-52.
2. Roser, M., *Life Expectancy.* 2019.
3. Prospects, U.N.W., *World Population Prospects - Population Division - United Nations.* 2015.
4. Institute, N.C., *NCI Dictionary of Cancer Terms.* 2019.
5. Goedert, M. and A. Compston, *Parkinson's disease - the story of an eponym.* Nat Rev Neurol, 2018. **14**(1): p. 57-62.
6. Hirsch, E.C. and S. Hunot, *Neuroinflammation in Parkinson's disease: a target for neuroprotection?* Lancet Neurol, 2009. **8**(4): p. 382-97.
7. Pickrell, A.M. and R.J. Youle, *The roles of PINK1, parkin, and mitochondrial fidelity in Parkinson's disease.* Neuron, 2015. **85**(2): p. 257-73.
8. Pellicano, C., et al., *Prodromal non-motor symptoms of Parkinson's disease.* Neuropsychiatr Dis Treat, 2007. **3**(1): p. 145-52.
9. Sarkar, S., J. Raymick, and S. Imam, *Neuroprotective and Therapeutic Strategies against Parkinson's Disease: Recent Perspectives.* Int J Mol Sci, 2016. **17**(6).
10. Poewe, W., et al., *Parkinson disease.* Nat Rev Dis Primers, 2017. **3**: p. 17013.
11. de Rijk, M.C., et al., *Prevalence of Parkinson's disease in Europe: A collaborative study of population-based cohorts. Neurologic Diseases in the Elderly Research Group.* Neurology, 2000. **54**(11 Suppl 5): p. S21-3.
12. Lix, L.M., et al., *Socioeconomic variations in the prevalence and incidence of Parkinson's disease: a population-based analysis.* J Epidemiol Community Health, 2010. **64**(4): p. 335-40.
13. Dorsey, E.R., et al., *Projected number of people with Parkinson disease in the most populous nations, 2005 through 2030.* Neurology, 2007. **68**(5): p. 384-6.
14. Haaxma, C.A., et al., *Gender differences in Parkinson's disease.* J Neurol Neurosurg Psychiatry, 2007. **78**(8): p. 819-24.
15. Dluzen, D., *Estrogen decreases corpus striatal neurotoxicity in response to 6-hydroxydopamine.* Brain Res, 1997. **767**(2): p. 340-4.
16. Datla, K.P., et al., *Differences in dopaminergic neuroprotective effects of estrogen during estrous cycle.* Neuroreport, 2003. **14**(1): p. 47-50.
17. Parkinson Study Group, P.I., *A randomized pilot trial of estrogen replacement therapy in post-menopausal women with Parkinson's disease.* Parkinsonism Relat Disord, 2011. **17**(10): p. 757-60.
18. Ascherio, A. and M.A. Schwarzschild, *The epidemiology of Parkinson's disease: risk factors and prevention.* Lancet Neurol, 2016. **15**(12): p. 1257-1272.
19. Chillag-Talmor, O., et al., *Use of a refined drug tracer algorithm to estimate prevalence and incidence of Parkinson's disease in a large israeli population.* J Parkinsons Dis, 2011. **1**(1): p. 35-47.
20. Reed, X., et al., *The role of monogenic genes in idiopathic Parkinson's disease.* Neurobiol Dis, 2019. **124**: p. 230-239.
21. Koprich, J.B., et al., *Progressive neurodegeneration or endogenous compensation in an animal model of Parkinson's disease produced by decreasing doses of alpha-synuclein.* PLoS One, 2011. **6**(3): p. e17698.
22. Albert, K., et al., *AAV Vector-Mediated Gene Delivery to Substantia Nigra Dopamine Neurons: Implications for Gene Therapy and Disease Models.* Genes (Basel), 2017. **8**(2).
23. Zampese, E., Galtieri, D. J., Schumacker, P. T., & Surmeier Jr, D. J., *Determinants of Selective Vulnerability of Dopamine Neurons in Parkinson's Disease. .* In Handbook of Behavioral Neuroscience (pp. 821-837). (Handbook of Behavioral Neuroscience; Vol. 24), 2016.

24. Gonzalez-Hernandez, T., et al., *Vulnerability of mesostriatal dopaminergic neurons in Parkinson's disease.* Front Neuroanat, 2010. **4**: p. 140.
25. Barone, P., *Neurotransmission in Parkinson's disease: beyond dopamine.* Eur J Neurol, 2010. **17**(3): p. 364-76.
26. Nelson, A.B. and A.C. Kreitzer, *Reassessing models of basal ganglia function and dysfunction.* Annu Rev Neurosci, 2014. **37**: p. 117-35.
27. Lee, H.J., et al., *Activation of Direct and Indirect Pathway Medium Spiny Neurons Drives Distinct Brain-wide Responses.* Neuron, 2016. **91**(2): p. 412-24.
28. Calabresi, P., et al., *Direct and indirect pathways of basal ganglia: a critical reappraisal.* Nat Neurosci, 2014. **17**(8): p. 1022-30.
29. Lim, S.A., U.J. Kang, and D.S. McGehee, *Striatal cholinergic interneuron regulation and circuit effects.* Front Synaptic Neurosci, 2014. **6**: p. 22.
30. Fino, E. and L. Venance, *Spike-timing dependent plasticity in striatal interneurons.* Neuropharmacology, 2011. **60**(5): p. 780-8.
31. Kravitz, A.V., et al., *Regulation of parkinsonian motor behaviours by optogenetic control of basal ganglia circuitry.* Nature, 2010. **466**(7306): p. 622-6.
32. Dorszewska, J., et al., *Molecular Effects of L-dopa Therapy in Parkinson's Disease.* Curr Genomics, 2014. **15**(1): p. 11-7.
33. Maiti, P., J. Manna, and G.L. Dunbar, *Current understanding of the molecular mechanisms in Parkinson's disease: Targets for potential treatments.* Transl Neurodegener, 2017. **6**: p. 28.
34. Hadaczek, P., et al., *Eight years of clinical improvement in MPTP-lesioned primates after gene therapy with AAV2-hAADC.* Mol Ther, 2010. **18**(8): p. 1458-61.
35. Palfi, S., et al., *Long-term safety and tolerability of ProSavin, a lentiviral vector-based gene therapy for Parkinson's disease: a dose escalation, open-label, phase 1/2 trial.* Lancet, 2014. **383**(9923): p. 1138-46.
36. McIver, E.L., et al., *Maladaptive Downregulation of Autonomous Subthalamic Nucleus Activity following the Loss of Midbrain Dopamine Neurons.* Cell Rep, 2019. **28**(4): p. 992-1002 e4.
37. McGregor, M.M. and A.B. Nelson, *Circuit Mechanisms of Parkinson's Disease.* Neuron, 2019. **101**(6): p. 1042-1056.
38. Stoker, T.B., N.F. Blair, and R.A. Barker, *Neural grafting for Parkinson's disease: challenges and prospects.* Neural Regen Res, 2017. **12**(3): p. 389-392.
39. Yasuhara, T., et al., *Cell Therapy for Parkinson's Disease.* Cell Transplant, 2017. **26**(9): p. 1551-1559.
40. Torper, O. and M. Gotz, *Brain repair from intrinsic cell sources: Turning reactive glia into neurons.* Prog Brain Res, 2017. **230**: p. 69-97.
41. Waddington, C., *The strategy of the genes: a discussion of some aspects of theoretical biology. 1957*. London: Allen & Unwin.
42. Ladewig, J., P. Koch, and O. Brustle, *Leveling Waddington: the emergence of direct programming and the loss of cell fate hierarchies.* Nat Rev Mol Cell Biol, 2013. **14**(4): p. 225-36.
43. Takahashi, K. and S. Yamanaka, *Induction of pluripotent stem cells from mouse embryonic and adult fibroblast cultures by defined factors.* Cell, 2006. **126**(4): p. 663-76.
44. Iwafuchi-Doi, M. and K.S. Zaret, *Pioneer transcription factors in cell reprogramming.* Genes Dev, 2014. **28**(24): p. 2679-92.
45. Niu, W., et al., *Phenotypic Reprogramming of Striatal Neurons into Dopaminergic Neuron-like Cells in the Adult Mouse Brain.* Stem Cell Reports, 2018. **11**(5): p. 1156-1170.
46. Vierbuchen, T., et al., *Direct conversion of fibroblasts to functional neurons by defined factors.* Nature, 2010. **463**(7284): p. 1035-41.
47. Heins, N., et al., *Glial cells generate neurons: the role of the transcription factor Pax6.* Nat Neurosci, 2002. **5**(4): p. 308-15.

48. Gascon, S., et al., *Direct Neuronal Reprogramming: Achievements, Hurdles, and New Roads to Success.* Cell Stem Cell, 2017. **21**(1): p. 18-34.
49. Gascon, S., et al., *Identification and Successful Negotiation of a Metabolic Checkpoint in Direct Neuronal Reprogramming.* Cell Stem Cell, 2016. **18**(3): p. 396-409.
50. Lang, A.E. and A.M. Lozano, *Parkinson's disease. Second of two parts.* N Engl J Med, 1998. **339**(16): p. 1130-43.
51. Zaret, K.S. and J.S. Carroll, *Pioneer transcription factors: establishing competence for gene expression.* Genes Dev, 2011. **25**(21): p. 2227-41.
52. Wapinski, O.L., et al., *Hierarchical mechanisms for direct reprogramming of fibroblasts to neurons.* Cell, 2013. **155**(3): p. 621-35.
53. Chanda, S., et al., *Generation of induced neuronal cells by the single reprogramming factor ASCL1.* Stem Cell Reports, 2014. **3**(2): p. 282-96.
54. Gao, Z., et al., *Neurod1 is essential for the survival and maturation of adult-born neurons.* Nat Neurosci, 2009. **12**(9): p. 1090-2.
55. Chen, Y.C., et al., *A NeuroD1 AAV-Based Gene Therapy for Functional Brain Repair after Ischemic Injury through In Vivo Astrocyte-to-Neuron Conversion.* Mol Ther, 2020. **28**(1): p. 217-234.
56. Guo, Z., et al., *In vivo direct reprogramming of reactive glial cells into functional neurons after brain injury and in an Alzheimer's disease model.* Cell Stem Cell, 2014. **14**(2): p. 188-202.
57. Rodriguez-Traver, E., et al., *Role of Nurr1 in the Generation and Differentiation of Dopaminergic Neurons from Stem Cells.* Neurotox Res, 2016. **30**(1): p. 14-31.
58. Arenas, E., M. Denham, and J.C. Villaescusa, *How to make a midbrain dopaminergic neuron.* Development, 2015. **142**(11): p. 1918-36.
59. Saijo, K., et al., *A Nurr1/CoREST pathway in microglia and astrocytes protects dopaminergic neurons from inflammation-induced death.* Cell, 2009. **137**(1): p. 47-59.
60. Friling, S., et al., *Efficient production of mesencephalic dopamine neurons by Lmx1a expression in embryonic stem cells.* Proc Natl Acad Sci U S A, 2009. **106**(18): p. 7613-8.
61. Caiazzo, M., et al., *Direct generation of functional dopaminergic neurons from mouse and human fibroblasts.* Nature, 2011. **476**(7359): p. 224-7.
62. Torper, O., et al., *In Vivo Reprogramming of Striatal NG2 Glia into Functional Neurons that Integrate into Local Host Circuitry.* Cell Rep, 2015. **12**(3): p. 474-81.
63. Rivetti di Val Cervo, P., et al., *Induction of functional dopamine neurons from human astrocytes in vitro and mouse astrocytes in a Parkinson's disease model.* Nat Biotechnol, 2017. **35**(5): p. 444-452.
64. Jansen, R., et al., *Identification of genes that are associated with DNA repeats in prokaryotes.* Mol Microbiol, 2002. **43**(6): p. 1565-75.
65. Bolotin, A., et al., *Clustered regularly interspaced short palindrome repeats (CRISPRs) have spacers of extrachromosomal origin.* Microbiology, 2005. **151**(Pt 8): p. 2551-61.
66. Mojica, F.J., et al., *Intervening sequences of regularly spaced prokaryotic repeats derive from foreign genetic elements.* J Mol Evol, 2005. **60**(2): p. 174-82.
67. Pourcel, C., G. Salvignol, and G. Vergnaud, *CRISPR elements in Yersinia pestis acquire new repeats by preferential uptake of bacteriophage DNA, and provide additional tools for evolutionary studies.* Microbiology, 2005. **151**(Pt 3): p. 653-63.
68. Bhaya, D., M. Davison, and R. Barrangou, *CRISPR-Cas Systems in Bacteria and Archaea: Versatile Small RNAs for Adaptive Defense and Regulation.* Annual Review of Genetics, 2011. **45**(1): p. 273-297.
69. Shabbir, M.A., et al., *Survival and Evolution of CRISPR-Cas System in Prokaryotes and Its Applications.* Front Immunol, 2016. **7**: p. 375.
70. Jinek, M., et al., *A programmable dual-RNA-guided DNA endonuclease in adaptive bacterial immunity.* Science, 2012. **337**(6096): p. 816-21.
71. Mali, P., K.M. Esvelt, and G.M. Church, *Cas9 as a versatile tool for engineering biology.* Nat Methods, 2013. **10**(10): p. 957-63.

72. Gaj, T., C.A. Gersbach, and C.F. Barbas, 3rd, *ZFN, TALEN, and CRISPR/Cas-based methods for genome engineering.* Trends Biotechnol, 2013. **31**(7): p. 397-405.
73. Mushtaq, M., et al., *CRISPR/Cas approach: A new way of looking at plant-abiotic interactions.* J Plant Physiol, 2018. **224-225**: p. 156-162.
74. Knott, G.J. and J.A. Doudna, *CRISPR-Cas guides the future of genetic engineering.* Science, 2018. **361**(6405): p. 866-869.
75. Koonin, E.V., K.S. Makarova, and F. Zhang, *Diversity, classification and evolution of CRISPR-Cas systems.* Curr Opin Microbiol, 2017. **37**: p. 67-78.
76. Murugan, K., et al., *The Revolution Continues: Newly Discovered Systems Expand the CRISPR-Cas Toolkit.* Mol Cell, 2017. **68**(1): p. 15-25.
77. Dominguez, A.A., W.A. Lim, and L.S. Qi, *Beyond editing: repurposing CRISPR-Cas9 for precision genome regulation and interrogation.* Nat Rev Mol Cell Biol, 2016. **17**(1): p. 5-15.
78. Qi, L.S., et al., *Repurposing CRISPR as an RNA-guided platform for sequence-specific control of gene expression.* Cell, 2013. **152**(5): p. 1173-83.
79. Maeder, M.L., et al., *CRISPR RNA-guided activation of endogenous human genes.* Nat Methods, 2013. **10**(10): p. 977-9.
80. Chavez, A., et al., *Highly efficient Cas9-mediated transcriptional programming.* Nat Methods, 2015. **12**(4): p. 326-8.
81. Konermann, S., et al., *Genome-scale transcriptional activation by an engineered CRISPR-Cas9 complex.* Nature, 2015. **517**(7536): p. 583-8.
82. Chavez, A., et al., *Comparison of Cas9 activators in multiple species.* Nat Methods, 2016. **13**(7): p. 563-567.
83. Soriano, P., *Generalized lacZ expression with the ROSA26 Cre reporter strain.* Nat Genet, 1999. **21**(1): p. 70-1.
84. Zaiss, A.K. and D.A. Muruve, *Immune responses to adeno-associated virus vectors.* Curr Gene Ther, 2005. **5**(3): p. 323-31.
85. Mattugini, N., et al., *Inducing Different Neuronal Subtypes from Astrocytes in the Injured Mouse Cerebral Cortex.* Neuron, 2019. **103**(6): p. 1086-1095 e5.
86. Grieger, J.C. and R.J. Samulski, *Packaging capacity of adeno-associated virus serotypes: impact of larger genomes on infectivity and postentry steps.* J Virol, 2005. **79**(15): p. 9933-44.
87. Foglieni, C., et al., *Split GFP technologies to structurally characterize and quantify functional biomolecular interactions of FTD-related proteins.* Sci Rep, 2017. **7**(1): p. 14013.
88. Gregorian, C., et al., *Pten deletion in adult neural stem/progenitor cells enhances constitutive neurogenesis.* J Neurosci, 2009. **29**(6): p. 1874-86.
89. Grealish, S., et al., *Characterisation of behavioural and neurodegenerative changes induced by intranigral 6-hydroxydopamine lesions in a mouse model of Parkinson's disease.* Eur J Neurosci, 2010. **31**(12): p. 2266-78.
90. Schlachetzki, J.C., et al., *Increased tyrosine hydroxylase expression accompanied by glial changes within the non-lesioned hemisphere in the 6-hydroxydopamine model of Parkinson's disease.* Restor Neurol Neurosci, 2014. **32**(4): p. 447-62.
91. Boix, J., T. Padel, and G. Paul, *A partial lesion model of Parkinson's disease in mice--characterization of a 6-OHDA-induced medial forebrain bundle lesion.* Behav Brain Res, 2015. **284**: p. 196-206.
92. Buffo, A., et al., *Origin and progeny of reactive gliosis: A source of multipotent cells in the injured brain.* Proc Natl Acad Sci U S A, 2008. **105**(9): p. 3581-6.
93. Naso, M.F., et al., *Adeno-Associated Virus (AAV) as a Vector for Gene Therapy.* BioDrugs, 2017. **31**(4): p. 317-334.
94. Truong, D.J., et al., *Development of an intein-mediated split-Cas9 system for gene therapy.* Nucleic Acids Res, 2015. **43**(13): p. 6450-8.
95. Hie, B., B. Bryson, and B. Berger, *Efficient integration of heterogeneous single-cell transcriptomes using Scanorama.* Nat Biotechnol, 2019. **37**(6): p. 685-691.

96. Traag, V.A., L. Waltman, and N.J. van Eck, *From Louvain to Leiden: guaranteeing well-connected communities.* Scientific Reports, 2019. **9**(1): p. 5233.
97. Broom, L., et al., *A translational approach to capture gait signatures of neurological disorders in mice and humans.* Scientific Reports, 2017. **7**(1): p. 3225.
98. Vandeputte, C., et al., *Automated quantitative gait analysis in animal models of movement disorders.* BMC Neuroscience, 2010. **11**(1): p. 92.
99. Mirelman, A., et al., *Arm swing as a potential new prodromal marker of Parkinson's disease.* Mov Disord, 2016. **31**(10): p. 1527-1534.
100. Glajch, K.E., et al., *Sensorimotor assessment of the unilateral 6-hydroxydopamine mouse model of Parkinson's disease.* Behav Brain Res, 2012. **230**(2): p. 309-16.
101. Bejjani, B.P., et al., *Axial parkinsonian symptoms can be improved: the role of levodopa and bilateral subthalamic stimulation.* J Neurol Neurosurg Psychiatry, 2000. **68**(5): p. 595-600.
102. Amende, I., et al., *Gait dynamics in mouse models of Parkinson's disease and Huntington's disease.* J Neuroeng Rehabil, 2005. **2**: p. 20.
103. Brooks, S.P. and S.B. Dunnett, *Tests to assess motor phenotype in mice: a user's guide.* Nat Rev Neurosci, 2009. **10**(7): p. 519-29.
104. Dunnett, S.B. and E.M. Torres, *Rotation in the 6-OHDA-Lesioned Rat*, in *Animal Models of Movement Disorders: Volume I*, E.L. Lane and S.B. Dunnett, Editors. 2012, Humana Press: Totowa, NJ. p. 299-315.
105. Pang, Z.P., et al., *Induction of human neuronal cells by defined transcription factors.* Nature, 2011. **476**(7359): p. 220-3.
106. Black, J.B., et al., *Targeted Epigenetic Remodeling of Endogenous Loci by CRISPR/Cas9-Based Transcriptional Activators Directly Converts Fibroblasts to Neuronal Cells.* Cell Stem Cell, 2016. **19**(3): p. 406-14.
107. Zhou, H., et al., *In vivo simultaneous transcriptional activation of multiple genes in the brain using CRISPR-dCas9-activator transgenic mice.* Nat Neurosci, 2018. **21**(3): p. 440-446.
108. Savell, K.E., et al., *A neuron-optimized CRISPR/dCas9 activation system for robust and specific gene regulation.* eNeuro, 2019. **6**(1).
109. Levy, J.M., et al., *Cytosine and adenine base editing of the brain, liver, retina, heart and skeletal muscle of mice via adeno-associated viruses.* Nat Biomed Eng, 2020. **4**(1): p. 97-110.
110. Bove, J., et al., *Toxin-induced models of Parkinson's disease.* NeuroRx, 2005. **2**(3): p. 484-94.
111. Walsh, S., D. Finn, and E. Dowd, *Time-course of nigrostriatal neurodegeneration and neuroinflammation in the 6-hydroxydopamine-induced axonal and terminal lesion models of Parkinson's disease in the rat.* Neuroscience, 2011. **175**: p. 251-261.
112. Henning, J., et al., *Differential astroglial activation in 6-hydroxydopamine models of Parkinson's disease.* Neuroscience research, 2008. **62**(4): p. 246-253.
113. Magnusson, J.P., et al., *A latent neurogenic program in astrocytes regulated by Notch signaling in the mouse.* Science, 2014. **346**(6206): p. 237-41.
114. Sirko, S., et al., *Reactive glia in the injured brain acquire stem cell properties in response to sonic hedgehog. [corrected].* Cell Stem Cell, 2013. **12**(4): p. 426-39.
115. Terzioglu, M. and D. Galter, *Parkinson's disease: genetic versus toxin-induced rodent models.* FEBS J, 2008. **275**(7): p. 1384-91.
116. Weber, T., et al., *Caspase-mediated apoptosis induction in zebrafish cerebellar Purkinje neurons.* Development, 2016. **143**(22): p. 4279-4287.
117. Govindan, S. and D. Jabaudon, *Coupling progenitor and neuronal diversity in the developing neocortex.* FEBS Lett, 2017. **591**(24): p. 3960-3977.
118. Lodato, S. and P. Arlotta, *Generating neuronal diversity in the mammalian cerebral cortex.* Annu Rev Cell Dev Biol, 2015. **31**: p. 699-720.
119. Pereira, M., et al., *Direct Reprogramming of Resident NG2 Glia into Neurons with Properties of Fast-Spiking Parvalbumin-Containing Interneurons.* Stem Cell Reports, 2017. **9**(3): p. 742-751.

120. Herrero-Navarro, Á., et al., *Astrocytes and neurons share brain region-specific transcriptional signatures.* bioRxiv, 2020: p. 2020.04.21.038737.
121. Komor, A.C., A.H. Badran, and D.R. Liu, *CRISPR-Based Technologies for the Manipulation of Eukaryotic Genomes.* Cell, 2017. **168**(1-2): p. 20-36.
122. Matsuda, T., et al., *Pioneer Factor NeuroD1 Rearranges Transcriptional and Epigenetic Profiles to Execute Microglia-Neuron Conversion.* Neuron, 2019. **101**(3): p. 472-485 e7.
123. Bensinger, S.J. and P. Tontonoz, *A Nurr1 pathway for neuroprotection.* Cell, 2009. **137**(1): p. 26-8.
124. Huang, T., et al., *Wnt1-cre-mediated conditional loss of Dicer results in malformation of the midbrain and cerebellum and failure of neural crest and dopaminergic differentiation in mice.* J Mol Cell Biol, 2010. **2**(3): p. 152-63.
125. Rodriguez-Calvo, R., M. Tajes, and M. Vazquez-Carrera, *The NR4A subfamily of nuclear receptors: potential new therapeutic targets for the treatment of inflammatory diseases.* Expert Opin Ther Targets, 2017. **21**(3): p. 291-304.
126. Masserdotti, G., S. Gascón, and M. Götz, *Direct neuronal reprogramming: learning from and for development.* Development, 2016. **143**(14): p. 2494-2510.
127. Tepper, J. and T. Koos, *Gabaergic interneurons of the Striatum*, in *Handbook of Behavioral Neuroscience*. 2016, Elsevier. p. 157-178.
128. Mao, M., A. Nair, and G.J. Augustine, *A Novel Type of Neuron Within the Dorsal Striatum.* Front Neural Circuits, 2019. **13**: p. 32.
129. Grande, A., et al., *Environmental impact on direct neuronal reprogramming in vivo in the adult brain.* Nature communications, 2013. **4**(1): p. 1-12.
130. Planert, H., T.K. Berger, and G. Silberberg, *Membrane properties of striatal direct and indirect pathway neurons in mouse and rat slices and their modulation by dopamine.* PLoS One, 2013. **8**(3): p. e57054.
131. Gertler, T.S., C.S. Chan, and D.J. Surmeier, *Dichotomous anatomical properties of adult striatal medium spiny neurons.* J Neurosci, 2008. **28**(43): p. 10814-24.
132. Cepeda, C., et al., *Differential electrophysiological properties of dopamine D1 and D2 receptor-containing striatal medium-sized spiny neurons.* Eur J Neurosci, 2008. **27**(3): p. 671-82.
133. Burke, D.A., H.G. Rotstein, and V.A. Alvarez, *Striatal Local Circuitry: A New Framework for Lateral Inhibition.* Neuron, 2017. **96**(2): p. 267-284.
134. Bergman, H., T. Wichmann, and M.R. DeLong, *Reversal of experimental parkinsonism by lesions of the subthalamic nucleus.* Science, 1990. **249**(4975): p. 1436-8.
135. Bergman, H., et al., *The primate subthalamic nucleus. II. Neuronal activity in the MPTP model of parkinsonism.* J Neurophysiol, 1994. **72**(2): p. 507-20.
136. Salin, P., et al., *Changes to interneuron-driven striatal microcircuits in a rat model of Parkinson's disease.* Neurobiol Dis, 2009. **34**(3): p. 545-52.
137. Lozovaya, N., et al., *GABAergic inhibition in dual-transmission cholinergic and GABAergic striatal interneurons is abolished in Parkinson disease.* Nat Commun, 2018. **9**(1): p. 1422.
138. Ortega-de San Luis, C., et al., *Substantia nigra dopaminergic neurons and striatal interneurons are engaged in three parallel but interdependent postnatal neurotrophic circuits.* Aging Cell, 2018. **17**(5): p. e12821.
139. Breunig, C.T., et al., *One step generation of customizable gRNA vectors for multiplex CRISPR approaches through string assembly gRNA cloning (STAgR).* PLoS One, 2018. **13**(4): p. e0196015.
140. Heinrich, C., et al., *Generation of subtype-specific neurons from postnatal astroglia of the mouse cerebral cortex.* Nat Protoc, 2011. **6**(2): p. 214-28.
141. Zolotukhin, S., et al., *Recombinant adeno-associated virus purification using novel methods improves infectious titer and yield.* Gene Ther, 1999. **6**(6): p. 973-85.
142. D'Costa, S., et al., *Practical utilization of recombinant AAV vector reference standards: focus on vector genomes titration by free ITR qPCR.* Mol Ther Methods Clin Dev, 2016. **5**: p. 16019.

143. Hölter, S.M. and L. Glasl, *High-Throughput Mouse Phenotyping*, in *Animal Models of Movement Disorders: Volume I*, E.L. Lane and S.B. Dunnett, Editors. 2012, Humana Press: Totowa, NJ. p. 109-133.
144. Zimprich, A., et al., *Analysis of locomotor behavior in the German Mouse Clinic.* J Neurosci Methods, 2018. **300**: p. 77-91.
145. Luecken, M.D. and F.J. Theis, *Current best practices in single-cell RNA-seq analysis: a tutorial.* Mol Syst Biol, 2019. **15**(6): p. e8746.
146. Wolf, F.A., P. Angerer, and F.J. Theis, *SCANPY: large-scale single-cell gene expression data analysis.* Genome Biol, 2018. **19**(1): p. 15.
147. Satija, R., et al., *Spatial reconstruction of single-cell gene expression data.* Nat Biotechnol, 2015. **33**(5): p. 495-502.
148. Traag, V.A., L. Waltman, and N.J. van Eck, *From Louvain to Leiden: guaranteeing well-connected communities.* Sci Rep, 2019. **9**(1): p. 5233.
149. Melville, J., L. McInnes, and J. Healy, *UMAP: uniform manifold approximation and projection for dimension reduction.* Preprint at arXiv https://arxiv. org/abs/1802.03426, 2018.

9.6 Acronyms

6-OHDA	6-hydroxy dopamine
A	Ascl1, Mash1
AAV	Adeno-associated virus
ABC	Avicin biotin complex
aCRISPR	CRISPR activation
ANOVA	Analysis of variance
AP	Actionpotential
Ascl1	Achaete-scute homolog 1
BBB	Blood brain barrier
BDNF	Bone marrow derived growth factor
BG	Basal ganglia
bp	Base pairs
BSA	Bovine serum albumin
Ca	Calcium
cAMP	Cyclic adenosine monophosphate
Cas	CRISPR associated proteins
cDNA	Complementary DNA
CHAT	Choline acetyltransferase
CMV	Cytomegalovirus
COMT	Catechol-O-Methyltransferase
CRISPR	Clustered regulatory interspaced short palindromic repeats
crRNA	CRISPR-RNA
D1	Dopamine D1 receptor
D2	Dopamine D2 receptor
DA	Dopamine
DAB	3,3´-Diaminobenzidine
DARPP32	Dopamine- and cAMP-regulated phosphoprotein, Mr 32 kDa
dCas9	Dead Cas9, nuclease-deficient Cas9
DMEM	Dulbecco´s modified eagle medium
DNA	Deoxyribonucleic acid
ECL	Enhanced chemoluminescence
EGF	Epidermal growth factor
ESC	Embryonic stem cell
FACS	Fluorescence-activated cell sorting

FGF	Fibroblast growth factor
GABA	Gamma-aminobutyric acid
GAD65/67	Glutamate decarboxylase 65/67kDa
GBA	β-Glucocerebrosidase
GC	Gene copy
GFAP	Glial fibrillary acidic protein
GFP	Green fluorescent protein
GLAST	Glutamata-aspartate transporter
Glc	Glucose
Gluta	Glutamate
GPe	Globus pallidus externus
GPi	Globus pallidus internus
GWAS	Genome-wide association study
HBSS	Hank´s balanced salt solution
HCl	Hydrochloric acid
HEK	Human embryonic kidney
HiFi	High fidelity
HSF1	Heat shock factor 1
HVG	Highly variable genes
iPSC	Induced pluripotent stem cell
K	Potassium
kb	Kilobase
kDa	Kilo Dalton
L	Lmx1a
LB	Lewy body
L-DOPA	L-Dihydroxyphenylalanin
Lmx1a	LIM homeobox transcription factor 1, alpha
Lrrk2	Leucine-rich repeat kinase 2
MAP2	Microtubule-associated protein 2
MAO	Monoaminoxidase
MB	MasterBlaster
MEF	Mouse embryonic fibroblast
MFB	Medium forebrain bundle
Mg	Magnesium
mir218	MicroRNA218
MPTP	1-METHYL-4-PHENYL-1,2,3,6-tetrahydropyridin

mRNA	Messenger RNA
MS2	MS2 bacteriophage coat protein
MSN	Medium spiny neurons
N	Nr4a2/Nr4A2
Na	Sodium
NaOH	Sodiumhydroxid
Ne	NeuroD1
NeuN	Fox-3, Rbfox3, or Hexaribonucleotide Binding Protein-3
NeuroD1	Neurogenic differentiation 1
NPY	Neuropeptide Y
Nt	Nucleotides
Nr4a2	Nuclear receptor related 1 protein
OXPHOS	Oxidative phosphorylation
P2A	2A peptide of porcine teschovirus-1
P65	P65 subunit of NF-κB
PAM	Protospacer adjacent motif
PCR	Polymerase chain reaction
PD	Parkinson´s Disease
PFA	Paraformaldehyde
PV	Parvalbumin
QC	Quality control
qRT-PCR	Quantitative real-time PCR
rAAV	Recombinant AAV
R_{in}	Input resistance
RNA	Ribonucleic acid
rpm	Rounds per minute
Rta	Regulator of transcriptional activation
SAM	Synergistic activation mediator
SB	Southern blot
scRNA-seq	Single cell RNA sequencing
SD	Standard deviation
sgRNA	Single-guide RNA
SNCA	α-Synuclein
SN*pc*	Substantia nigra *pars compacta*
SNr	Substantia nigra reticulate
SpCas9	Streptococcus pyogenes Cas9

SSC	Saline sodium citrate
STAGR	String assembly gRNA cloning
STN	Subthalamic nucleus
TALEN	Transcription activator-effector nuclease
TBS-T	Tris-buffered saline with Tween-20
TH	Tyrosine hydroxylase
tracrRNA	Transactivating crRNA
UMAP	Uniform Manifold Approximation and Projection
vGLUT1	Vesicular glutamate transporter 1
Vm	Resting membrane potential
VP16, VP64	Herpes simplex virus protein 16 and repeats
VPR	VP64, p65, Rta
VTA	Ventral tegmental area
WB	Western blot
wpi	Weeks post injection
ZFN	Zinc finger nuclease

9.8 Danksagung

An erster Stelle möchte ich mich bei Dr. Florian Giesert bedanken, ohne ihn wäre dieses Projekt nicht möglich gewesen. Nicht nur auf wissenschaftlicher, sondern auch auf persönlicher Ebene, konnte ich mich jederzeit auf seine Unterstützung und seinen Rat verlassen.
Danke Florian – ohne dich hätte ich die tiefsten Tiefs nicht überstanden!

Meinem Doktorvater Prof. Dr. Wolfgang Wurst möchte ich dafür danken, dass er mich in meiner Begeisterung für die Forschung immer unterstützt und bestärkt hat, durch seine Hilfe war es mir möglich die nötigen Ressourcen auszuschöpfen und viele meiner Ideen umzusetzen.

Vielen Dank an die Mitglieder meiner Prüfungskommission, Prof. Dr. Erwin Grill als Vorsitzenden und Prof. Dr. Wolfgang Wurst, sowie Prof. Dr. Magdalena Götz und Prof. Dr. Angelika Schnieke als Prüfer.

Ich möchte mich bei meinem Thesis Komitee bedanken, insbesondere bei Prof. Dr. Magdalena Götz, durch ihre Hilfe und Kooperation konnten viele Versuche schneller und manchmal sogar überhaupt erst durchgeführt werden. Hierbei möchte ich mich auch bei den Mitgliedern der AG Götz, Dr. Chu Lan Lao, Dr. Giacomo Masserdotti, Dr. Judith Fischer und Manja Thorwirth für ihre Hilfe bedanken.

Einen großen Dank an Dr. Daniela Vogt-Weisehorn für die Hilfe beim Schreiben des Tierversuchsantrages und die Unterstützung bei den stereotaktischen Operationen.

Vielen Dank an Dr. Sandrine Lefort für ihr Hilfe bei der Elektrophysiologie.

Vielen Dank an Christina Koupourtidou und Prof. Dr. Jovica Ninkovic für die Hilfe bei der Planung und Durchführung des scRNA-seq Experimente, und auch an Dr. Ignacio Ibarra del Río und Dr. Malte Lücken für die Hilfe bei der bioinformatischen Analyse.

Herzlichen Dank an Susanne Bourier und Susanne Badeke, für die Hilfe und Unterstützung vor allem beim Genotypisieren und bei der Immunohistochemie.

Danke auch an die anderen Mitglieder der AG Wurst, vor allem Annerose Kurz-Drexler und Irina Rodionova für die vielen Tipps und Hilfestellungen im Labor.

Vielen Dank an das Verhaltensteam, Dr. Sabine Hölter-Koch, Dr. Annemarie Zimprich und Jan Einicke, für die Hilfe bei der Planung, Durchführung und Auswertung der Verhaltenstests.

Besonderen Dank an Jeffery Truong für zahlreiche Diskussionen und Plasmide und natürlich die Hilfe bei den FACS-Einstellungen.

Ebenfalls vielen Dank an das C-Streifen Team, besonders an Nenad Radic, auf den ich mich bei der Betreuung meiner Tiere immer verlassen konnte. In diesem Zusammenhang auch vielen Dank an Heidi Krause und Anja Folchert für die seelische Unterstützung im C-Streifen.

Vielen Dank an Dr. Benedict Rauser, welcher durch seine *in vitro* Versuche die Basis für meine *in vivo* Experimente geliefert hat.

Vielen Dank an alle meine Doktorandenkollegen, vor allem Petra, Artem, Consti, Christoph, Bianca und Kristina.

Und einen ganz lieben Dank an alle Mitglieder des Genetic Tools Seminars und des Reprogramming Clubs für zahlreiche Diskussionen.

Ganz lieben Dank an alle meine Freunde, die mich immer wieder in meiner Doktorarbeit bestärkt haben.

Unglaublich großen Dank an meine Familie!
An Einhard und Pia, dass ihr euch immer wieder nach dem Stand meiner Arbeit erkundigt habt, obwohl ihr totale Naturwissenschafts-Nieten seid.
An meine Eltern die mich von Anfang an unterstützt haben und immer hinter mir standen, ich danke euch von ganzem Herzen, ihr seid die Besten!

Zuletzt möchte ich der für mich wichtigsten Person danken, meinem Schatz Bernhard, ohne dich hätte ich es nicht geschafft!

Für Bernhard

9.9 Eidesstattliche Erklärung

Ich erkläre an Eides statt, dass ich die bei der Fakultät Wissenschaftszentrum Weihenstephan für Ernährung, Landnutzung und Umwelt (promotionsführende Einrichtung) der Technischen Universität München zur Promotionsprüfung vorgelegte Arbeit mit dem Titel:

Rescuing motor behavior in a Parkinson´s disease model by aCRISPR mediated reprogramming of striatal astrocytes into induced neurons

unter der Anleitung und Betreuung durch Professor Dr. Wolfgang Wurst ohne sonstige Hilfe erstellt und bei der Abfassung nur die gemäß § 6 Abs. 6 und 7 Satz 2 angegebenen Hilfsmittel benutzt habe.

Ich habe keine Organisation eingeschaltet, die gegen Entgelt Betreuerinnen und Betreuer für die Anfertigung von Dissertationen sucht, oder die mir obliegenden Pflichten hinsichtlich der Prüfungsleistungen für mich ganz oder teilweise erledigt. Weder habe ich diese Dissertation in dieser oder ähnlicher Form in einem anderen Prüfungsverfahren als Prüfungsleistung vorgelegt. Ich habe den angestrebten Doktorgrad noch nicht erworben und bin nicht in einem früheren Promotionsverfahren für den angestrebten Doktorgrad endgültig gescheitert. Die öffentlich zugängliche Promotionsordnung der TUM ist mir bekannt, insbesondere habe ich die Bedeutung von § 28 (Nichtigkeit der Promotion) und § 29 (Entzug des Doktorgrades) zur Kenntnis genommen. Ich bin mir der Konsequenzen einer falschen Eidesstattlichen Erklärung bewusst.

Mit der Aufnahme meiner personenbezogenen Daten in die Alumni-Datei der TUM bin ich einverstanden.

München,

Ort, Datum, Unterschrift